6-2011

The Impact of Modern Weathering on the Geochemistry of a Marine Permo-Triassic Boundary Section

Jeremy Christopher Williams
University of Massachusetts Boston

THE IMPACT OF MODERN WEATHERING ON THE GEOCHEMISTRY OF A NEO-TETHYAN PERMO-TRIASSIC BOUNDARY SECTION

A Thesis Presented

by

JEREMY CHRISTOPHER WILLIAMS

Submitted to the Office of Graduate Studies,
University of Massachusetts Boston,
in partial fulfillment of the requirements for the degree of

MASTER IN SCIENCE

June 2011

Environmental, Earth, and Ocean Science

THE IMPACT OF MODERN WEATHERING ON THE GEOCHEMISTRY OF A NEO-TETHYAN PERMO-TRIASSIC BOUNDARY SECTION

A Thesis Presented

by

Jeremy Christopher Williams

Approved as to style and content by:

_____
Robyn Hannigan, Professor
Chairperson of Committee

_____
Curtis Olsen, Professor
Member

_____
Allen Gontz, Assistant Professor
Member

_____
John Duff, Program Director
Environmental, Earth, and Ocean Sciences Program

_____
Robyn Hannigan, Chairperson
Environmental, Earth, and Ocean Sciences Department

ABSTRACT

THE IMPACT OF MODERN WEATHERING ON THE GEOCHEMISTRY OF A MARINE PERMO-TRIASSIC BOUNDARY SECTION

June 2011

Jeremy Christopher Williams, B.S., Hampton University
M.S., University of Massachusetts Boston

Directed by Professor Robyn Hannigan

The Permian-Triassic Boundary (PTB) marks the end-Permian extinction, the greatest mass extinction recorded in Earth's history. The Attargoo PTB section located in Spiti Valley, Himachal Pradesh, India was situated along the north continental margin of Gondwana-land in the Neo-Tethys Ocean during the end-Permian extinction. In Spiti Valley, PTB sections such as Attargoo are exposed by a thin (~ 2cm) ferruginous layer separating the Permian black shale from Triassic Limestone. Studies that have presented geochemical data to support a theory of the end-Permian extinction lack any interpretation of post-depositional effects on Spiti Valley PTB sections. In order to accurately present a cause for the end Permian extinction one must understand if the Spiti PTB sections contain any

original chemical signature. In this study we present the major element geochemistry of the Attargoo PTB section to see if this section has experienced any post-depositional alteration and assess the major element geochemistry of the ferruginous layer. X-ray fluorescence (ED-XRF), Inductively Coupled Plasma Optical Emission Spectroscopy (ICP-OES), and Loss on Ignition (LOI) were used to gather major element, organic, and inorganic carbon values for the Attargoo PTB section. From our analysis we suggest that the Attargoo section has experienced intermediate weathering, very little chloritzation, no K-metasomatism, and is diagenetically altered. Intermediate weathering is supported by the CIA values quantified at the Gungri formation. The major element chemistry suggests that the Triassic limestone contains dolomitic characteristics. The extent of chemical weathering and chloritization do not appear to be significant in which samples are altered from the original chemical composition this is reflective in the shale CIA values and both ternary plots. The ferruginous layer can be divided into three sections: lower, middle and upper ferruginous layer. The lower ferruginous layers has shale characteristics, whereas the middle and upper ferruginous layer has characteristics of an ironstone or iron rich shale. The CIA values of the middle and upper ferruginous layer suggest that it formed under arid or dry conditions. The Ca, Fe, P and C_{org} values suggest that the ferruginous layer formed *in situ* during a non-depositional event of subaerial origin.

ACKNOWLEDGEMENTS

I would like to thank my advisor Robyn Hannigan for providing with a wonderful opportunity to do exciting and once in a life time research. I also would like to thank her for academic guidance, emotional, and financial support throughout this process. I would like to thank the Environmental, Earth, and Ocean Science department for providing an excellent work atmosphere. A special thanks to my committee members Robyn Hannigan, Allen Gontz, and Curtis Olsen for your guidance throughout research process.

I would like to thank the Southern Region Education Board Doctoral Fellowship and National Science Foundation University of Massachusetts Boston Watershed-Integrated Science Partnership GK12 Program for funding me during this process.

I would like to thank the people involved in the Indo-US bilateral workshop and field conference for allowing me to go to Spiti Valley. The people from the Centre of Advanced Studies in Geology at Panjab University for their hospitality, and holding the Indo-US bilateral workshop and field conference. A special thanks to Dr. Asish Basu from the University of Rochester for academic guidance, expanding my geological interest, and pulling this entire event together. To the people affiliated with University of Rochester: Neil Basu, Arundhuti Ghatak, Amanda Carey, Stephanie Yuchik, and Nilotpal Ghosh for their hard work. Also, a special thanks to Dr. Ellen

Douglass for going to India with me and being there for me and Mythreyi Balaji for her hard work in the field.

To my lab mates Dr. Thomas Darrah, Melanie Campbell, Nicole Henderson, Bryanna Broadaway, Eric Wilcox Freeburg, Jenny Flashman Geldart, and Alex Eisen-Cuadra, for laboratory assistance and emotional support. I would like to thank Dr. Curtis Olsen and Jun Zhu for assisting me in my research project and letting me use the XRF, Dr. Deyang Qu and his lab group for their assistance and letting me use the ICP-OES, and Dr. Alan Christian and the Freshwater Ecology lab group for laboratory assistance and letting me burn the table during the LOI process. A special thanks to Dr. Peter Abanda for helping me with my research project and Melika Uter for assisting me in completing the LOI analysis.

Lastly, I would like to thank my Eddie Williams Sr. (father), Karen Williams (mother), Eddie Williams Jr. (brother), Sharonda Williams (sister-in-law), Elbert Moore (grandfather), Barbara Moore (grandmother), Eddie "Trey" Williams (nephew), other family members, and friends for your prayers, support, and patience. I could not ask for a better family, you have always been there for me, and most importantly you gave me guidance and support no matter what the circumstances were.

TABLE OF CONTENTS

CHAPTER Page

LIST OF FIGURES

LIST OF FIGURES

FIGURE Page

LIST OF TABLES

TABLE Page

CHAPTER 1

INTRODUCTION

Statement of Purpose

This thesis centers on the geochemical record of the Permian-Triassic (PT) sequence exposed in Spiti Valley known as Attargoo (Himachal Himalaya, India). The exposed PT section at Attargoo includes the uppermost Permian Gungri Shale and the lowermost Triassic Mikin Limestone. The boundary itself is thought to be marked by a 2-5 cm ferruginous layer lying unconformably between the Permian Gungri Shale and Triassic Mikin Limestone. Even though this boundary is marked by an unconformity, we will treat this section as a complete section in order to meet the objectives set for this thesis. This thesis focuses on the geochemistry of these units and the evaluation of the impact of post-depositional processes on the geochemical record and will cover the following relevant topics: (1) an overview of the depositional records preserved in Tethyan Permian-Triassic marine sequences and (2) an overview of major element geochemical approaches to evaluating post-depositional alteration in sedimentary units.

1. Introduction

During the late Permian- early Triassic (~ 250 mya) there were two continental masses, Laurasia and Gondwanaland, joined together to form the supercontinent of Pangea (Figure 1.1). Pangea partially enclosed the Tethys Ocean, while the Panthalassa Sea surrounded Pangea (Zhao et al., 2004). The southern Tethyan PT sequences include complete to nearly complete sections in the Himalayas of India, Kashmir, Pakistan, and Tibet. A thorough review of the geology and paleontology of the majority of well studied Tethyan PT sequences is presented elsewhere in the published literature (Hongfu et al., 2000; Sweet et al., 1992). Since this thesis focuses on a section of the PT exposed in the high Himalaya of India, a brief overview of the PT geology of the northern Indian continental margin and the PT sequences that are exposed in this region. The sedimentary record of the PT in northern India represents the deformed remnants of the continental margin of the Indian subcontinent (Gaetani and Garzanti, 1991b). The Tethys sediments in this region are exposed in the Zanskar-Spiti synclinorium (Figure 1.2).

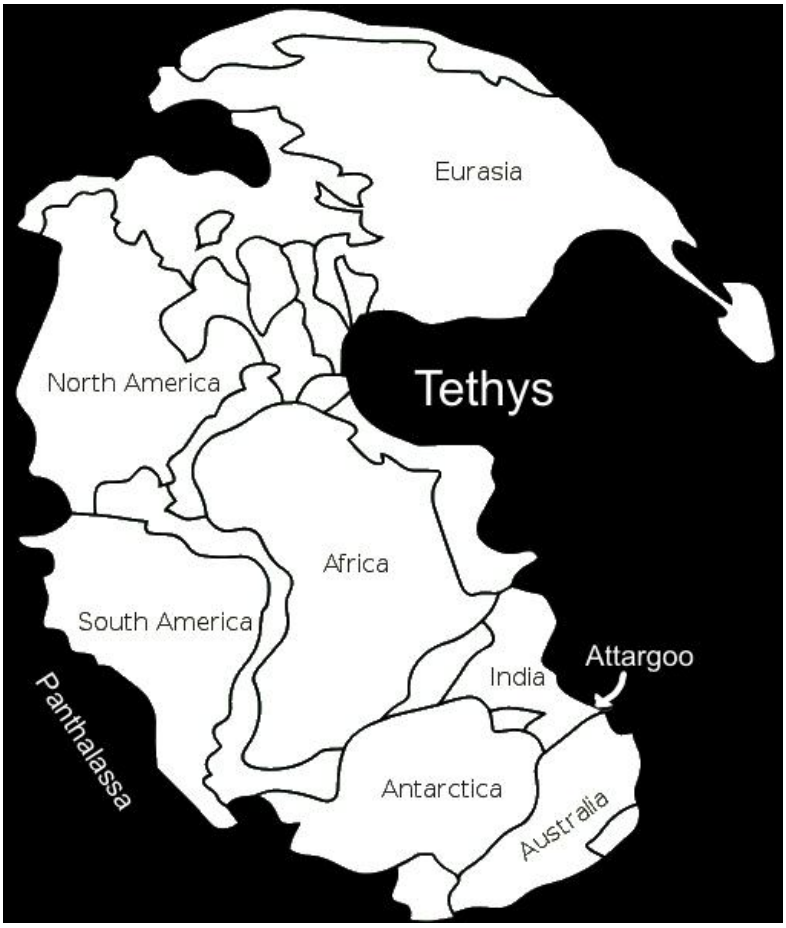

Figure 1.1. Paleogeography of Pangea showing the location of the study section at Attargoo based on estimates of paleolatitude derived from Guryul Ravine, Kashmir (Algeo et al., 2007).

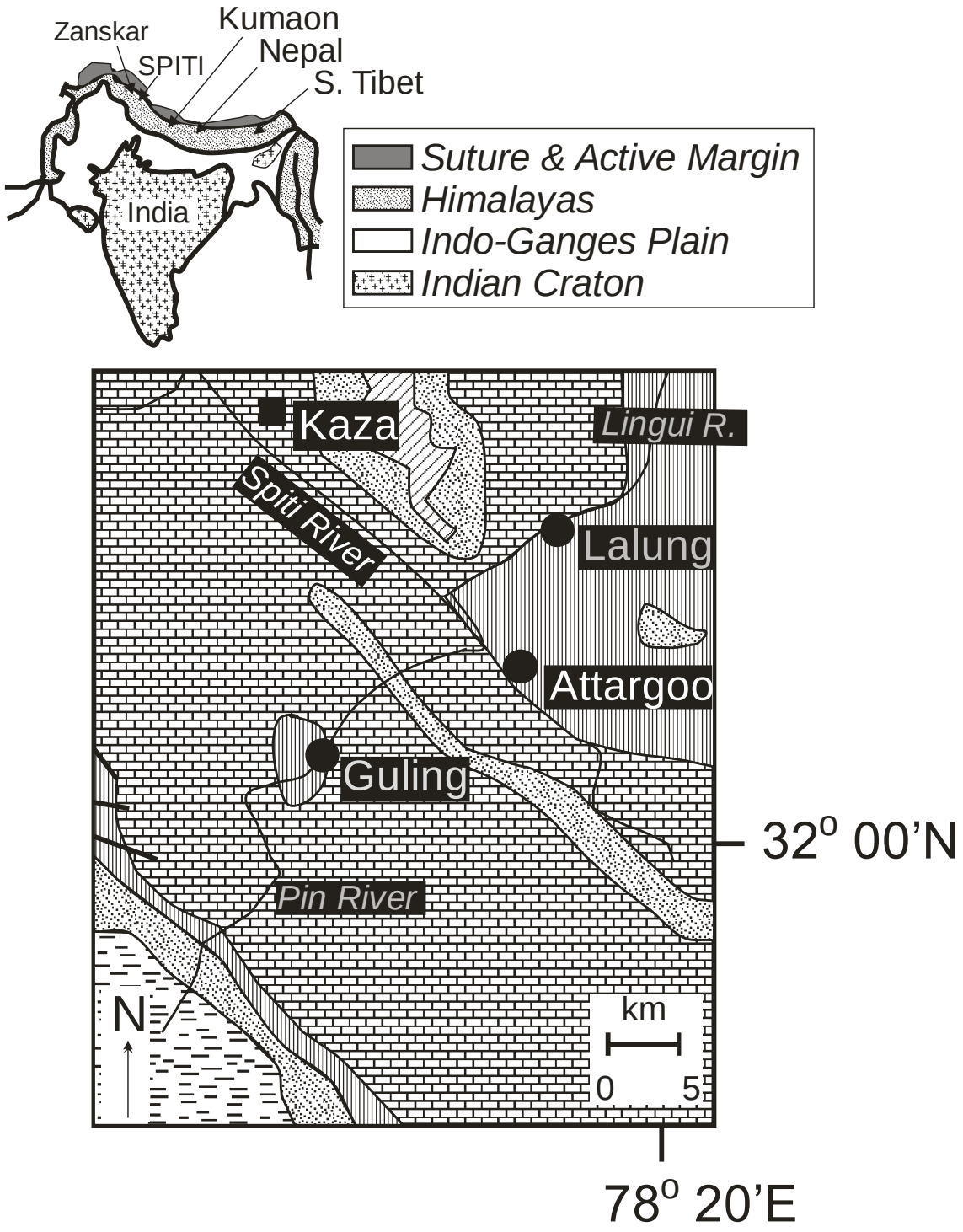

Figure 1.2. Geology of the northwestern Himalaya showing location of study site (Attargoo).

Towards the end Permian rifting caused detachment of the Peri-Gondwanian microplate and the initial opening of the neo-Tethys (Sengor et al., 1988). During the early Permian the margin was covered by transgressive shallow marine sediments followed by fluvial-deltaic siliciclastics (Gaetani and Garzanti, 1991b). Within these early Permian fluvial sediments is the first record of rift volcanism (Panjal Traps) (Garzanti, 1993b). The major transgressive episode that is defined by this sequence corresponds to the end of Gondwana glaciations and the initial opening of the neo-Tethys (Veevers and Powell, 1987). Paleontological evidence also supports the Early Permian neo-Tethys opening with late Early Permian as marina faunas have been identified in these sections and to the north in modern-day Afghanistan and northern Karakorum to Ladakh (Bassoullet et al., 1983). Following this tectono-eustatic event thick intraplate basaltic lavas, the Panjal Traps filled the rift valleys with rift volcanism ending in the mid-Permian (Baud et al., 1989). The Panjal Traps were located off the continental margin of Gondwana-land near the Kashmir and Spiti Valley Basin. In the late Permian transgressive shallow marine arenites of the Kuling Group mark the onlapping of marine waters, with these units of arenites becoming more distal until the maximum transgression is reached with this being marked by turbidites preserved in the Markha (central) region of the High Himalaya (Stutz, 1988). In the early Triassic rapid thermo-tectonic subsidence and submergence of rift valleys caused starvation of sediments and deepening of the outer shelf and upper slope marked by deposition of condensed nodular limestones of Tamba Kurkur Formation, Lilang Group, equivalent to Mikin Formation of Spiti. Proximal inner continental margin conditions are well preserved in the units at the Guryul Ravine PTB

section in Kashmir (Algeo et al., 2007a) and Salt Range PTB section in Pakistan (Waterhouse, 2010). The early Triassic is marked by renewed carbonate productivity and mud supply with a thick shallowing upward sequence rapidly deposited by the Mid-Triassic. These thick sequences for a thick continental terrace in Zanskar and Spiti (Garzanti et al., 1995). By the end Triassic these offshore marly limestones (Hanse Formation) are overlain by subtidal and, finally, peritidal carbonates of the Zozar Formation.

1.1. The Permo-Triassic of Spiti Valley (Himachal Pradesh) at Attargoo

The Paleozoic and Mesozoic Tethyan sequences in the Indian Plate are primarily preserved in the inner part of the Higher Himalaya. These units are well exposed in the Western Himalaya at Kashmir, Zanskar- Spiti and Uttrakhand; and the Central (Nepal) Himalaya (Kapoor, 2004). Spiti Valley forms part of the district of Lahul & Spiti located in the northern part of the Himachal Pradesh, which occupies a central position in the Western Himalaya (Figure 1.2). Spiti Valley became famous for its well exposed and complete Triassic sedimentary succession [~1400 m; (Diener, 1908; Diener, 1912; Hayden, 1904)] and rich fossil content (Stoliczka, 1866). During the Triassic this region formed part of the tropical Gondwana margin [also known as Peri-Gondwana Tethyan succession; (Matsuda, 1985)]. The mid-low paleolatitude allowed for the development of a large and highly diverse mixed pelagic fauna which are very well preserved in these rocks (e.g., Diener, 1897; Krafft and Diener, 1909)].

The section exposed at Attargoo (Chapter 2, Figure 2.1) contains late Permian gray-black shales of the Gungri Formation apart of the Kuling Group overlain by early Triassic limestone of the Mikin Formation apart of the Lilang Group. The units are separated by a 2-5 cm ferruginous layer marking a sharp transition from the shale to limestone (Figure 1.3). The biostratigraphy across the boundary is not firmly established due to the apparent lack of uppermost Permian strata at this location (Garzanti et al., 1998). The Gungri shale grades upward from gray to black suggesting a change in oxygen availability close to the PT boundary (Shukla et al., 2002a). The regional extent of this layer (Spiti Valley, Lahaul Valley and Guryul Raving, Kashmir) (Algeo et al., 2007c; Singh et al., 1995) and the mineralogical and sedimentological character suggest that this layer represents period of subaerial exposure or a sedimentary hiatus (Bhargava, 1987; Bhatt et al., 1981; Srikantia and Bhargava, 1998). It is important to note, however, that the overall stratigraphic record of the Tethys Himalaya documents a major long-term stepwise transgression which began after continental breakup in the mid-early Permian and ended at the PT boundary with transgression, draping, in the Lower Triassic, deep water limestone atop the terrigenous shelf (Gardner, 1992; Garzanti et al., 1996; Garzanti et al., 1995).

1.1.1. The Gungri Shale

Little information about the Gungri Shale at Attargoo has been published. Based on our field observations the uppermost Gungri is consistent in character with that exposed at Muth (Garzanti et al., 1996). This unit consists of black shale with

intercalations, stratigraphically below our samples, of thin siltstone (Figure 1.3). Phosphate nodules and Fe-rich concretions are locally present in the uppermost Gungri as well. Fragments of brachiopods and corals are also present sporadically in the lower samples. Macroscopic evidence of bioturbation (e.g., *Zoophycos*) such as noted at Muth and other Spiti Valley sections (Bhargava, 1987; Bhargava et al., 1985) is at the base of the Gungri. Garzanti et al. (1996) state that based on paleontological and sedimentology data, that the uppermost member of the Gungri was deposited in an offshore shelf environment episodically disturbed by "exceptional" storm events.

1.1.2. The Ferruginous Layer

At Attargoo the ferruginous layer contains goethite, quartz, gypsum and feldspar (Shukla et al., 2002b). Though Shukla et al. (2002b) performed X-Ray Diffraction and Scanning Electron-Energy Dispersion X-Ray Spectroscopy measurements of the ferruginous layer they do not report mineralogy for these shales. Oolitic ironstones like the ferruginous layer at Attargoo are found at several intervals in sections across the globe including the Frasnian (end Devonian), Sakmarian (lower Permian), Djulfian (upper Permian), Norian (upper Triassic), Callovian (mid Jurassic), Aptian to Cenomanian (lower to upper Cretaceous) and Paleocene (Garzanti, 1993a). Garzanti (1993) suggests that ironstones such as the ferruginous layer in Spiti Valley marks a major drowning unconformity associated with time gaps several million years long and that it corresponds in time to peak global transgressions. While many assume that the ferruginous layer marks the PT Boundary the fact that, globally, these units represent

maximum high stand events and significant missing time and, in Spiti, the end Permian fossil record is incomplete makes it difficult to constrain this unit in time. Regardless of the precise age, throughout the Spiti Valley, there is a sedimentation break across the PT which likely caused by strongly reduced carbonate production as a consequence of the end-Permian biotic crisis. This coupled with sediment reworking on sediment starved shelf during deepening may have caused the lack of sedimentation and consequent absence of the Dorashamian age sediments at Attargoo (Bhatt et al., 1981).

1.1.3. The Mikin Limestone

At Attargoo the earliest Triassic (Dorashamian) is missing. Condensed limestones with pelagic fauna *Otoceras* sp. were deposited on the outer shelf to upper slope during peak transgressive stages. It rests unconformably over the Gungri Formation and comprises gray to dark gray limestone in basal part, sporadic argillaceous (marl) limestone and subordinate thin shale bands in middle and predominantly limestone in upper parts (Figure I-3). At Attargoo the lowest member is exposed with this member comprised of ferruginous limestone grading upwards into gray concretionary limestone rich in ammonoids and, occasionally, pteriid bivalves (Bhargava et al., 2004). The Mikin at Attargoo preserves the basal Mikin and is a bioturbated thin to thick-shelled packstone (Bhargava et al., 2004). The macrofauna of the Mikin indicate deposition in shallow marine waters above mean wave base (Bhargava et al., 2004).

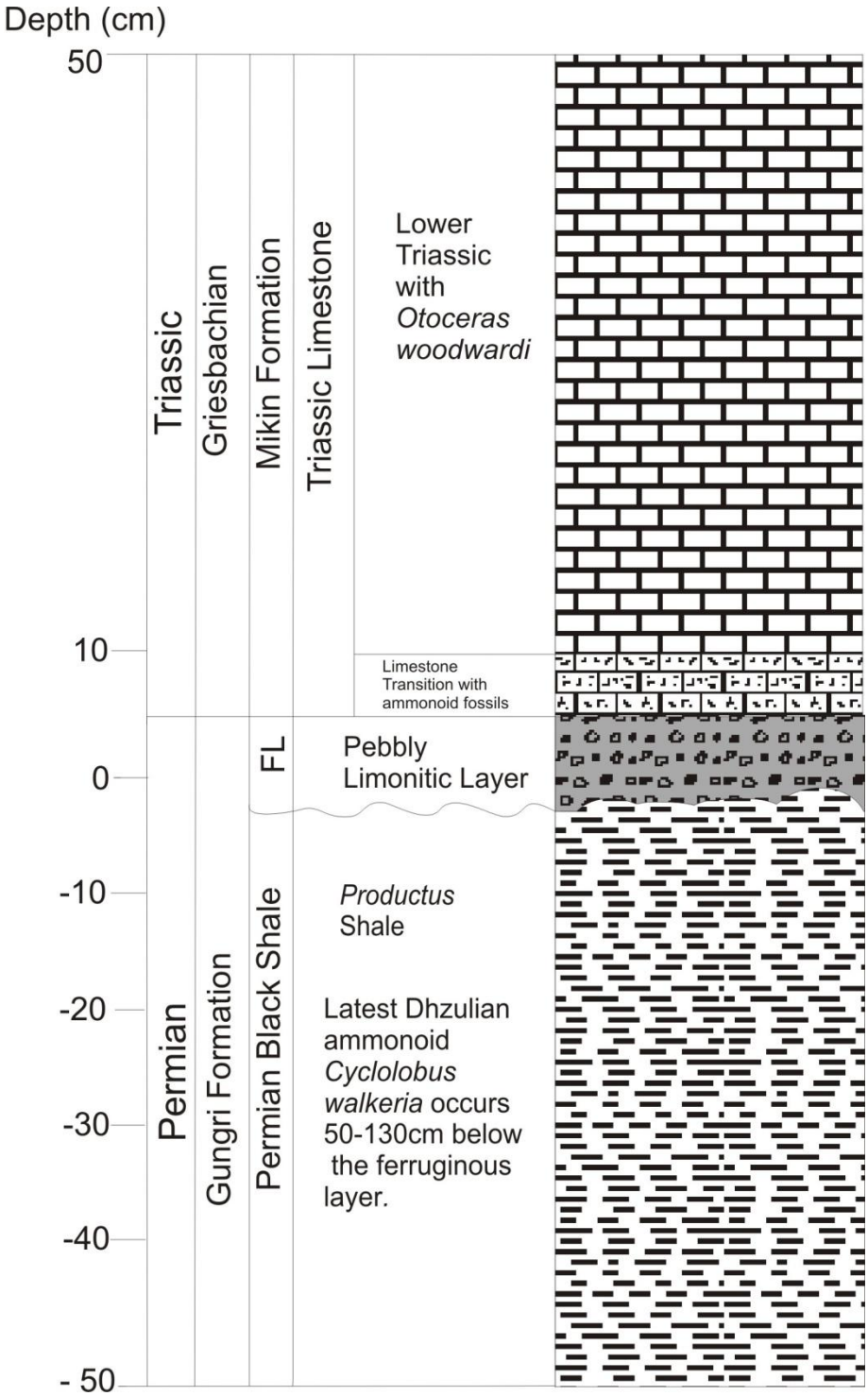

Figure 1.3. Litho and biostratigraphy of the Attargoo PTB in Spiti Valley. FL stands for ferruginous layer, based off of Kapoor (2004) and Shukla et al. (2002b).

1.2. Context and Significance

This research represents a portion of a larger project centered on geochemically based paleoenvironmental reconstruction of the Tethys at the end Permian. The Spiti Valley PT sections, such as Attargoo, are poorly studied geochemically. Of benefit to this research is that the Spiti Valley PT sections have been remarkably well studied paleontologically, sedimentologically and tectonically meaning that the geochemistry of the units can be considered in a context of other paleoenvironmental indicators. One primary motivation for developing geochemical paleoenvironmental reconstructions of the marine PT is that the end-Permian is marked by one of the greatest extinctions in Earth's history. However, in order to leverage the geochemical record of Spiti to better understand the processes operating at that time we must confirm that the record has not been significantly altered since the deposition of these units. This requires a thorough investigation of the major element geochemistry of these rocks and an evaluation of the relative impact of diagenesis and modern weathering on these rocks.

1.3. The End-Permian Biotic Crisis – Causes and Geochemical Proxies

The Permo-Triassic extinction took place at the end of the Permian approximately 251.5 mya. The extent of the Permo-Triassic (PT) extinction is significant and marked by a loss of over 90% of marine and nearly 70% of terrestrial species (Erwin, 1994). Gradual environmental change and/or a combination of catastrophic events are invoked to explain the PT extinction. Many questions remain unanswered as to the succession and timing of the events, the nature and relative importance of controlling factors, and the ultimate

causes of the ecological disaster that marks the PTB (Haas et al., 2007). Our lack of agreement stems from the fact that there are relatively few geologic sections that are demonstrably continuous across the boundary, and even fewer in which relatively thick sections allow individual late Permian events to be identified.

The assumed cause(s) for this biotic crisis [see (Korte and Kozur, 2010) and references therein) are still under discussion and include:

(1) large-scale volcanic activity of Siberian flood basalt and contemporaneous volcanism in South China as well as smaller eruptions in the southern Tethys (Panjal Traps)
(2) ocean anoxia reaching unusually shallow depths accompanied by CO_2 degassing, and/or methane release
(3) an oceanic acidification crisis due to increase in atmospheric CO_2 concentrations
(4) low atmospheric oxygen levels
(5) worldwide depletion of stratospheric ozone
(6) climate change caused by strong volcanism (volcanic winter) and/or impact of a celestial body

Most of these mechanisms rely on geochemical indicators which require that the units under study have not been impacted by late diagenetic/metamorphic alteration or by modern weathering.

1.4. Geochemical Indicators of Mechanism(s) of the PT Extinction

Regardless of the cause the scientific community agrees that the mass extinction and the associated environmental changes were accompanied by major perturbations of the global carbon cycle with nearly all end-Permian marine sections preserving a pronounced negative carbon-isotope excursion (e.g., Spiti Valley, Figure 1.4; Ghosh et al., 2002), Guryul Ravine, Kashmir, India (Algeo et al., 2007b), Meishan, China (Jin et al., 2000; Xie et al., 2006; Yin et al., 2007) Dongpan, China (Yin et al., 2007), Iran (Kozur, 2006), Seis/Siusi, Italy (Kraus et al., 2009), Coalsack Bluff, Antarctica (Retallack et al., 2007), Guizhou, China (Payne et al., 2004), Chaohu/Anhul, China (Tong et al., 2005), Tethys (Baud et al., 1996; Corsetti et al., 2005), Zhuodeng, West Guangxi, China (Zhang et al., 2005), Wenjiangsi, China (Shao et al., 2000), Caucasia area, Russia (Zakharov et al., 2005), Abadeh, Iran (Korte et al., 2004a), Shahreza, Iran (Korte et al., 2004b), Nammal, India (Baud et al., 1996), and Kamura (Isozaki et al., 2007) (Figure 1.5).

The timing of the initial negative $\delta^{13}C$ excursions is often coincident with the end-Permian extinction and is thought to represent a crisis of the carbon cycle probably caused by the shut-down of biological productivity, and the development of Strangelove Ocean or ocean acidification conditions (e.g., Payne et al., 2007; Payne et al., 2010). However, some PT sections such as Guryul Ravine and Meishan (the type section) show more than one negative $\delta^{13}C$ excursion (Algeo et al., 2007b; Yin et al., 2007). The number and timing of these excursions may indicate a series of extinction events or pulsed catastrophic events prior to and following the end Permian (Yin et al., 2007).

Broadly, the negative $\delta^{13}C$ excursions are explained by contemporaneous catastrophic events and gradual or punctuated global events.

Recently it was recognized that, more often than not, up to 10 ‰ ($\delta^{13}C$) negative shifts also occur in the early Triassic; this suggests that the ocean, once thought to return to "normal" after the extinction, continued to experience disturbances (Algeo et al., 2007b). This further suggests that the cause of the extinction could not have been a single catastrophic event, rather the cause(s) may be a series of events that combined to destabilize the carbon cycle (Yin et al., 2007). Such events may include (1) catastrophic release of methane from the gas hydrate reservoir with $\delta^{13}C \sim -60‰$ (Retallack et al., 1996), (2) the input of CO_2 from volcanic out-gassing with $\delta^{13}C \sim -6‰$ (Renne and Basu, 1991), and (3) the release of CO_2 from decomposing terrestrial biomass after a catastrophic die-off with $\delta^{13}C$ - ~25‰.

Another, more controversial explanation is a bolide impact event (Basu et al., 2003; Farley and Mukhopadhyay, 2001; Isozaki et al., 2007) which could have led to both the proposed methane release and volcanism. Gradual causes for the $\delta^{13}C$ negative excursion include ocean stratification/turnover and re-organization of the carbon cycle (Retallack et al., 1996). The ocean stratification model proposes that isotopically light organic matter in the surface water sinks and is remineralized at depth causing an isotopically heavy surface ocean and isotopically light deep ocean. Overturn of the deep water would return light carbon to the surface resulting in a negative $\delta^{13}C$ in shallow water limestones. Re-organization of the carbon cycle proposed reduction in the burial flux of terrestrial biomass versus marine biomass. This is supported by the terrestrial

"coal gap" and shift from arborescent to herbaceous plants recorded at the PTB (Retallack et al., 1996). This shift would impact the burial proportion of terrestrial versus marine organic carbon and cause a long-term negative shift in the $\delta^{13}C$ of the oceans. This theory can be invoked for long-term excursions but fails to explain the series of excursions that typify the early Triassic.

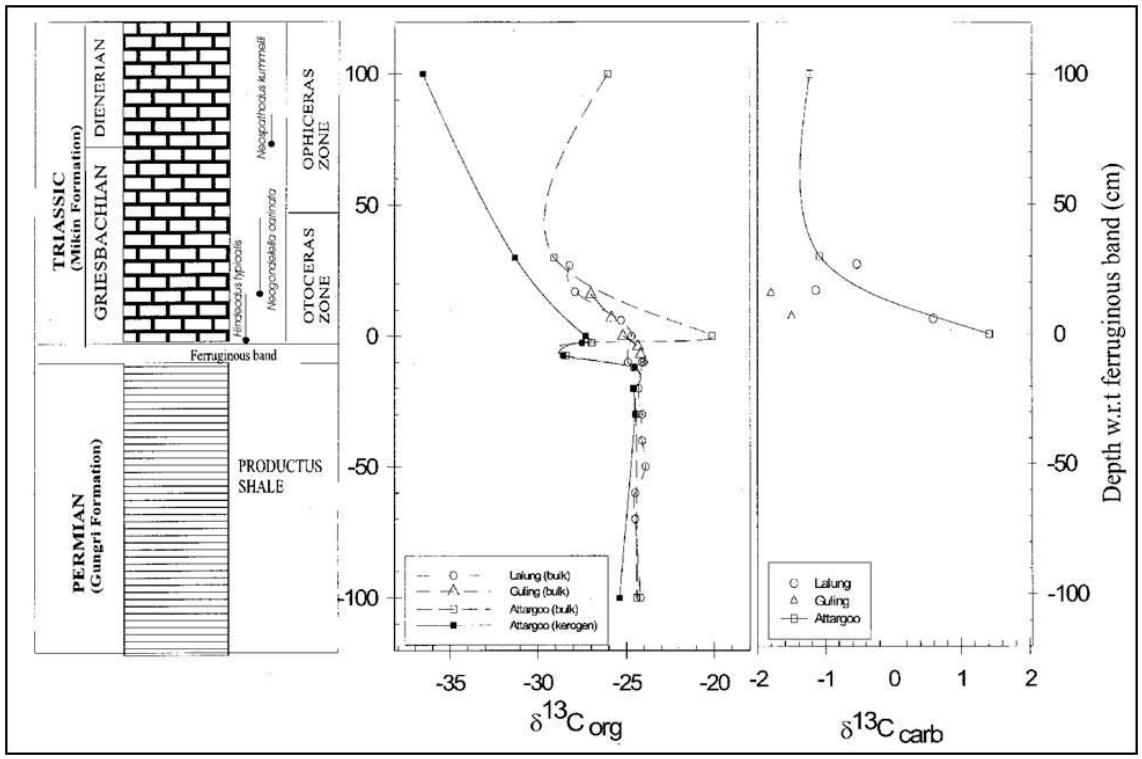

Figure 1.4. From (Ghosh et al., 2002). General litho-, biostratigraphy, δ13C org, and $\delta^{13}C$ carb of Permian-Triassic Boundary sections in Spiti Valley.

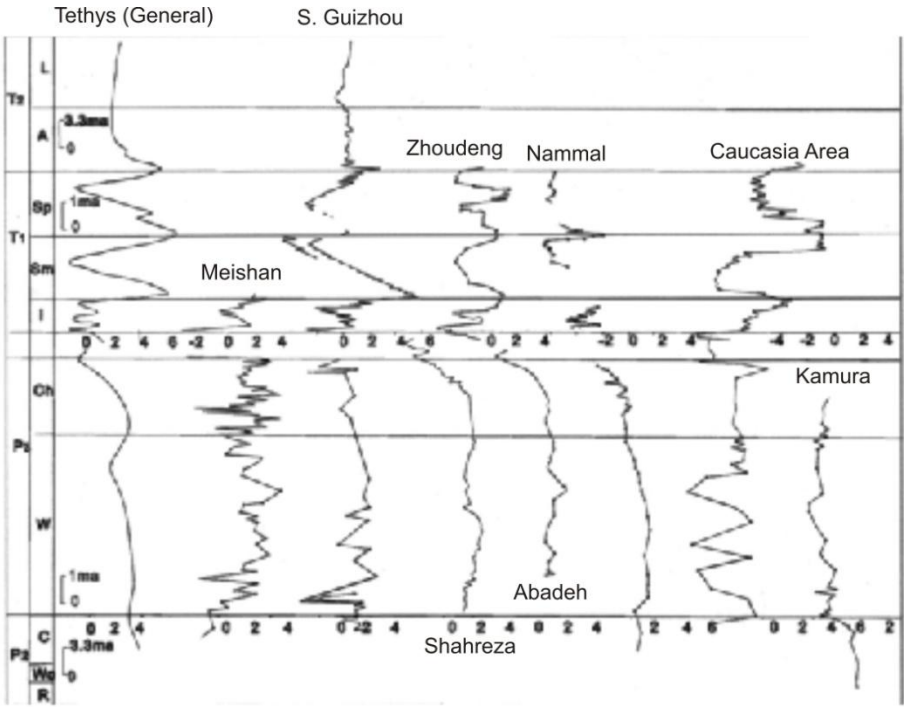

Figure 1.5. From (Yin et al., 2007 and references therein). The $\delta^{13}C$ stratigraphic profiles of the Tethys, Meishan, S. Guizhou, Zhuodeng, Chaohu, Wenjiangsi, Caucasia area, Abadeh, Shahreza, Nammal, and Kamura.

1.5. Wide-spread Anoxia

One of the widely accepted theories explaining the end Permian extinction is global ocean anoxia. Evidence for wide-spread anoxia include facies changes within the PTB sections such as increased deposition of black shales, formation of framboidal pyrite (Wignall et al., 2004) dwarfism of organisms (Brookfield et al., 2003; Yin et al., 2007), positive cerium anomaly recorded at Guryul Ravine PTB section (Algeo et al., 2007b), the change in fauna across the PTB section (loss of diversity and abundance in marine sections), and closing the paleo-Tethys. However, the cause of wide-spread anoxia remains controversial.

Anoxia is a condition where oxygen in the water is depleted to near or at 0 mg/L. Anoxia may occur in the sediment or the entire water column. In either case these conditions preclude the persistence of aerobic biota. Anoxia can be subdivided into three categories: (1) hypoxia - meaning low oxygen within the sediment or water column (< 2 mg/L), (2) suboxia - the water column is under-saturated with respect to oxygen (< 5 umol O_2 per liter water), and (3) dysoxia – the water column, including the sediment-water interface, is depleted of oxygen (0 mg/L). Under anoxic conditions, anaerobic biota persist in the sediment where they produce methane (Schubert et al., 2006). Widespread water column anoxia can be driven by an over-abundance of anaerobic bacteria in the sediment where decomposition of proteins leads to the release of hydrogen sulfide gas from sulfur bacteria (Şengör and Atayman, 2009). This reaction produces carbonic acid which enables the conversion of hydrogen sulfide to solid sulfide minerals (e.g., pyrite) under anoxic sediment-water interface conditions (Şengör and Atayman,

2009). Oxidation of HS in a suboxic or fully-oxygenated water column leads to the dissolution of carbonate minerals and precipitation of sulfates (Şengör and Atayman, 2009). Sulfate reduction at the anoxic sediment-water interface forms calcium sulfide and releases CO_2 which is then converted, in the water column, to carbonic acid which leads to further carbonate dissolution and delivery of organic matter to the sediments (Meunier and Velde, 1976). If additional carbon and sulfur are introduced into the system than oxidation can occur, thus continuing the production of CO_2 and hydrogen sulfide (Şengör and Atayman, 2009).This cycle depletes the water column of oxygen leading, ultimately, to global ocean anoxia.

In anoxic waters, the sediments will generally contain chemically reduced organic carbon, sulfur, and iron. In these conditions, deep marine sediments will be dominated by clay minerals and contain variable, but high, concentrations of organic carbon and pyrite (FeS_2). These units, referred to as shale, are variable in color. The colors red and purple suggest the presence of hematite indicating oxidizing conditions (Şengör and Atayman, 2009). In general, black shales contain up to 30% unoxidized carbon (Şengör and Atayman, 2009; Wignall, 1994). Gray-black shales contain organic carbon as well as authigenic pyrite produced *in situ* (McBride, 1974); and black or gray shales are indicators of anoxia in the rock record (Wignall, 1994). In unmetamorphosed sedimentary rocks, green shales represent the absence of hematite (oxidized Fe) and organic matter with the color imparted by the clay mineral, illite; green shales indicate sufficient oxygen at the time of deposition (Şengör and Atayman, 2009). Green shales are thought to represent suboxic conditions. This criteria cannot be applied to

metamorphosed shales where chlorite is present (Şengör and Atayman, 2009) due to the fact that chloritization produces a green color in shales. Therefore the lowest metamorphic grade (greenschist facies) color is a poor indicator of original depositional conditions. Sediment composition can also be impacted by modern weathering. Organic carbon can be oxidized upon exposure or leached from sediments. Pyrite can similarly be oxidized to form hematite and/or limonite.

High abundance of framboidal pyrite at the PTB provides support for the contention that the end Permian ocean was anoxic. Framboidal pyrite is a common diagenetic phase in many shales; they are abundant in strata deposited under low oxygen conditions (Raiswell and Berner, 1985). Though it is not established how framboids form it is clear that they form under weakly reducing conditions immediately above the sulfidic zone developed within marine sediments (Wignall et al., 2004). At this level (depth will vary depending on extent of anoxia), ferrous iron and hydrogen sulfide react rapidly to produce abundant iron monosulfide microcysts (Wignall et al., 2004). The iron monosulfide microcysts compress into spheres and form greigite (Fe_3S_4) due to the magnetic properties of the iron monosulfide microcysts. In order for greigite to form, partially oxidized sulfur species must be present; therefore the framboid formation occurs within the redox boundary (Canfield and Thamdrup, 1994; Wilkin and Barnes, 1997). Greigite is converted to pyrite during early diagenesis (Wignall et al., 2004). For that reason, pyrite framboid formation occurs within the surface layers of sediments beneath dysoxic bottom waters where the redox boundary is located close to the sediment surface. Wignall et al. (2004) found pyrite frambroids in the Khunamuh Formation at PTB section

Guryul Ravine. Pyrite framboids are found in the silty shales and brachiopod shell beds of the lower part of Late Permian Event Horizon units (Wignall et al., 2004). The presence of framboidal pyrite in Khunamuh formation at Guryul Ravine suggests that there was a wide-spread anoxia event occurred in the Tethys during the late Permian period.

The Cerium (Ce) anomaly is, geochemically, a marker of depletion or enrichment in Ce (a lanthanide element) compared to its neighbors Lanthanum (La) and Praseodymium (Pr). A negative cerium anomaly, in rocks and sediments, occurs when Ce is depleted and positive when Ce is enriched. Ce has two redox states, III and IV. Unlike other lanthanide elements, which are trivalent (except Eu which can be divalent), Ce^{3+} can be oxidized to Ce^{4+} under alkaline conditions. Ce (IV) is insoluble and, under oxidizing conditions, is precipitated as CeO_2. Sediments deposited under oxic or anoxic conditions can preserve on the long term the geochemical signature of Ce^{3+} or Ce^{4+} though this signature can be altered, post-depositionally, by late diagenesis and metamorphism. Positive cerium anomalies indicate anoxia in the water column enhancing Ce (III) concentrations in the sediment (Kato et al., 2002; Sholkovitz et al., 1994). Negative Ce anomalies suggest suboxic conditions wherein aqueous Ce(III) is depleted (Kakuwa and Matsumoto, 2006).

Algeo et al. (2007b) observed positive Ce anomalies in the end-Permian sediments of Guryul Ravine supporting the contention that there were two episodes of anoxia. The first 2 positive Ce anomalies straddle the Late Permian Event Horizon (LPEH) and are separated by 30 cm. Algeo et al. (2007) suggest that this represents

pulses of a single anoxic event associated with the end-Permian biotic crisis. A third positive Ce anomaly, also spanning the LPEH may indicate a separate event (Algeo et al., 2007b). The relation between anoxia and the PTB is not unique to Guryul Ravine and is seen in sections across southern China and Vietnam (Grice et al., 2005; Xie et al., 2006). Wignall et al. (2004) inferred diachronous onset of anoxia from the records of the late Griesbachian of northern India, Tibet, and western Canada. They base their conclusions on an assumption that anoxia was not as a causal factor in the end-Permian mass extinction but rather a coincidental contributor.

Wide-spread anoxia is also supported by the record of tectonism at the time. The formation of the Cathyasian Bridge (Şengör & Atayman, 2009) is proposed as the cause of wide-spread anoxia, resulting in the isolation of the paleo-Tethys from the Panthalassa Ocean. According to Şengör and Atayman (2009) some suggest that the formation of the Cathyasian Bridge, the closing of the paleo-Tethys, the isolation of the Panthalassa, and the opening of the Neo-Tethys all contributed to the depletion in the abundance and diversity of organisms in the Paleo-Tethys. At the time in the late Permian, the Paleo-Tethys was shallow, with bearing physical conditions similar to an epicontental sea. Once the Cathyasian Bridge formed, Paleo-Tethys was no longer significantly influenced by physical, chemical, or biological interactions with the Panthalassa Ocean. At the same time, Neo-Tethys began to open, leading to a closing of Paleo-Tethys similar to the present day situation Caspian Sea (Şengör and Atayman, 2009). Eventually, the isolation and closure led to a shut-down of circulation in Paleo-Tethys and the biological pump.

1.6. Atmospheric O_2 Drawdown

There is little debate that the end-Permian extinction was accompanied by, if not caused by, global ocean anoxia. Prior to the extinction, ocean oxygen levels in the Phanerzoic were at an all time high (Berner, 2005). The abundance of oxygen in the atmosphere led to high diversity and abundance of vascular plant flora which were at their maximum in the Carboniferous (~360 mya) (Berner et al., 2007; Raymond et al., 1985; Rowley et al., 1985). Thus, the peak of oxygen abundace in the atmosphere occurred at a time of continental assemblage which decreased aridification of the world's climate leading to an increase in plant diversity. However, a decline in total abundance of oxygen occurred in the late Carboniferous through the early Permain (Berner et al., 2007; Rowley et al., 1985; Willis and McElwain, 2002). Orogenic events which accompanied the formation of Pangea (e.g.,Huastecan, Appalachian, Hercynian, Uralian, Altaid, and New England) led to rapid loss of long stretches of subduction zones which resulted in diminshed volcanic activity, and contributing globally to the reduction of atmospheric CO_2 (Beerling and Berner, 2005). With the continuing of the formation of Pangea, aridity increased resulting in the diminished oxygen production. The geologic record of this time (Carboniferous) is marked by abundant red beds and coal with these units recording the increased draw down of CO_2 and O_2 (Berner, 2005). So much gas consumption, occuring in a short period of time (~ 20 Ma) led to decline of atmospheric O_2 to a low of 15%. This precipitous decline in O_2, coincident with the end Permian extinction (255 to 242 mya) had significant evolutionary consequences of organism (Berner, 2005).

1.7. Sea-Level Change

Sea level change, both regression and transgression, in the Tethys and the Panthalassa Ocean has been invoked as a contributing factor to the End Permian extinction. Yin et al. (2007) suggest, based on the stratigraphic record of the Dongspan China section, that regression occurred during the end-Permian extinction. This supposition is based on a suite of radiolarian (*Albailellaria*, *Latentifistularia*, *Entactinaria*, and *Spumellaria*) that are considered bathyal and indicative of water depths > 200m (Catalano et al., 1991; Yin et al., 2007). Transition to these shallow water fauna towards the end Permian suggests a regression event. Marine regression is also supported by the presence of terrigenous clasts and replacement of deep water fauna by shallow water agglutinated tests and ostracods (Yin et al., 2007).

In other sections a transgression is recorded. Brookfield et al. (2003) suggest a basin-wide transgression marked by an unconformity and subsidence phase. The subsidence phase is marked by Upper Permian marine deposits overlying all underlying structures including earlier Permian rift basalts (Gaetani and Garzanti, 1991a; Garzanti et al., 1998). Evidence of sea-level rise during the late Permian is found in the lowest Khunamuh Formation (Guryul Ravine). In the Khunamuh Formation there is a decrease in thickness and abundance of storm beds up section, and a general decrease in grain size (Brookfield et al., 2003; Kapoor, 2004). Faunal and lithological change in several sections also suggests that marine transgression occurred. At Guryul Ravine there is a depletion of diversity in the benthic community; the depletion in diversity results in the appearance of *Hindeodus parvus*, other nektonic ammonoids, and other Triassic taxa

(Brookfield et al., 2003). Hallam and Wignall (1997) observed a similar change in fauna other PTB sections worldwide. Marine transgression had a minor, if any, role in the end-Permian extinction (Brookfield et al., 2003). This is due to the fact that some PTB sections that recorded marine transgression (e.g. Guryul Ravine) were probably isolated events. Marine transgression coincides with, and probably caused the spread of oxygen-poor bottom waters over well oxygenated shallow shelves (Wignall and Hallam, 1996). The loss of benthic diversity and abundance that marks the end-Permian extinction is recorded, in the rock record, in the deposition of shell beds. The existence of these shell beds is controlled by water depth; as sea level rises through the basal Khunamuh Formation the shell beds eventually disappear (Brookfield et al., 2003). Therefore, the final loss in benthic diversity is directly related to the loss of habitat which is attributable to sea-level rise. Many "transgression" researchers believe the end Permian extinction to be gradual. The transgressive period led to the spread of low O_2 waters onto the shallow shelf which further impacted the species abundance and diversity (Brookfield, 1993; Wignall et al., 2004).

1.8. Bolide Impact

One of the most controversial scenarios for the cause of the end Permian extinction is extraterrestrial (bolide) impact. The bolide theory is inspired by the clear causative link between the Yucatan impact event and the late Cretaceous extinction. Several researchers have suggested a similar cause for the end Permian with the bolide being larger than that of the late Cretaceous. Evidence for a bolide impact at the time

include chondritic meteorite fragments in the Antarctic terrestrial end Permian strata (Basu et al., 2003), shocked quartz in the Antarctic terrestrial end Permian strata (Retallack et al., 1998), a suspect impact crater found offshore of northwestern Australia (Becker et al., 2004), positive Europium anomaly in the Spiti Valley PT section at Lalung (Bhandari et al., 1992), and the presence of a ferruginous layer in all Spiti Valley sections (Shukla et al., 2002b).

Chondritic meteorite fragments found in the terrestrial Graphite Peak PTB section in Antarctica supports the bolide impact theory (Basu et al., 2003). Basu et al. (2003) found magnetic fragments 0.8 m below the PTB in Antarctica. The fragments were comprised of Fe oxides and hydroxides only and lacked significant concentrations of Ni, S, and P (Basu et al., 2003). The fragments contained a number silicate rich particles displaying identical poikilitic and granular texture (Basu et al., 2003). Additionally, the fragments contained small euhedral and subhedral forsterite (olivine) grains enclosed in larger grains of clinoenstatite; these grains have chemical composition of low FeO and relatively high Mn/Fe ratios (Basu et al., 2003). Basu et al. (2003) state that the chemical composition of forsterite and clinoenstatite is distinct from other terrestrial olivines and pyroxenes; the fosterite contains high concentration of CaO and Cr_2O_3. Therefore, the authors concluded that these fragments are of extraterrestrial origin and the presence of high CaO and Cr_2O_3 concentrations imply that the bolide was a chondritic meteorite (Basu et al., 2003).

Retallack et al. (1998) investigated evidence of a bolide impact by focusing on terrestrial claystone breccias, shocked quartz, and iridium anomalies for terrestrial PTB

sections in Graphite Peak and Mount Crean Antarctica, and Wybung Head, Australia. They noted that the claystone breccias have been thoroughly leached of alkalis and alkaline earths compared to clastics in the underlying coals. The claystone breccias at Wynbung Head were leached to the same extent as Cretaceous-Tertiary boundary (KTB) sediments. No evidence of leaching was found in the claystone breccias of Antarctica (Retallack et al., 1998). Based on the differences in leaching of claystone breccias, the rare shocked quartz and iridium anomalies found in these sections were not considered primary deposition from direct impact fallout. Retallack et al. (Retallack et al., 1998) suggested redeposition from local soils as a source.

Shocked quartz is a form of quartz that has a different microscopic structure than regular quartz. It is formed under intense pressure; this causes the crystalline structure of quartz to be deformed along planes inside the crystal. Shoemaker (1959) noted that shocked quartz is found inside craters created by bolide impacts. Retallack et al. (1998) did not find any shocked quartz below the PTB. The shocked quartz found at the three PT-boundaries were smaller and less abundant than the shocked quartz at the KTB and late Precambrian (Retallack et al., 1998). But the authors noted that the shock quartz found at the three PTB sections were within the size range and abundance reported at the Cretaceous Tertiary boundary (KTB) (Izett, 1990), late Devonian (Warmer and Sandberg, 1996), late Triassic (Bice et al., 1992), and late Jurassic (Dyer et al., 1989). The planar deformation of the PT shocked quartz is comparable to that of the KTB and numerous other impact craters. Retallack et al. (1998) also looked for anomalously high concentrations of iridium (Ir) which marked the KTB. They found a positive Ir anomaly

at Mount Crean, but there was no significant positive Ir anomaly at Wybung Head and Graphite Peak. The Graphite Peak and Wybung Head Ir anomalies were similar to the Ir anomalies found in PTB sections in Italy, Austria, Armenia, India, and China. Since there is a lack of a positive Ir anomaly at several terrestrial and marine PTB sections; Retallack et al. (1998) suggested that Ir anomalies can be weakened by leaching through strong acids that are generated during the impact shocking of the atmosphere. Iridium anomalies can also be caused by microbial activity (Dyer et al., 1989). Retallack et al. (1998) proposed that microbial activity is an appealing explanation for peak Ir values at the base rather than the top of the Graphite Peak and Wybung Head sections. The base is characterized by abundant coal deposits which are suggestive of high microbial activity in the soils that once supported the flora.

Becker et al. (2004) suggested that a bolide impact crater of appropriate age exists, off shore, in northwestern Australia known as Bedout High. Becker et al. (2004) suggest that the large impact crater-like structure at Bedout is consistent with the global distribution of impact ejecta in the PTB, and the maximum grain sizes of shocked quartz matches the maximum sizes of shocked quartz at the KTB. Additionally, the Bedout shocked quartz is consistent with the size of the shocked quartz found at terrestrial PTB sections in Antarctica and Australia. Becker et al. (2004) suggest that shocked quartz is not present in other PTB sections because of stratospheric winds and the settling of particles was similar to that of the KTB. Such a dispersal of mechanism is not efficient for latitudinal transport of debris, therefore an impact at Bedout would disperse shocked quartz over the Southern Hemisphere particularly Australia and Antarctica (Becker et al.,

2004). Lastly, the bolide impact could have acted as a trigger for massive continental volcanism coincident with the end Permian extinction. Ar-Ar dating of continental flood basalts at Deccan and Siberia show contemporaneous ages for the volcanism and the extinction associated with them. In the case of the Deccan traps the basalts are contemporaneous with the impact of the KTB. The coincidence of the Siberian traps and end-Permian extinction and the proposed Bedout impact are causatively linked by Becker et al. (2004) such that the impact event enhanced the eruption of a pre-existing plume.

Others proposed evidence of a eucritic meteorite was the cause of the end Permian extinction due to the positive europium (Eu) anomaly and the ferruginous layer found at some of the PTB sections. Bhandari et al. (1992) found a positive Eu anomaly at the Lalung PTB section in Spiti Valley. They proposed that the positive Eu anomaly could be attributed to an extraterrestrial body or volcanism. They suggest that a eucritic meteorite was responsible for the end Permian extinction. Eucritic meteorites have positive Eu anomaly and are low in Ir, because their parent magma is believed to be enriched in europium, this would explain the low Ir anomaly and positive Eu anomaly found at several PTB sections (Bhandari et al., 1992). Therefore, these authors suggest that a eucritic meteorite maybe responsible for the end Permian extinction. Also invoked as evidence of a meteorite is the ferruginous layer found in PTB sections of Spiti Valley, India. The formation of the ferruginous layer could be evidence of strong regression at the end Permian and the layer is thought by some to contain extraneous material and dominated by allogenic minerals (Shukla et al., 2002b).

1.9. Continental Volcanism

Volcanism is another mechanism that contributed, to some extent, to the end Permian extinction. The hypothesis is that the Siberian Traps erupted in a sequence over a very short period of time (~1 Ma). According to Renne et al. (1995) continental Siberian flood volcanism produced an episodic outpouring of basaltic magma, whose volume and eruption rate led to the emplacement of up to 3 million km^3 over 1Ma. This eruption was significantly larger than any volcanism in any other geological settings. The hypothesis state that the eruption led to global cooling caused by sulfate aerosol accumulation and acid production resulting from reduction and coalescence of sulfates (Renne et al., 1995). Many supporters of continental volcanism suggest that the positive Eu anomaly is indicative of flood volcanism eruption.

1.10. Methane Release

The end Permian extinction was caused by catastrophic release of methane (Şengör and Atayman, 2009). Methane gas is produced as a result of decomposition under anoxic conditions (Schubert et al., 2006). Three critical gases (CO_2, HS, and CH_4) accumulate in massive quantities under anoxic conditions. Over time and under anoxic water column conditions the water temperature increases leading to density inversion and ultimately release of gas to the surface ocean and atmosphere (Şengör and Atayman, 2009). Schubert et al. (2006) showed that methanogensis in the water column in the anoxic water column is negligible. The sediments from the Black Sea are sinks for methane in the water column, in contrast to the claim of (Reeburgh et al., 1991). Thus,

the major contributions of methane must come from seeps and mud volcanoes (Schubert et al., 2006).

1.11. Multi-Episode Extinction

Many geologists and paleontologists agree that the end-Permian extinction was caused by multiple events. Yin et al. (2007) suggest that there were multi-events that occurred before the end-Permian extinction. Evidence for multi-episodes can be seen in the $\delta^{13}C$ stratigraphic profile of PTB sections; these sections have more than one negative $\delta^{13}C$ excursion in the stratigraphic section (Figure 1.5). The Meishan PTB section provides strong evidence of multiple events; biomarkers such as 2-methylhopane, Pr/Ph, $\gamma C_{31}HP$, and Ts/Tm^{1}, vary in association with anoxic conditions which coincide $\delta^{13}C$ values (Yin et al., 2007). The first "event" impacts the corals, fusulinids, ammonoids, deep water radiolarians, and brachiopods (Yin et al., 2007). Yin et al. (2007) note the miniaturization of marine invertebrates signifies the presence of environmental stress such as degradation of habitats, which could have serve as a prelude to the mass extinction. Yin et al. (2007) state that these ecological changes at the PTB were induced by a major change in the carbonate system and represent a prelude to the mass extinction. Which suggest that two extinction episodes occurred in deep-water environments, after the first extinction, the mass extinction was caused by one or more events including those discussed previously in this chapter.

1.12. Geochemical Proxies for Evaluation of Post-Depositional Alteration

The geochemical study of ancient marine sediments poses problems, due to the different source compositions as well as to weathering history, hydraulic sorting, and diagenesis. These processes complicate the original signal by controlling the abundances of major and trace elements (Abanda and Hannigan, 2006; Condie, 1993).

1.12.1. Modern Weathering

Weathering indices are widely used in studies of both modern and ancient *in situ* weathering profiles. A useful chemical weathering index should provide values that do more than simply vary relative to one another on a given weathering profile. The most commonly applied, in ancient marine sediments, in the Chemical Index of Alteration (CIA) (Nesbitt and Young, 1982). CIA assesses the extent of weathering on siliciclastic material. The CIA is calculated as (100) [Al_2O_3/ (Al_2O_3 + CaO* +Na_2O+K_2O)] using molar proportions and only that portion of CaO associated with silicate minerals. Samples are considered fresh if the CIA is less than or equal to 50, weathered if the value reaches 100. Upward trends in increasing CIA reflect an increase in weathering. CIA does not allow for mobility of Al_2O_3. In sediments such as the Gungri Shale the CIA measures the degree of weathering of feldspars, relative to unweathered protoliths (Nesbitt and Young, 1982). Values for unweathered plagioclase and K-feldspars are approximately equal to 50, as are values of unweathered upper crustal rocks. Higher CIA values represent higher degrees of weathering, however low CIA values may suggest arid or cool conditions (Fedo et al. 1995). CIA can be applied to marly limestones such as

the Mikin however care must be taken in interpreting the values since none of the CaO is associated with silicate minerals and alkali-alkali earth content is minimal which may skew the CIAs towards higher than true values. Another issue is that, in the case of the ferruginous layer, iron content is very high and CIA does not account for iron mobility meaning that the calculated CIA may underestimate the degree of weathering of those samples. Therefore when looking at a sequence of rocks such as at Attargoo, it is probably most appropriate to use the CIA values of the shales as a proxy for weathering of the entire section.

1.12.2. Diagenesis/Metamorphism

The PT sequence at Attargoo is complicated by having shale, an iron rich ferruginous layer, and limestone which have undergone not only modern weathering but also diagenesis and, potentially, metamorphism (chloritization) (Algeo et al., 2007c). Chemical Index of Alteration is insufficient for evaluating post-depositional alteration such as metamorphism and diagenesis. Growing concerns regarding potassium metasomatism in shale (Condie, 1993) point to the complex processes involved in chemical weathering *in situ* (production of clay minerals), mechanical breakdown, and continued chemical alteration during transport, burial, and diagenesis.

The chemical compositions of sedimentary rocks can be plotted as molar proportions within Al_2O_3, CaO* (CaO associated with silicates) + Na_2O, and K_2O (A-CN-K) compositional space, where CaO* represents Ca in silicate-bearing minerals only (Figure 1.6). The A-CN-K system is useful for evaluating fresh rock compositions

and examining their weathering trends because the upper crust is dominated by plagioclase- and K-feldspar–rich rocks (Nesbitt and Young, 1984, 1989) and their weathering products, the clay minerals. Average Paleoproterozoic shale and its probable source composition, average Upper Archean upper crust, are plotted in Figure 1A. The weathering trend for Upper Archean crust, predicted from kinetic leach rates (Nesbitt and Young, 1984; Nesbitt, 1992), is also plotted in Figure 1.6 (arrow b). The accumulated weathering products of Upper Archean crust, as represented by average Paleoproterozoic shale, should plot on this trend, but instead plot well below it; the average shale contains considerably more K_2O than expected and therefore has undergone K metasomatism (Nesbitt, 1992). As shown in Figure I.6 different amounts of K_2O can be added during metasomatism to all three "types" of samples. Variable degrees of diagenesis/metamorphism will lead to K enrichment. Addition of K_2O to aluminous clays follows a path towards the K_2O apex of the triangle. It is useful also to note that the position of samples on the A-CN-K can also be used to establish changes in provenance in that if the source of sediment did not change during the deposition of the sequence all samples will plot together following a single trend if impacted by metamorphism.

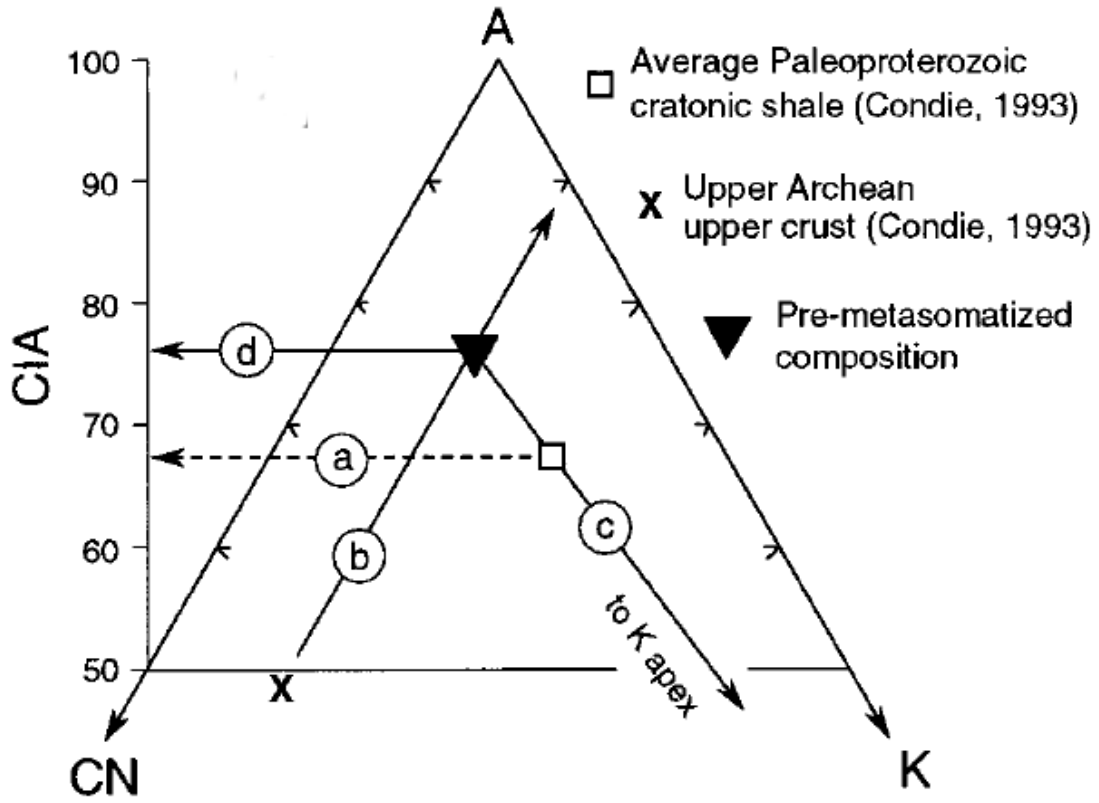

Figure I-6. From (Fedo et al., 1995). Average shale and continental crust plotted as molar proportions Effect of K metasomatism (metamorphism) on weathered residue of Archean crust to produce average Paleoproterozoic shale. Dashed arrow a shows chemical index of alteration (CIA) of shale; arrow b, predicted weathering trend of Archean crust; arrow c, addition of K to weathered residues; arrow d, CIA of weathered residues (before metasomatism).

1.13. Summary

The goal of this research is to ultimately assess the paleoenvironmental conditions that typify the Neo-Tethys across the PT Boundary. As previously discussed many of the hypotheses regarding the cause(s) of the end-Permian extinction rely on multiple proxies including geochemical signatures. All too often the geologic record of the PTB has been impacted by diagenetic, metamorphic and weathering events. The ability to use geochemical proxies to reconstruct paleoenvironments requires that the relative over-print of each process be identified and the extent of alteration known. The goal of this thesis is to geochemically explore the extent of weathering and the impact of modern weathering on the geochemistry Attargoo PTB section. If this section has been geochemically altered such that no record of original composition is present, then it will not be possible to use this section to reconstruct the paleoenvironment or to inform our understanding of the mechanisms/processes that might have been operating at the time of the extinction.

Reference List

Abanda, P.A., and Hannigan, R., 2006, Diagenetic controls of trace element partitioning in shales: Chemical Geology, v. 230, p. 42-59.

Algeo, T.J., Ellwood, B., Nguyen, T.K.T., Rowe, H., and Maynard, J.B., 2007a, The Permian-Triassic boundary at Nhi Tao, Vietnam: Evidence for recurrent influx of sulfidic water masses to a shallow-marine carbonate platform: Palaeogeography, Palaeoclimatology, Palaeoecology, v. 252, p. 304-327.

Algeo, T.J., Hannigan, R., Rowe, H., Brookfield, M., Baud, A., and Krystyn, L., 2007b, Sequencing events across the Permian-Triassic boundary, Guryul Ravine (Kashmir, India): Palaeogeography Palaeoclimatology Palaeoecology, v. 252, p. 328-346.

Algeo, T.J., Hannigan, R., Rowe, H., Brookfield, M., Baud, A., Krystyn, L., and Ellwood, B.B., 2007c, Sequencing events across the Permian-Triassic boundary, Guryul Ravine (Kashmir, India): Palaeogeography, Palaeoclimatology, Palaeoecology, v. 252, p. 328-346.

Bassoullet, J.P., Colchen, M., Juteau, T., Marcoux, J., Mascle, G., and Reibel, F., 1983, Geological studies in the Indus suture zone of Ladakh (Himalayas), *in* Gupta, V.J., ed., Stratigraphy and structure of Kashmir and Ladakh Himalaya: Contributions to Himalayan Geology, Volume 2: India, HPC Publishers, p. 96-124.

Basu, A.R., Petaev, M.I., Poreda, R.J., Jacobsen, S.B., and Becker, L., 2003, Chondritic meteorite fragments associated with the Permian-Triassic boundary in Antarctica: Science, v. 302, p. 1388-1392.

Baud, A., Atudorei, V., and Sharp, Z., 1996, Late Permian and early Triassic evolution of the Northern Indian margin: Carbon isotope and sequence stratigraphy: Geodinamica Acta, v. 9, p. 57-77.

Baud, A., Magaritz, M., and Holser, W.T., 1989, Permian-Triassic of the Tethys: Carbon isotope studies: International Journal of Earth Sciences, v. 78, p. 649-677.

Becker, L., Poreda, R.J., Basu, A.R., Pope, K.O., Harrison, T.M., Nicholson, C., and Iasky, R., 2004, Bedout: A possible end-Permian impact crater offshore of Northwestern Australia: Science, v. 304, p. 1469-1476.

Beerling, D.J., and Berner, R.A., 2005, Feedbacks and the coevolution of plants and atmospheric CO2: Proceedings of the National Academy of Sciences of the United States of America, v. 102, p. 1302-1305.

Berner, R.A., 2005, The carbon and sulfur cycles and atmospheric oxygen from middle Permian to middle Triassic: Geochimica Et Cosmochimica Acta, v. 69, p. 3211-3217.

Berner, R.A., VandenBrooks, J.M., and Ward, P.D., 2007, Evolution - Oxygen and evolution: Science, v. 316, p. 557-558.

Bhandari, N., Shukla, P.N., and Azmi, R.J., 1992, POSITIVE EUROPIUM ANOMALY AT THE PERMO-TRIASSIC BOUNDARY, SPITI, INDIA: Geophysical Research Letters, v. 19, p. 1531-1534.

Bhargava, O.N., 1987, Stratigraphy, microfacies and paleoenvironment of the Lilang group (Scythian-Dogger), Spiti Valley, Himachal Himalaya, India: Journal of the Palaeontological Society of India, v. 25, p. 91-107.

Bhargava, O.N., Krystyn, L., Balini, M., Lein, R., and Nicora, A., 2004, Revised litho- and seq
uence stratigraphy of the Spiti Triassic: Albertiana, v. 30, p. 21-39.

Bhargava, O.N., Srivastava, R.N., and Gadhoke, S.K., 1985, *Zoophycos* from the Permian Gungri Member (Kuling Formation), Spiti Valley, Himachal Himalaya: Journal of the Geological Society of India, v. 26, p. 137-140.

Bhatt, D.K., Fuchs, G., Prashara, K.C., Krysten, L., Arora, R.K., and Golebiowski, R., 1981, Conodonts of Otoceras beds of Spiti: Journal of the Palaeontological Society of India, v. 25, p. 130-134.

Bice, D.M., Newton, C.R., McCauley, S., Reiners, P.W., and McRoberts, C.A., 1992, SHOCKED QUARTZ AT THE TRIASSIC-JURASSIC BOUNDARY IN ITALY: Science, v. 255, p. 443-446.

Brookfield, M.E., 1993, THE HIMALAYAN PASSIVE MARGIN FROM PRECAMBRIAN TO CRETACEOUS TIMES: Sedimentary Geology, v. 84, p. 1-35.

Brookfield, M.E., Twitchett, R.J., and Goodings, C., 2003, Palaeoenvironments of the Permian-Triassic transition sections in Kashmir, India: Palaeogeography Palaeoclimatology Palaeoecology, v. 198, p. 353-371.

Canfield, D.E., and Thamdrup, B., 1994, THE PRODUCTION OF S-34-DEPLETED SULFIDE DURING BACTERIAL DISPROPORTIONATION OF ELEMENTAL SULFUR: Science, v. 266, p. 1973-1975.

Catalano, R., Distefano, P., and Kozur, H., 1991, PERMIAN CIRCUMPACIFIC DEEP-WATER FAUNAS FROM THE WESTERN TETHYS (SICILY, ITALY) - NEW EVIDENCES FOR THE POSITION OF THE PERMIAN TETHYS: Palaeogeography Palaeoclimatology Palaeoecology, v. 87, p. 75-108.

Condie, K.C., 1993, Chemical-composition and evolution of the upper continental crust - contrasting results from surface samples and shales: Chemical Geology, v. 104, p. 1-37.

Corsetti, F.A., Baud, A., Marenco, P.J., and Richoz, S., 2005, Summary of Early Triassic carbon isotope records: Comptes Rendus Palevol, v. 4, p. 473-486.

Diener, C., 1897, Himalayan fossils. The Cephalopoda of the Lower Trias: Palaeontologia Indica, (ser.15), v. 2, p. 1-191.

Diener, C., 1908, Ladinic, Carnic and Noric faunae of Spiti: Palaeontologia Indica, (ser.15), v. 5, p. 1-157.

Diener, C., 1912, The Trias of the Himalayas: Memoirs of the Geological Survey of India, v. 36, p. 202-367.

Dyer, B.D., Lyalikova, N.N., Murray, D., Doyle, M., Kolesov, G.M., and Krumbein, W.E., 1989, ROLE FOR MICROORGANISMS IN THE FORMATION OF IRIDIUM ANOMALIES: Geology, v. 17, p. 1036-1039.

Erwin, D.H., 1994, THE PERMO-TRIASSIC EXTINCTION: Nature, v. 367, p. 231-236.

Farley, K.A., and Mukhopadhyay, S., 2001, An extraterrestrial impact at the Permian-Triassic boundary?: Science, v. 293, p. 2343-+.

Fedo, C.M., Wayne Nesbitt, H., and Young, G.M., 1995, Unraveling the effects of potassium metasomatism in sedimentary rocks and paleosols, with implications for paleoweathering conditions and provenance: Geology, v. 23, p. 921-924.

Gaetani, M., and Garzanti, E., 1991a, MULTICYCLIC HISTORY OF THE NORTHERN INDIA CONTINENTAL-MARGIN (NORTHWESTERN HIMALAYA): Aapg Bulletin-American Association of Petroleum Geologists, v. 75, p. 1427-1446.

Gaetani, M., and Garzanti, E., 1991b, Multicyclic history of the northern India continental margin (Northwestern Himalaya): American Association of Petroleum Geologists Bulletin, v. 75, p. 1427-1446.

Gardner, L.R., 1992, Long-term isovolumetric leaching of aluminum from rocks during weathering: Implications for the genesis of saprolite: CATENA, v. 19, p. 521-537.

Garzanti, E., 1993a, Himalayan ironstones, "superplumes," and the breakup of Gondwana: Geology, v. 21, p. 105-108.

Garzanti, E., 1993b, Sedimentary evolution and drowning of a passive margin shelf (Giumal Group; Zanskar Tethys Himalaya, India): palaeoenvironmental changes during final break-up of Gondwanaland: Geological Society, London, Special Publications, v. 74, p. 277-298.

Garzanti, E., Angiolini, L., and Sciunnach, D., 1996, The Permian Kuling Group (Spiti, Lahaul and Zanskar; NW Himalaya): sedimentary evolution during rift/drift transition and initial opening of Neo-Tethys: Rivista Italiana di Paleontologia e Stratigrafia, v. 102, p. 175-200.

Garzanti, E., Jadoul, F., Nicora, A., and Berra, F., 1995, Triassic of Spiti (Tethys Himalaya; N. India): Rivista Italiana di Paleontologia e Stratigrafia, v. 101, p. 267-300.

Garzanti, E., Nicora, A., and Rettori, R., 1998, Permo-Triassic boundary and lower to middle Triassic in South Tibet: Journal of Asian Earth Sciences, v. 16, p. 143-157.

Ghosh, P., Bhattacharya, S.K., Shukla, A.D., Shukla, P.N., Bhandari, N., Parthasarathy, G., and Kunwar, A.C., 2002, Negative delta C-13 excursion and anoxia at the Permo-Triassic boundary in the Tethys Sea: Current Science, v. 83, p. 498-502.

Grice, K., Cao, C.Q., Love, G.D., Bottcher, M.E., Twitchett, R.J., Grosjean, E., Summons, R.E., Turgeon, S.C., Dunning, W., and Jin, Y.G., 2005, Photic zone euxinia during the Permian-Triassic superanoxic event: Science, v. 307, p. 706-709.

Haas, J., Demeny, A., Hips, K., Zajzon, N., Weiszbury, T.G., and Sundar, M., 2007 Biotic and environmental changes in the Permian-Triassic boundaryinterval recorded on a western Tethyan ramp in the Bukk Mountains, Hungary: Global and Planetary Change, v. 55, p. 136-154

Hallam, A., and Wignall, P.B., 1997, Mass Extinction and their aftermath: Oxford University Press, New York.

Hayden, H.H., 1904, The geology of Spiti with parts of Bashahr and Rupshu: Memoirs of the Geological Survey of India, v. 36, p. 1-129.

Hongfu, Y., Dickins, J.M., Shi, G.R., and T.Jinnan, 2000, Permian-Triassic Evolution of Tethys and Western Circum-Pacific, Developments in Palaeontology and Stratigraphy: Amsterdam, Elsevier, p. 412.

Isozaki, Y., Kawahata, H., and Ota, A., 2007, A unique carbon isotope recordacross the Guadalupian-Lopingian (Middle-Upper Permian) boundary in the mid-oceanic paleo-atoll carbonates: The high productivity "Kamura event: and its collapse in Panthalassa.: Global and Planetary Change, v. 55, p. 21-38.

Izett, G.A., 1990, The Cretaceous-Tertiary (KT) boundary interval, Raton Basin Colorado and New Mexico, and its content of minerals: Evidence relevant to the Crateceous-Tertiary impact extinction hypothesis: Geological Society of America Special Papers, v. 249, p. 100.

Jin, Y.G., Wang, Y., Wang, W., Shang, Q.H., Cao, C.Q., and Erwin, D.H., 2000, Pattern of marine mass extinction near the Permian-Triassic boundary in South China: Science, v. 289, p. 432-436.

Kakuwa, Y., and Matsumoto, R., 2006, Cerium negative anomaly just before the Permian and Triassic boundary event - The upward expansion of anoxia in the water column: Palaeogeography Palaeoclimatology Palaeoecology, v. 229, p. 335-344.

Kapoor, H.M., 2004, Permo-Triassic of the Indian subcontinent and its intercontinental correlation In: Sweet, W.C., Yang, Z., Dickens, J.M., Yin, H. (Eds.), 2004. Permo-Triassic Events in the Eastern Tethys. Stratigraphy, Classification and Relations with the Western Tethys.: Cambridge University Press, Cambridge.

Kato, Y., Nakao, K., and Isozaki, Y., 2002, Geochemistry of Late Permian to Early Triassic pelagic cherts from southwest Japan: implications for an oceanic redox change: Chemical Geology, v. 182, p. 15-34.

Korte, C., Kozur, H., and Mohtat-Aghai, P., 2004a, Dzhulfian tolowermost Triassic d13C record at the Permian/Triassic section at Shahreza, Central, Iran In: Yin, H., Feng, Q., Lai, X., Baud, A., Tong, J (Eds). 2007. The protracted Perno-Triassic crisisand multi-episode extinction around the Permian-Triassic boundary. Global

and Planetary Change 55, 1-20: Hallesches Jahrbuch der Geowissenchaften, B, v. 18, p. 73-78.

Korte, C., and Kozur, H.W., 2010, Carbon-isotope stratigraphy across the Permian-Triassic boundary: A review: Journal of Asian Earth Sciences, v. 39, p. 215-235.

Korte, C., Kozur, H.W., Joachimski, M.M., Strauss, H., Veizer, J., and Schwark, L., 2004b, Carbon, sulfur, oxygen,and strontium isotope records, organic geochemistry and biostratigraphy across the Permian /Triassic boundary in Abadeh, Iran In: Yin, H., Feng, Q., Lai, X., Baud, A., Tong, J (Eds). 2007. The protracted Perno-Triassic crisisand multi-episode extinction around the Permian-Triassic boundary. Global and Planetary Change 55, 1-20: Geological Rundschau, v. 93, p. 565-581.

Kozur, H., 2006, Biostratigraphy and event stratigraphy in Iran around the Permo-Triassic Boundary Implications forthe causes of the PTB biotic crisis In: Yin, H., Feng, Q., Lai, X., Baud, A., Tong, J (Eds). 2007. The protracted Perno-Triassic crisisand multi-episode extinction around the Permian-Triassic boundary. Global and Planetary Change 55, 1-20: Global and Planetary Change, v. 55, p. 155-176.

Krafft, A., and Diener, C., 1909, Himalayan fossils. Lower Triassic Cephalopoda from Spiti, Malla Johar, and Byans: Palaeont. Indica, (ser. 15), v. 6, p. 1-186.

Kraus, S.H., Siegert, S., Mette, W., Struck, U., and Korte, C., 2009, Stratigraphic significance of carbon isotope variations in the shallow-marine Seis/Siusi Permian-Triassic boundary section (Southern Alps, Italy): Fossil Record, v. 12, p. 197-205.

Matsuda, T., 1985, Late Permian to early Triassic conodont paleobiogeography in the "Tethys Realm", *in* Nakazawa, K., and Dickens, J.M., eds., The Tethys–Her Paleogeography and Paleobiogeography from Paleozoic to Mesozoic: Tokyo, Tokai University Press, p. 157–170.

McBride, E.F., 1974, Significance of color in red, green, olive, brown, and grey beds of Difunta Group, northeastern Mexico.: Journal of Sedimentary Petrology, v. 44, p. 760-773.

Meunier, A., and Velde, B., 1976, Mineral Reactions At Grain Contacts In Early Stages Of Granite Weathering: Clay Miner., v. 11(3), p. 235-240.

Nesbitt, H.W., and Young, G.M., 1982, Early Proterozoic climates and plate motions inferred from major element chemistry of lutites: Nature, v. 299, p. 715-717.

Payne, J.L., Lehrmann, D.J., Follett, D., Seibel, M., Kump, L.R., Riccardi, A., Altiner, D., Sano, H., and Wei, J., 2007, Erosional truncation of uppermost Permian shallow-marine carbonates and implications for Permian-Triassic boundary events: Geological Society of America Bulletin, v. 119, p. 771-784.

Payne, J.L., Lehrmann, D.J., Wei, J.Y., Orchard, M.J., Schrag, D.P., and Knoll, A.H., 2004, Large perturbations of the carbon cycle during recovery from the end-Permian extinction: Science, v. 305, p. 506-509.

Payne, J.L., Turchyn, A.V., Paytan, A., DePaolo, D.J., Lehrmann, D.J., Yu, M.Y., and Wei, J.Y., 2010, Calcium isotope constraints on the end-Permian mass extinction: Proceedings of the National Academy of Sciences of the United States of America, v. 107, p. 8543-8548.

Raiswell, R., and Berner, R.A., 1985, PYRITE FORMATION IN EUXINIC AND SEMI-EUXINIC SEDIMENTS: American Journal of Science, v. 285, p. 710-724.

Raymond, A., Parker, W.C., and Parrish, J.T., 1985, Phtyogeography and paleoclimate of the early Carboniferous in Tiffney B.H. (eds). Geological Factors and the Evolution of Plants.: New Haven, Yale University Press, p. 166-222.

Reeburgh, W.S., Ward, B.B., Whalen, S.C., Sandbeck, K.A., Kilpatrick, K.A., and Kerkhof, L.J., 1991, Black Sea methane geochemistry: Deep-Sea Res., v. 38, p. 1189–1210.

Renne, P.R., and Basu, A.R., 1991, RAPID ERUPTION OF THE SIBERIAN TRAPS FLOOD BASALTS AT THE PERMO-TRIASSIC BOUNDARY: Science, v. 253, p. 176-179.

Renne, P.R., Zhang, Z.C., Richards, M.A., Black, M.T., and Basu, A.R., 1995, SYNCHRONY AND CAUSAL RELATIONS BETWEEN PERMIAN-TRIASSIC BOUNDARY CRISES AND SIBERIAN FLOOD VOLCANISM: Science, v. 269, p. 1413-1416.

Retallack, G.J., Greaver, T., and Jahren, A.H., 2007, Return to Coalsack Bluff and the Permian-Triassic boundary in Antarctica: Global and Planetary Change, v. 55, p. 90-108.

Retallack, G.J., Seyedolali, A., Krull, E.S., Holser, W.T., Ambers, C.P., and Kyte, F.T., 1998, Search for evidence of impact at the Permian-Triassic boundary in Antarctica and Australia: Geology, v. 26, p. 979-982.

Retallack, G.J., Veevers, J.J., and Morante, R., 1996, Global coal gap between Permian-Triassic extinction and Middle Triassic recovery of peat-forming plants: Geological Society of America Bulletin, v. 108, p. 195-207.

Rowley, D.B., Raymond, A., Parrish, J.T., Lottes, A.L., Scotese, C.R., and Ziegler, A.M., 1985, CARBONIFEROUS PALEOGEOGRAPHIC, PHYTOGEOGRAPHIC, AND PALEOCLIMATIC RECONSTRUCTIONS: International Journal of Coal Geology, v. 5, p. 7-42.

Schubert, C.J., Durisch-Kaiser, E., Klauser, L., Vazquez, F., Wehrli, B., and Holzner, C.P., 2006, Recent studies in sources and sinks of methane in Black Sea, in Neretin, L.N., (eds). Past Present Water Column Anoxia: Dordrecht Springer, p. 419-441.

Şengör, A.M.C., Altmer, D., Cin, A., Utsaomer, T., and Hsu, K.J., 1988, Origin and assembly of the Tethyside orogenic collage at the expense of Gondawana Land, *in* Audley-Charles, M.G., and Hallam, A., eds., Gondawa and Tethys, Volume 37: Special Publication: Boulder, Geological Society of America, p. 119-181.

Şengör, A.M.C., and Atayman, S., 2009, The Permian Extinction and the Tethys:An Exercise in Global Geology: geological Society of America Special Papers, v. 448.

Shao, L.Y., Zhang, P.F., Duo, J.W., and Shen, S.Z., 2000, Carbon isotope compositions of the late Permian carbonate rocks in southern China: their variations between Wujiaping and Changxing formations.: Palaeogeography Palaeoclimatology Palaeoecology, v. 161, p. 179-192.

Shoemaker, E.M., 1959, Impact mechanics at Meteor crater, Arizona, U.S.: Atomic Energy Commission Open File Report.

Sholkovitz, E.R., Landing, W.M., and Lewis, B.L., 1994, OCEAN PARTICLE CHEMISTRY - THE FRACTIONATION OF RARE-EARTH ELEMENTS BETWEEN SUSPENDED PARTICLES AND SEAWATER: Geochimica Et Cosmochimica Acta, v. 58, p. 1567-1579.

Shukla, A.D., Bhandari, N., and Shukla, P.N., 2002a, Chemical signatures of the Permian-Triassic transitional environment in Spiti Valley, India, *in* Koeberl, C., and MacLeod, K.G., eds., Catastrophic Events and Mass Extinctions: Impacts and Beyond, Volume Special Paper 356: Boulder, Geological Society of America, p. 445-453.

Shukla, A.D., Bhandari, N., and Shukla, P.N., 2002b, Chemical signatures of the Permian-Triassic transitional environment in Spiti Valley, India: Geological Society of America Special Papers, v. 356, p. 445-453.

Singh, T., Tiwari, R., Vijaya, S., and Avtar, R., 1995, Stratigraphy and palynology of Carboniferous-Permian-Triassic succession in Spiti Valley, Tethys Himalaya, India: Journal of the Palaeontological Society of India, v. 40, p. 55-76.

Srikantia, S.V., and Bhargava, O.N., 1998, Geology of Himachal Pradesh: Bangalore, Geological Society of India.

Stoliczka, F., 1866, Geological section across the Himalayan Mountains, from Wangtu bridge on the River Sutlej to Sungdo on the Indus: with an account of the formations of Spiti, accompanied by a revision of all known fossils from that district: Memoirs of the Geological Survey of India, v. 5, p. 1-173.

Stutz, E., 1988, Geologie de la chaine de Mylmaling aux confins du Ladakh et du Rupshu (NW Himalaya, Inde): Evolution, paleogeographique et tectonique d' un segment de la marge nord-indienne, 149 p.

Sweet, W.C., Zunyi, Y., Dickins, J.M., and Yin, H., 1992, Permo-Triassic Events in the Eastern Tethys: Cambridge, Cambridge University Press.

Tong, J.N., Erwin, D.H., Zuo, J.X., and Zhao, L.S., 2005, Lower Triassic carbon isotope stratigraphy in Chaohu, Anhui: implaction to biotic and ecological recovery.: Albertiana, v. 33, p. 75-76.

Veevers, J.J., and Powell, C.M., 1987, Late Paleozoic glacial episodes in Gondwanaland reflected in trasngressive-regressive depositional sequences in Euramerica: Geological Society of America Bulletin, v. 98, p. 475-487.

Warmer, J.G., and Sandberg, C.A., 1996, Alamo megabreccia: Record of late Devonian impact in southern Nevada, U.S.A.: GSA Today, v. 104, p. 171-176.

Waterhouse, J.B., 2010, Lopingian (Late Permian) stratigraphy of the Salt Range, Pakistan and Himalayan region: Geological Journal, v. 45, p. 264-284.

Wignall, P.B., 1994, Black Shales: Oxford, Oxford University Press, , v. 30.

Wignall, P.B., and Hallam, A., 1996, Facies change and the end-Permian mass extinction in SE Sichuan, China: Palaios, v. 11, p. 587-596.

Wignall, P.B., Newton, R., and Brookfield, M.E., 2004, Pyrite framboid for oxygen-poor deposition during the Permian-Triassic crisis in Kashmir: Palaeogeography Palaeoclimatology Palaeoecology, v. 216, p. 183-188.

Wilkin, R.T., and Barnes, H.L., 1997, Pyrite formation in an anoxic estuarine basin: American Journal of Science, v. 297, p. 620-650.

Willis, K., and McElwain, J.C., 2002, The Evolution of Plants: Oxford University Press, v. 378.

Xie, S.C., Pancost, R.P., Yin, E.F., Wang, H., and Evershed, R.P., 2006, Two episodes of microbial changes associated with Permo-Triassic faunal mass extinction.: Nature, v. 434, p. 494-497.

Yin, H.F., Feng, Q.L., Lai, X.L., Baud, A., and Tong, J.N., 2007, The protracted Permo-Triassic crisis and multi-episode extinction around the Permian-Triassic boundary: Global and Planetary Change, v. 55, p. 1-20.

Zakharov, Y.D., Biakov, A.S., Baud, A., and Kozur, H., 2005, Carbon isotope standard for the Upper Permian and Lower Triassic in Caucasus and its correlation with the Permian of northeastern Russia: Albertiana, v. 33, p. 102-103.

Zhang, H.J., Tong, J.N., and Zuo, J.X., 2005, Lower Triassic and carbon isotope excursion in West Guangxi, southwest China: Albertiana, v. 33, p. 103-104.

Zhao, G., Sun, M., Wilde, S.A., and Li, S.Z., 2004, A Paleo-Mesoproterozoic supercontinent: assembly, growth and breakup: Earth-Science Reviews, v. 67, p. 91-123.

CHAPTER 2

THE IMPACT OF MODERN WEATHERING ON THE GEOCHEMISTRY OF A NEO-TETHYAN PERMO-TRIASSIC SECTION

2.1. Introduction

The Permian-Triassic Boundary (PTB) marks the largest mass extinction in Earth's history; over 90% of all marine and 70% of terrestrial species became extinct at this time (~ 250 mya) (Erwin, 1993). A number of hypotheses have been proposed regarding the cause(s) of the extinction with many relying directly upon the geochemical record preserved in boundary sections. These "geochemical" signatures include variations in $\delta^{13}C_{carb}$ during Late Permian–Early Triassic, in all measured marine sections, that were more extreme (up to 8 to 10‰) that the variations recorded in the Early Triassic (e.g. Yin et al., 2007). These perturbations in the $\delta^{13}C_{carb}$ record are thought to reflect changes in the atmospheric and oceanic carbon cycles, and thus changes of environment on the Earth's surface. Geochemical signatures associated with bolide impact are less well preserved in the marine sections, though there has been a suggestion that the enrichments in Eu at the boundary in the Spiti Valley section at Attargoo (India) are evidence of a eucritic bolide impact (Bhandari et al., 1992). Other geochemical signatures of note include signatures associated with global ocean anoxia

(Algeo, 2007 and references therein), volcanism and aerosol loading of the atmosphere (Renne and Basu, 1991; Renne et al., 1995) and catastrophic methane release (Retallack et al., 2007; Şengör and Atayman, 2009). In all of these cases the interpretation of the geochemical record hinges on the whether the units have been affected by post-depositional processes including diagenesis, metamorphism and modern weathering.

For the most part, marine PT sections show evidence of global ocean anoxia during the late Permian and early Triassic (Hotinski et al., 2001; Isozaki, 1997b; Kakuwa, 2008; Kato and Isozaki, 2009; Wignall and Hallam, 1992; Wignall and Twitchett, 1996; Zhang et al., 2001). Shallow marine sections also show evidence of transient anoxia (Musashi et al., 2001). In the Spiti Valley section at Attargoo (Himachal Pradesh, Indian Himalaya), evidence of anoxia includes small increases in U concentration (from 4ppm to 8ppm) closer to the ferruginous layer (See Chapter 1) and positive $(Ce/La)_N$ ratio (~1.3) within the ferruginous layer (Shukla et al., 2002). Shukla et al. (2002) measured two samples at the ferruginous layer, five samples in the Gungri formation (Permian shale) and two samples in the Mikin formation (Triassic limestone) therefore, it is difficult to ascertain whether these increases represent prolonged changes in depositional conditions. Most authors, who have worked on the Spiti Valley sections, have neglected the potential impact of post-depositional processes on the geochemical records and have focused on the cause of the end-Permian extinction as recorded in the geochemical record (Bhandari et al., 1992; Shukla et al., 2002).

Another PT section located in the neo-Tethys is Guryul Ravine located in Kashmir, India. This section has been studied for both records of the cause(s) of the mass

extinction as well as evaluation of the geochemical record for post-depositional alteration (Algeo et al., 2007; Brookfield et al., 2003). Geochemical investigations at Guryul Ravine can be used to inform our interpretation of the records at Spiti Valley. For example, both appear to be post-depositionally altered with much of the Tethyan sequence in Kashmir impacted by greenschist facies metamorphism (Dèzes, 1999; Herren, 1987). Though not known it appears that the Tethyan sediments in the Spiti Valley have also been impacted by low-grade metamorphism based on thermal alteration indices of 3 to 5 which is indicative of thermally mature sediments (Krystyn et al., 2007; Richoz et al., 2007; Singh et al., 2004).

In the case of the Spiti Valley sections there has been little work done on diagenetic overprint and far less on the effect of surficial weathering. Therefore, perturbations of the geochemical record attributable to weathering may occur. For instance, high concentrations of Zr, REE, Y, and Sc can be attributed to weathering and retention of heavy minerals. This weathering could occur post-depositionally once the sequences are exposed to surface conditions or could represent, as was the case in the Tethyan Guryul Ravine section (Kashmir,Algeo et al., 2007), winnowing of outer-shelf sediments during sea level rise just prior to the end-Permian extinction. It is crucial therefore that we examine the Spiti Valley section geochemistry from the perspective of post-depositional alteration prior to evaluating its position in the global PT chemostratigraphy or attempting to ascribe extinction-related causal meaning to the geochemical signatures preserved in the sequence.

Spiti Valley PTB sections have not been sufficiently studied and so their exact position in the global PT chemostratigraphy is not known. The conodont and ammonite biostratigraphy of the units is well defined (Kapoor, 2004) and the paleodiversity is well constrained in the sections (e.g. Diener, 1908, 1912; Hayden, 1904; Stoliczka, 1865). Many PT sections in Spiti Valley are incomplete and, in the case of the Attargoo where the boundary is preserved, are considered significantly weathered and diagenetically altered (Krystyn et al., 2007; Richoz et al., 2007; Singh et al., 2004). The extent of post-depositional alteration in the Spiti Valley sections is consistent with that observed for the Guryul Ravine section in neighboring Kashmir (Dèzes, 1999; Herren, 1987). Since both sections are geographically close to each other, they may have commonalities in terms of metamorphic history and modern weathering. If this is the case then the Spiti Valley PTB section at Attargoo may, like the Guryul Ravine section, retain some of the original geochemical depositional signatures.

Chemical weathering strongly affects major and trace element geochemistry as well as mineralogy (Fedo et al., 1995; Nesbitt and Young, 1982) of sedimentary rocks. For example, as clay content increases during weathering, via the transformation of feldspars to clay, whole rock Al_2O_3 content increases relative to CaO, K_2O and Na_2O (Nesbitt and Young, 1982; Sheldon and Tabor, 2009). The relative abundance of Al_2O_3 to other alkali and alkali earth metals is known as the Chemical Index of Alteration (Nesbitt and Young, 1982). Using the three stages of weathering defined by Taylor and McLennan (1985) we can place CIA values in context and allows us to assess the extent of weathering and loss of original depositional signatures. These three stages are (1)

early – weathering of primary minerals and formation of amorphous, unstable secondary minerals, (2) intermediate – clay minerals are formed and are dominated by illite and smectite, and (3) late – clay minerals dominate with multi-component compositions of kaolinite-gibbsite-quartz-iron oxide.

Metamorphism will also impact the geochemistry of sedimentary rocks. In addition to mineral transformation, low-grade metamorphism significantly impacts the trace element chemistry of sedimentary rocks (Taylor and McLennan, 1985). In thermally mature sediments such as those preserved at Attargoo (Krystyn et al., 2007; Richoz et al., 2007; Singh et al., 2004) the likelihood of low-grade metamorphism and associated chloritization will also impact the geochemistry of the units. Chloritization of rocks will impact the Mg, Fe, Ni, Mn, Zn, Li and Ca concentrations due to the formation of chlorite minerals such as clinochlore, chamosite, nimite, and pennantite. In the absence of mineralogical data we used the geochemistry of the units to assess the extent of metamorphism and the potential impact on original geochemical signatures (Algeo et al., 2007).

This study focuses specifically on the major element chemistry of the Spiti Valley PTB section at Attargoo, explores the extent of post-depositional weathering across the PT boundary, assesses whether the Attargoo section is suitable for a paleo-environmental reconstruction study, and evaluates the environmental conditions during the formation of the ferruginous layer. In all, this work is part of a larger research endeavor that seeks to place the Spiti Valley sections within the global PT chemostratigraphy.

2.2. The Permian-Triassic Geology of the Spiti Valley

The Neo-Tethyan sequences (Paleozoic and Mesozoic) of the Indian Plate are primarily preserved in the inner part of the Higher Himalaya. These sequences often occur in tectonically decoupled contact over crystalline bedrock. These units are well exposed in the Western (Kashmir, Zanskar- Spiti and Uttrakhand) and the Central (Nepal) Himalaya (Brookfield et al. 2003 and references there in; Figure 1.2). Spiti Valley became famous for its well exposed and complete Triassic sedimentary succession [~1400 m; (Diener, 1908, 1912; Hayden, 1904)] and rich fossil content (Stoliczka, 1865).

At Attargoo, the Triassic Mikin Formation rests over the Permian Gungri Formation with a minor break where a part of Dorashmian is missing and the PT Boundary (PTB) is assumed to be marked by a "ferruginous layer" (Figure 1.3 and 2.1). During the Triassic this region formed part of the tropical Gondwanan-land margin [a.k.a. Peri-Gondwana-land Tethyan succession; (Matsuda, 1985)]. The mid-low paleolatitude allowed for the development of a large and highly diverse mixed pelagic fauna which are very well preserved in these rocks [e.g., (Diener, 1897; Kraft von and Diener, 1909b)].

The biostratigraphy at Spiti Valley varies between the Gungri and Mikin Formation. The lower part of the Gungri formation contains brachiopods and bryozoans (Kapoor, 2004). In the upper part of the Gungri formation several *Cyclolobus* particularly *C. walker* specimen are abundant in the Gungri formation; the highest bed that contains *Cyclolobus* are 20-120cm from the bottom of the Mikin Formation where phosphatic nodules are present (Figure 1.3 Kapoor, 2004; Shukla et al., 2002). The lower Triassic biostratigraphy at Spiti is similar to Kashmir, however the lower Triassic section is

condensed and varies in thickness from 18 to 25cm (Kapoor, 2004).The base of the Mikin formation contains *Otoceras* and *Ophiceras* beds, while *Hedenstroemia* beds lie on top of the *Otoceras* and *Ophiceras* bed (Kapoor, 2004).

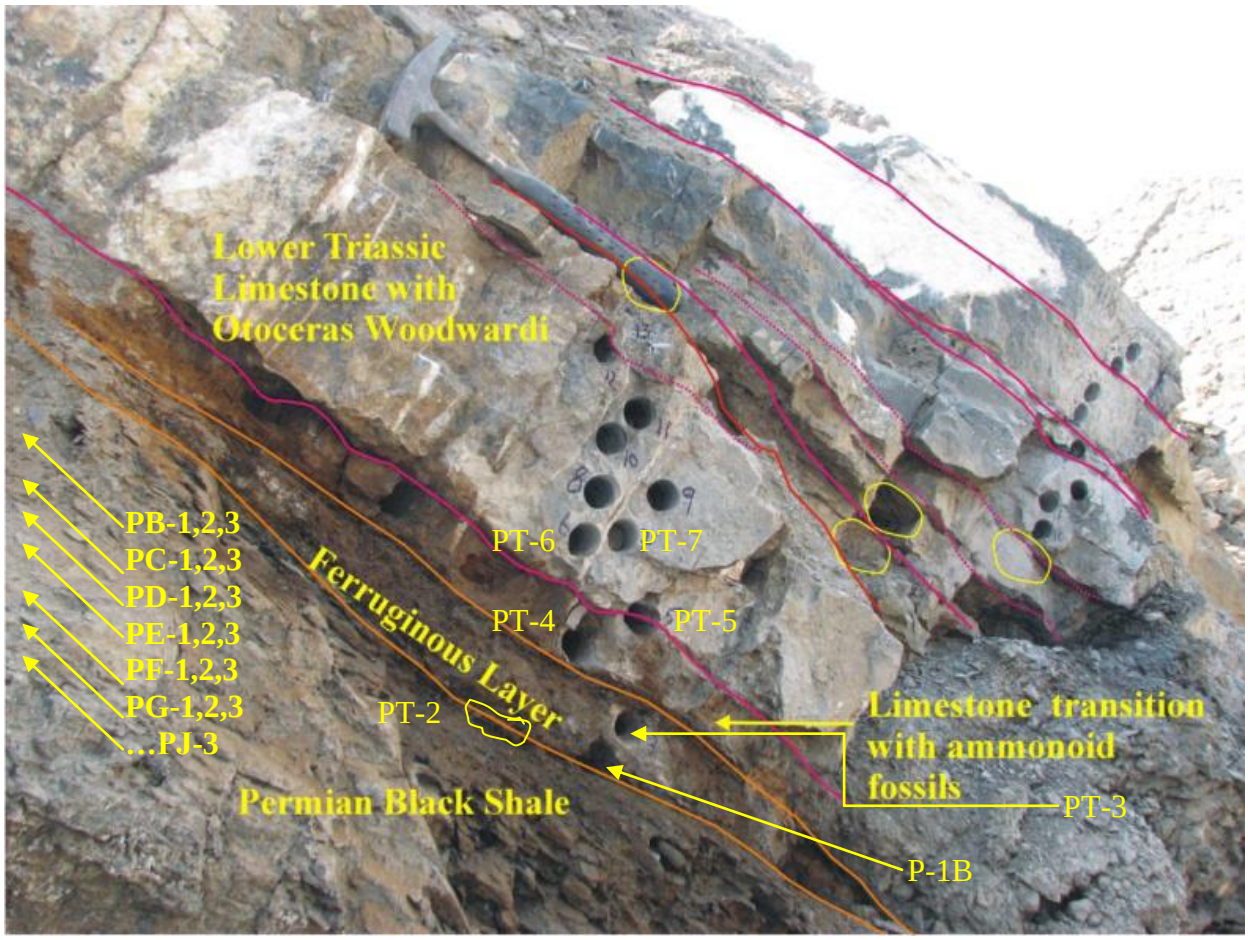

Figure 2.1. Photograph of the section at Attargoo showing the ferruginous layer. Drill core holes are shown were we sampled the limestone in June 2009. Samples of shale were taken every 1-cm as described in the method section.

The Spiti Valley forms part of the district of Lahul & Spiti located in the northern part of the Himachal Pradesh, which occupies a central position in the Western Himalaya. The PTB is marked, in the sections exposed at Attargoo, Kaza, Lalung, and Guling

(Figure 1.2), by a thin (~ 2cm) ferruginous layer separating the Permian black shale (Gungri Fm. *Productus* shale) from the Griesbachian Triassic Limestone (Mikin Fm., *Otoceras-Ophiceras* zone) (Figure 1.3; Shukla et al., 2002). The major geochemical characteristics of the PTB, globally, include several chemostratigraphic trends such as the sharp negative excursion of $\delta^{13}C_{carb}$ noted in a number of PTB sections globally from the southern Alps (Austria-Italy) (Kraus et al., 2009), southern China, western Canada (Isozaki, 1997a), Transcaucasia (northwest Iran) (Korte et al., 2004b), Iran (Kozur, 2006), Japan, New Zealand (Krull et al., 2000), and Kashmir (Algeo et al., 2007; Baud et al., 1989; Grossman, 1994; Holser et al., 1989; Kozur, 2007; Wang et al., 1994). The Spiti Valley PT sections record a number of trends observed in other sections [e.g., negative $\delta^{13}C_{carb}$ excursion; (Ghosh et al., 2002; Richoz et al., 2007)] as well as some that appear unique to the region such as high Eu, Sb, U, and Zn concentrations within the ferruginous layer [Eu/Eu* max = 1.9; (Bhandari et al., 1992; Shukla et al., 2002)], nano-sized iron oxyhydroxide phases, gypsum, and deformed quartz (Shukla et al., 2002).

2.3. Methods

At Attargoo both bulk rock (shale) and drill core (limestone) samples (n=32) were collected at high stratigraphic resolution in June 2009. Samples were collected continuously every 1cm from approximately ~50 cm below (shale) and ~70 cm above (limestone) the ferruginous layer (Figure 1.2). Limestone (Triassic Mikin Fm.) samples were collected using a Pomeroy EZ Core Drill Model D026-C (water cooled; 1" diameter, 5 cm length). Sample orientation (up section) was marked on the exposed core

end and samples were placed in whirlpaks for transport back to the laboratory. Shale (Permian Gungri Fm.) samples were collected using rock hammer and chisel. Weathered surfaces were trenched approximately 7" into the rock face and approximately 3 cm thick slabs were removed every 3 cm. Prior to removal from the outcrop the up section orientation was marked. Strike and dip exposure of Spiti PTB sections are noted as high angles, and a non-diastrophic fold is particularly in the Mikin formation (Bhargarva, 1987). Because the shale is very fissile, sample "packets" were tightly wrapped in newspaper taped and placed in zip-lock bags for transport back to the laboratory.

Sub-samples were taken from field samples for analysis in the laboratory. For shales, the samples were carefully opened, and using dental picks, the layers of the shale separated. Samples for analysis were taken from the "center" layer approximately 2 cm back from the up-section mark. For drill core samples sub-samples were taken 2 cm back from the up-section mark using a chisel. For both shale and limestone sub-samples approximately 7 g of material was excised.

2.3.1. Analytical Methods

Sub-samples representing homogenized 1cm intervals were powdered by Spex Ball Mill. The powdered samples (< 60 mesh) were analyzed for major element oxide (except Na_2O) using a SPECTRO XEPOS Benchtop Energy Dispersive X-ray Fluorescence (ED-XRF) as described by Smith (2007). 3 to 5 g of sample were measured, in triplicate, under He purge and calibrated against SDO-1 (USGS Devonian Shale). Reported errors represent the propagated error of repeat/replicate measures and the

certified measurement (MC) ratio for each element (Table 2.1). SGR-1 (USGS Green River Shale) was measured as an unknown to monitor accuracy of the ED-XRF. Measured values for SGR-1 were better than 95% of the known values for measured major elements.

For Na concentration measurements, 16mg of powdered sample was dissolved completely through ultra-pure acid digestion (Murray and Leinen, 1993). Samples were digested in 7mL Savillex teflon bombs on a hot plate (200-260°C) (Algeo et al., 2007; Bayon et al., 2002). Samples were digested for 24hrs and dried down repetitively after each digestion step. Once the samples were dried down after the removal of concentrated HF, they were acidified with 0.5mL of concentrated ultrapure HNO_3 and diluted with 50mL of milli-q water. Acid digested samples were quantified for Na using a PerkinElmer Optima 3000XL Inductively Coupled Plasma Optical Emission Spectrometer (ICP-OES) (Table 2.1). Samples were measured in triplicate under Ar purge. We measured Na using a 3 point calibration curve (500ppm, 20ppm, and 10ppm). The 3-point calibration served as verification for instrument accuracy and precision. SDO-1 was analyzed for calibration as well. Unknown values were corrected by the SDO-1 measured to certified ratio. SGR-1 was measured as an unknown to monitor accuracy. Measured values for SGR-1 were better than 95% of the known Na values.

Organic carbon and carbonate were estimated by loss on ignition (LOI) using the method outline in Dean (1974) (Table 2.1). LOI results were calibrated against SDO-1.

2.3.2. Chemical Index of Alteration (CIA)

Chemical Index of Alteration (CIA) was calculated to assess the degree of weathering. CIA uses molar proportions of Al_2O_3, Na_2O, and K_2O. This approach is commonly applied to silicate and sedimentary rocks(Nesbitt and Young, 1982). It is less commonly applied to limestones. Here we calculate the CIA for all samples and only, where appropriate, assess the Gungri formation samples (Permian Shales) in the context of CIA-weathering.

$$\boldsymbol{CIA = [Al_2O_3/(Al_2O_3 + CaO^* + Na_2O + K_2O)] \times 100}$$

Equation 2. 1

CaO*, used in the CIA calculation, is the amount of CaO incoroporated in the silicate fraction of the rock (Nesbitt and Young, 1982), hence the reason it is not directly applicable to limestones. In several samples CaO* was negative. We assumed, in these cases, that CaO content was neglibly associated with silicate. CaO* was determined as in Equation 2.2.

$$\boldsymbol{CaO^* = mol\ CaO - mol\ CO_2 - (0.5 \times mol\ CO_2) - [(10/3) \times mol\ P_2O_5]}$$

Equation 2. 2

2.4. Results

The Gungri formation has a high content of clay minerals. This is indicated by the high content of SiO_2, TiO_2, and Al_2O_3. The shales also had typical, relatively low, concentrations of Fe_2O_3, MnO, MgO, CaO, P_2O_5, Na_2O, and K_2O (Figure 2.2). The high clay mineral content suggests that the Gungri formation is, sedimentologically, mature. The Mikin formation has a high content of MgO and CaO and low, overall,

concentrations of SiO_2, TiO_2, Al_2O_3, Fe_2O_3, MnO, P_2O_5, Na_2O, and K_2O (Figure 2.2) as is typical for limestones. The MgO values suggest that the area (PT-4-PT-7) of the Mikin formation has dolomitic characteristics. The ferruginous layer can be separated into three layers bottom, middle, and top. The bottom or lower part of the ferruginous layer resembles, geochemically, the Gungri formation. The middle and upper ferruginous layer samples are low in SiO_2, TiO_2, Al_2O_3, MnO, MgO, Na_2O, and K_2O and have higher concentrations of Fe_2O_3, CaO, and P_2O_5 than other samples in the section (Figure 2.2).

The C_{org} content (calculated from LOI) between the two formations and the ferruginous layer are, as expected, significantly different. The Gungri formation and lower part of the ferruginous layer have C_{org} contents ranging from 2.14 to 4.04%, the Mikin formation (Triassic Limestone) ranges from 0.67 to 1.42%, the middle part of the ferruginous layer has a value of 3.69%, and the upper part of the ferruginous has a value of 5.31% (Table 2.1; Figure 2.2). The C_{org} content for the middle and upper parts of the ferruginous layer are significantly higher than the Permian or Triassic formations in the Attargoo section. The C_{Inorg} and LOI content in the Mikin formation are significantly higher than the ferruginous layer and Gungri formation. This is due to the high content of inorganic carbon found in limestones.

The CIA values for the Gungri formation range from 68.24-74.73, the CIA values indicate that the Gungri formation contains, as shales do, clay minerals which is reflected in the high content of Al_2O_3 (Table 2.1; Figure 2.2). The CIA values for the ferruginous layer suggest a decrease in clay content from the bottom to the top of the layer. The sample PT-2, located at the bottom of the ferruginous layer, has a CIA value of 73.05.

This value suggests that the base of the the ferruginous layer has a higher clay mineral content more like the Gungri shales. The sample PT-1B, middle ferruginous layer, has a CIA value of 29.19. The PT-3 sample, top of the ferruginous layer, has a CIA value of 31.57. The low CIA values of the middle and top of the ferruginous layer are probably due to low Al_2O_3, high CaO, cool, and/or arid conditions (Fedo et al., 1995). The Mikin formation CIA values range from 1.05-7.39 with these samples having high concentrations of alkali earth metals typical of limestones.

Table 2. 1. Major element composition of the Attargoo Section. PT 4 to 7 = Mikin Formation, PT 2-3 = Ferruginous Layer, PB to PJ = Gungri formation. LS=Limestone, FL=Ferruginous Layer, S=Shale, BDL = below detection limit. Standard deviation for CO_2, Organic Carbon, and LOI represent SDO-1, because samples were corrected by SDO-1.

Sample	Rock Type	Depth (cm)	SiO_2 (wt. %)	TiO_2 (wt. %)
PT-7	Mikin Fm. (LS)	10	14.07 +/-0.30	0.05 +/-0.00
PT-6	Mikin Fm. (LS)	7	6.44 +/-0.14	0.03 +/-0.00
PT-5	Mikin Fm. (LS)	5	14.31 +/-0.27	0.13 +/-0.01
PT-4	Mikin Fm. (LS)	3	7.98 +/-0.14	0.05 +/-0.00
PT-3	FL	1.0	18.26 +/-0.32	0.09 +/-0.00
PT-1b	FL	0	33.84 +/-0.84	0.35 +/-0.02
PT-2	FL	-1.5	60.99 +/-1.04	1.13 +/-0.06
PB-1	Gungri Fm. (S)	-6	64.68 +/-0.87	1.13 +/-0.06
PB-2	Gungri Fm. (S)	-8	48.43 +/-0.65	0.74 +/-0.03
PB-3	Gungri Fm. (S)	-10	62.63 +/-0.84	1.13 +/-0.07
PC-1	Gungri Fm. (S)	-11	50.38 +/-0.72	0.74 +/-0.04
PC-2	Gungri Fm. (S)	-13	46.69 +/-0.66	0.78 +/-0.04
PC-3	Gungri Fm. (S)	-15	51.15 +/-0.70	0.80 +/-0.05
PD-1	Gungri Fm (S)	-16	59.90 +/-0.80	1.02 +/-0.06
PD-2	Gungri Fm. (S)	-18	59.32 +/-0.80	0.97 +/-0.04
PD-3	Gungri Fm. (S)	-20	60.75 +/-0.82	1.04 +/-0.07
PE-1	Gungri Fm. (S)	-21	64.95 +/-0.87	1.09 +/-0.05
PE-2	Gungri Fm. (S)	-23	66.19 +/-0.91	0.98 +/-0.04
PE-3	Gungri Fm. (S)	-25	64.03 +/-0.86	1.09 +/-0.05
PF-1	Gungri Fm. (S)	-27	53.65 +/-0.73	0.87 +/-0.04
PF-2	Gungri Fm. (S)	-28	63.04 +/-0.84	1.09 +/-0.05
PF-3	Gungri Fm. (S)	-30	63.59 +/-0.90	1.07 +/-0.07
PG-1	Gungri Fm. (S)	-32	54.01 +/-0.76	0.95 +/-0.04
PG-2	Gungri Fm. (S)	-33	52.62 +/-0.72	0.87 +/-0.04
PG-3	Gungri Fm. (S)	-35	52.05 +/-0.70	0.78 +/-0.03
PH-1	Gungri Fm. (S)	-37	60.37 +/-0.81	1.03 +/-0.05
PH-2	Gungri Fm. (S)	-38	59.30 +/-0.80	0.96 +/-0.04
PH-3	Gungri Fm. (S)	-40	61.63 +/-0.82	1.04 +/-0.05
PI-1	Gungri Fm. (S)	-42	61.09 +/-0.87	0.87 +/-0.05
PI-2	Gungri Fm. (S)	-44	60.91 +/-0.83	1.04 +/-0.06
PI-3	Gungri Fm. (S)	-45	60.36 +/-0.81	1.00 +/-0.04
PJ-1	Gungri Fm. (S)	-47	52.70 +/-0.74	0.86 +/-0.04
PJ-2	Gungri Fm. (S)	-49	52.72 +/-0.79	0.96 +/-0.06
PJ-3	Gungri Fm. (S)	-50	57.80 +/-0.77	0.93 +/-0.06

Table 2.1. Continued.

Sample	Al_2O_3 (wt. %)	Fe_2O_3 (wt. %)	MnO (wt. %)	MgO (wt. %)
PT-7	0.38 +/- 0.01	6.12 +/-0.20	1.47 +/-0.23	14.81 +/-2.50
PT-6	0.34 +/-0.02	5.23 +/-0.17	1.12 +/-0.18	13.87 +/-2.38
PT-5	2.20 +/-0.06	10.07 +/-0.34	1.06 +/-0.17	8.69 +/-1.46
PT-4	0.75 +/-0.03	11.07 +/-0.33	1.85 +/-0.29	9.97 +/-1.67
PT-3	5.53 +/-0.13	30.51 +/-0.92	0.08 +/-0.01	BDL
PT-1b	9.67 +/-0.28	9.88 +/-0.34	0.08 +/-0.01	1.49 +/-0.34
PT-2	20.18 +/-0.49	2.74 +/-0.08	0.01 +/-0.00	0.27 +/-0.05
PB-1	21.61 +/-0.64	1.87 +/-0.04	0.01 +/-0.00	0.78 +/-0.21
PB-2	16.06 +/-0.49	19.67 +/-0.45	0.01 +/-0.00	0.53 +/-0.21
PB-3	20.61 +/-0.62	3.34 +/-0.08	0.01 +/-0.00	0.63 +/-0.17
PC-1	14.90 +/-0.54	17.35 +/-0.40	0.01 +/-0.00	BDL
PC-2	14.47 +/-0.53	18.93 +/-0.44	0.01 +/-0.00	BDL
PC-3	16.08 +/-0.48	14.75 +/-0.35	0.01 +/-0.00	0.42 +/-0.23
PD-1	19.58 +/-0.59	4.27 +/-0.10	0.01 +/-0.00	0.32
PD-2	19.60 +/-0.58	6.89 +/-0.16	0.01 +/-0.00	0.56 +/-0.34
PD-3	20.47 +/-0.61	4.41 +/-0.10	0.01 +/-0.00	0.86 +/-0.30
PE-1	20.32 +/-0.61	2.22 +/-0.05	0.01 +/-0.00	1.01 +/-0.25
PE-2	20.54 +/-0.61	3.28 +/-0.08	0.01 +/-0.00	0.77 +/-0.20
PE-3	20.03 +/-0.60	3.41 +/-0.08	0.01 +/-0.00	0.89 +/-0.23
PF-1	17.02 +/-0.51	12.62 +/-0.29	0.02 +/-0.00	BDL
PF-2	20.11 +/-0.60	2.80 +/-0.07	0.01 +/-0.00	0.61 +/-0.37
PF-3	20.26 +/-0.61	3.21 +/-0.07	0.01 +/-0.00	0.64 +/-0.22
PG-1	17.82 +/-0.56	12.03 +/-0.28	0.02 +/-0.00	0.32 +/-0.31
PG-2	16.86 +-/0.50	13.18 +/-0.30	0.03 +/-0.00	BDL
PG-3	14.90 +/-0.51	10.55 +/-0.24	0.02 +/-0.00	BDL
PH-1	20.67 +/-0.62	3.79 +/-0.09	0.01 +/-0.00	1.56 +/-0.42
PH-2	20.40 +/-0.61	4.78 +/-0.11	0.02 +/-0.00	1.43 +/-0.35
PH-3	20.30 +/-0.61	3.93 +/-0.09	0.01 +/-0.00	1.20 +/-0.38
PI-1	17.50 +/-0.53	5.58 +/-0.13	0.01 +/-0.00	0.63 +/-0.18
PI-2	20.64 +/-0.62	5.09 +/-0.12	0.03 +/-0.01	1.14 +/-0.34
PI-3	20.09 +/-0.60	5.87 +/-0.14	0.04 +/-0.01	1.25 +/-0.32
PJ-1	18.20 +/-0.57	8.33 +/-0.19	0.02 +/-0.00	0.92 +/-0.50
PJ-2	18.98 +/-0.57	7.36 +/-0.17	0.02 +/-0.00	1.11 +/-0.28
PJ-3	19.27 +/-0.58	5.20 +/-0.12	0.02 +/-0.00	0.89 +/-0.31

Table 2.1. Continued

Sample	CaO (wt. %)	Na_2O (wt. %)	K_2O (wt. %)	P_2O_5 (wt. %)
PT-7	31.79 +/-1.54	0.11 +/-0.03	0.23 +/-0.01	0.08 +/-0.01
PT-6	37.49 +/-1.82	0.11 +/-0.02	0.13 +/-0.00	0.05 +/-0.00
PT-5	31.18 +/-1.53	0.11 +/-0.02	0.67 +/-0.02	0.07 +/-0.00
PT-4	33.95 +/-1.59	0.09 +/-0.03	0.23 +/-0.01	0.09 +/-0.01
PT-3	9.92 +/-0.47	0.16 +/-0.03	0.37 +/-0.01	1.24 +/-0.08
PT-1b	14.10 +/-0.69	0.30 +/-0.02	1.88 +/-0.05	1.18 +/-0.08
PT-2	0.24 +/-0.01	0.72 +/-0.07	5.38 +/-0.12	0.12 +/-0.01
PB-1	0.22 +/-0.01	0.48 +/-0.07	5.87 +/-0.11	0.11 +/-0.01
PB-2	0.63 +/-0.03	0.37 +/-0.03	4.49 +/-0.08	0.13 +/-0.01
PB-3	0.26 +/-0.01	0.44 +/-0.01	5.61 +/-0.11	0.12 +/-0.01
PC-1	0.21 +/-0.01	0.33 +/-0.02	4.25 +/-0.08	0.12 +/-0.01
PC-2	0.84 +/-0.04	0.35 +/-0.03	4.28 +/-0.08	0.11 +/-0.01
PC-3	0.23 +/-0.01	0.52 +/-0.07	4.48 +/-0.08	0.11 +/-0.01
PD-1	0.20 +/-0.01	0.51 +/-0.05	5.43 +/-0.10	0.12 +/-0.01
PD-2	0.20 +/-0.01	0.42 +/-0.06	5.39 +/-0.10	0.12 +/-0.01
PD-3	0.23 +/-0.01	0.54 +/-0.03	5.58 +/-0.10	0.12 +/-0.01
PE-1	0.20 +/-0.01	0.56 +/-0.10	5.45 +/-0.10	0.12 +/-0.01
PE-2	0.21 +/-0.01	0.68 +/-0.07	5.31 +/-0.10	0.11 +/-0.01
PE-3	0.22 +/-0.01	0.62 +/-0.01	5.44 +/-0.10	0.12 +/-0.01
PF-1	0.30 +/-0.01	0.56 +/-0.03	4.78 +/-0.09	0.12 +/-0.01
PF-2	0.21 +/-0.01	0.54 +/-0.08	5.47 +/-0.10	0.11 +/-0.01
PF-3	0.20 +/-0.01	0.27 +/-0.04	5.47 +/-0.11	0.12 +/-0.01
PG-1	0.37 +/-0.02	0.55 +/-0.05	4.85 +/-0.09	0.11 +/-0.01
PG-2	0.20 +/-0.01	0.54 +/-0.04	4.68 +/-0.09	0.11 +/-0.01
PG-3	0.19 +/-0.01	0.51 +/-0.08	4.08 +/-0.08	0.10 +/-0.01
PH-1	0.23 +/-0.01	0.59 +/-0.05	5.12 +/-0.10	0.11 +/-0.01
PH-2	0.21 +/-0.01	0.68 +/-0.08	5.16 +/-0.10	0.11 +/-0.01
PH-3	0.21 +/-0.01	0.59 +/-0.08	5.21 +/-0.10	0.11 +/-0.01
PI-1	0.24 +/-0.01	0.62 +/-0.06	4.52 +/-0.09	0.12 +/-0.01
PI-2	0.22 +/-0.01	0.79 +/-0.07	5.21 +/-0.10	0.12 +/-0.01
PI-3	0.23 +/-0.01	0.72 +/-0.07	4.92 +/-0.10	0.11 +/-0.01
PJ-1	0.25 +/-0.01	0.67 +/-0.08	4.85 +/-0.10	0.11 +/-0.01
PJ-2	0.22 +/-0.01	0.73 +/-0.03	4.88 +/-0.09	0.12 +/-0.01
PJ-3	0.20 +/-0.01	0.57 +/-0.04	4.81 +/-0.09	0.11 +/-0.01

Table 2.1. Continued

Sample	$C_{Inorganic.}$ (wt. %)	$C_{Organic}$ (wt. %)	LOI (wt. %)	CIA
PT-7	9.23 +/-0.21	1.06 +/-0.45	30.4 +/-0.0	1.44
PT-6	10.48 +/-0.21	0.67 +/-0.45	33.5 +/-0.0	1.05
PT-5	8.59 +/-0.21	1.11 +/-0.45	28.5 +/-0.0	7.39
PT-4	9.16 +/-0.21	1.42 +/-0.45	30.9 +/-0.0	2.43
PT-3	1.08 +/-0.21	5.31 +/-0.45	13.5 +/-0.0	31.57
PT-1b	0.60 +/-0.21	3.69 +/-0.45	8.9 +/-0.0	29.19
PT-2	0.54 +/-0.21	2.41 +/-0.45	6.3 +/-0.0	73.05
PB-1	0.47 +/-0.21	2.39 +/-0.45	6.0 +/-0.0	74.13
PB-2	0.88 +/-0.21	4.04 +/-0.45	10.5 +/-0.0	70.85
PB-3	2.10 +/-0.21	2.59 +/-0.45	11.4 +/-0.0	73.93
PC-1	0.58 +/-0.21	3.66 +/-0.45	8.8 +/-0.0	72.97
PC-2	0.85 +/-0.21	3.70 +/-0.45	9.7 +/-0.0	68.24
PC-3	0.76 +/-0.21	3.00 +/-0.45	8.1 +/-0.0	72.44
PD-1	0.52 +/-0.21	2.73 +/- 0.45	6.8 +/-0.0	73.43
PD-2	0.58 +/-0.21	2.86 +/-0.45	7.3 +/-0.0	74.02
PD-3	0.51 +/-0.21	3.80 +/-0.45	8.9 +/-0.0	73.61
PE-1	0.53 +/-0.21	2.43 +/-0.45	6.3 +/-0.0	73.89
PE-2	0.50 +/-0.21	2.19 +/-0.45	5.8 +/-0.0	73.93
PE-3	0.49 +/-0.21	2.63 +/-0.45	6.5 +/-0.0	73.26
PF-1	0.79 +/-0.21	2.99 +/-0.45	8.2 +/-0.0	71.92
PF-2	0.55 +/-0.21	2.44 +/-0.45	6.4 +/-0.0	73.69
PF-3	0.50 +/-0.21	2.37 +/-0.45	6.1 +/-0.0	75.07
PG-1	0.37 +/-0.21	3.59 +/-0.45	8.0 +/-0.0	72.26
PG-2	0.66 +/-0.21	3.27 +/-0.45	8.3 +/-0.0	72.74
PG-3	0.60 +/-0.21	3.60 +/-0.45	8.8 +/-0.0	72.67
PH-1	0.59 +/-0.21	3.22 +/-0.45	8.0 +/-0.0	74.91
PH-2	0.53 +/-0.21	2.89 +/-0.45	7.2 +/-0.0	74.24
PH-3	0.51 +/-0.21	2.89 +/-0.45	7.1 +/-0.0	74.38
PI-1	0.52 +/-0.21	2.50 +/-0.45	6.4 +/-0.0	73.38
PI-2	0.55 +/-0.21	2.63 +/-0.45	6.7 +/-0.0	73.79
PI-3	0.53 +/-0.21	2.72 +/-0.45	6.9 +/-0.0	74.37
PJ-1	0.78 +/-0.21	3.04 +/-0.45	8.2 +/-0.0	72.78
PJ-2	0.58 +/-0.21	2.97 +/-0.45	7.5 +/-0.0	73.40
PJ-3	0.73 +/-0.21	2.40 +/-0.45	6.8+/-0.0	74.73

Figure 2.2. Stratitgraphy of major element weight percentages for the Attargoo PTB section. (A) SiO_2, (B) TiO_2, (C) Al_2O_3, (D) Fe_2O_3, (E) MnO, (F) MgO, (G) CaO, (H) Na_2O, (I) K_2O, (J) P_2O_5, (K) $C_{Organic}$, (L) $C_{Inorganic}$, (M) Loss on Ignition (LOI), and (N) Chemical Index of Alteration (CIA) . Dashed lines bracket the ferruginous layer. Depth 0 is defined as PT-1B.

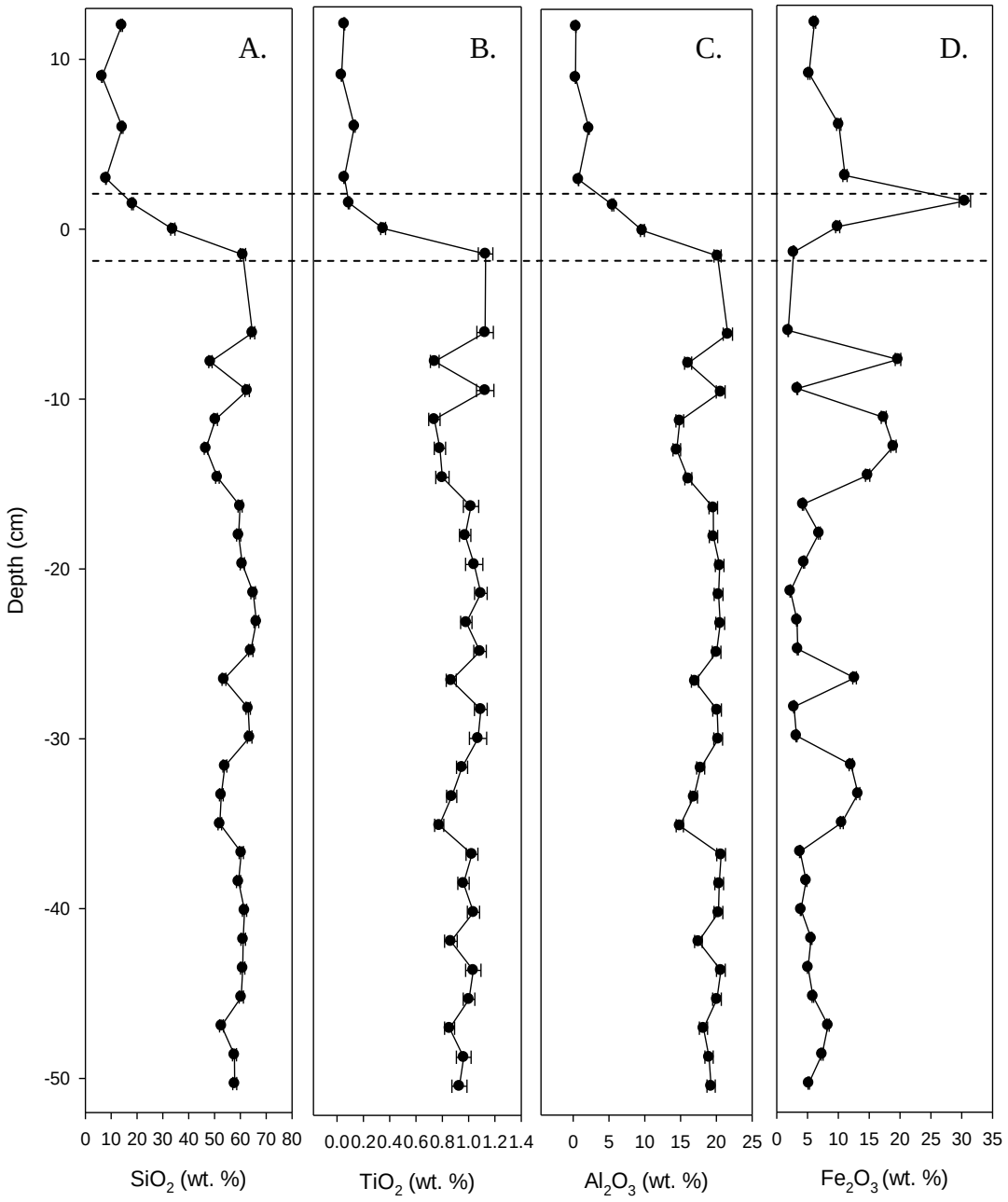

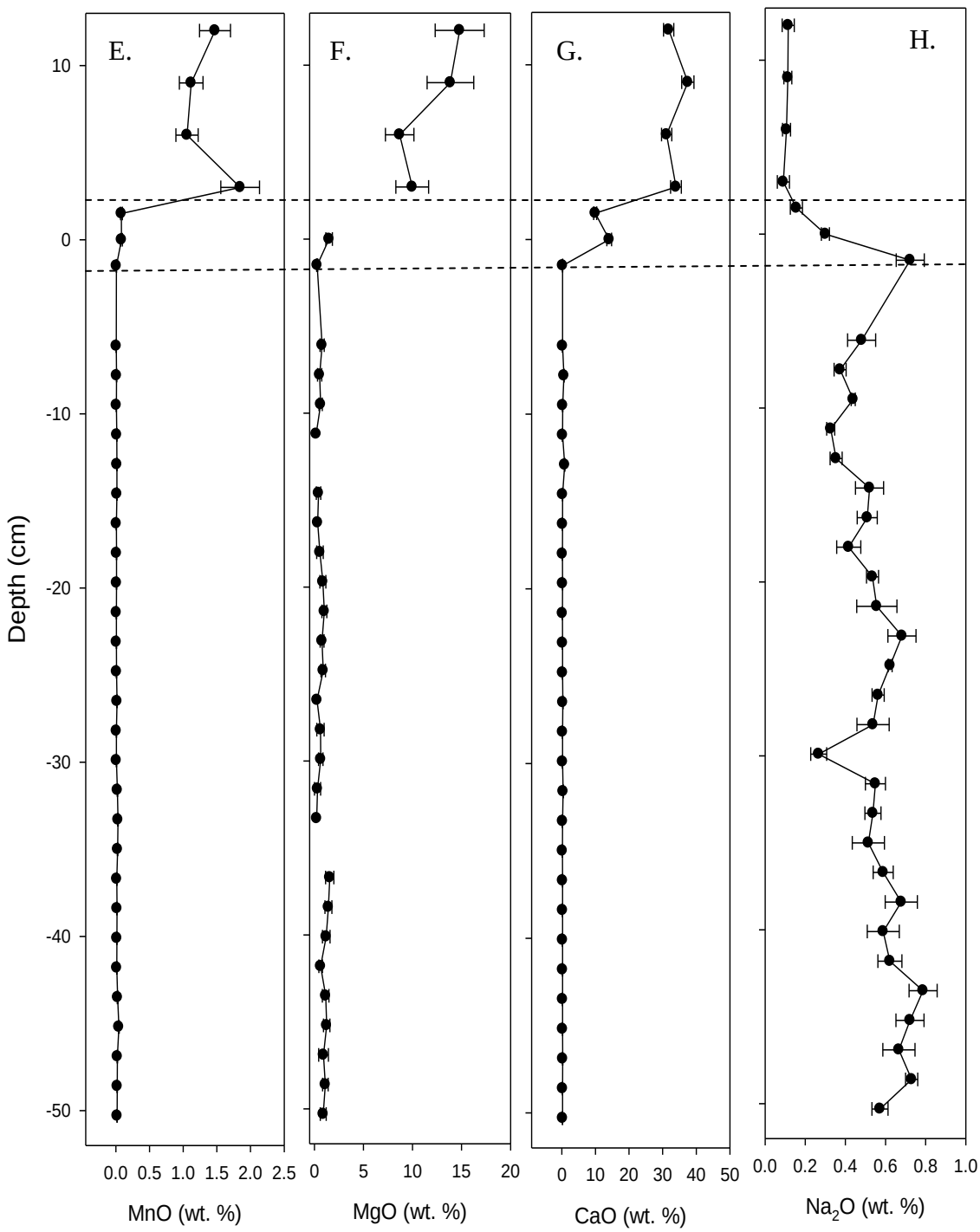
E.
F.
G.
H.
Depth (cm)
10
0
-10
-20
-30
-40
-50
0.0 0.5 1.0 1.5 2.0 2.5
MnO (wt. %)
0 5 10 15 20
MgO (wt. %)
0 10 20 30 40 50
CaO (wt. %)
0.0 0.2 0.4 0.6 0.8 1.0
Na2O (wt. %)

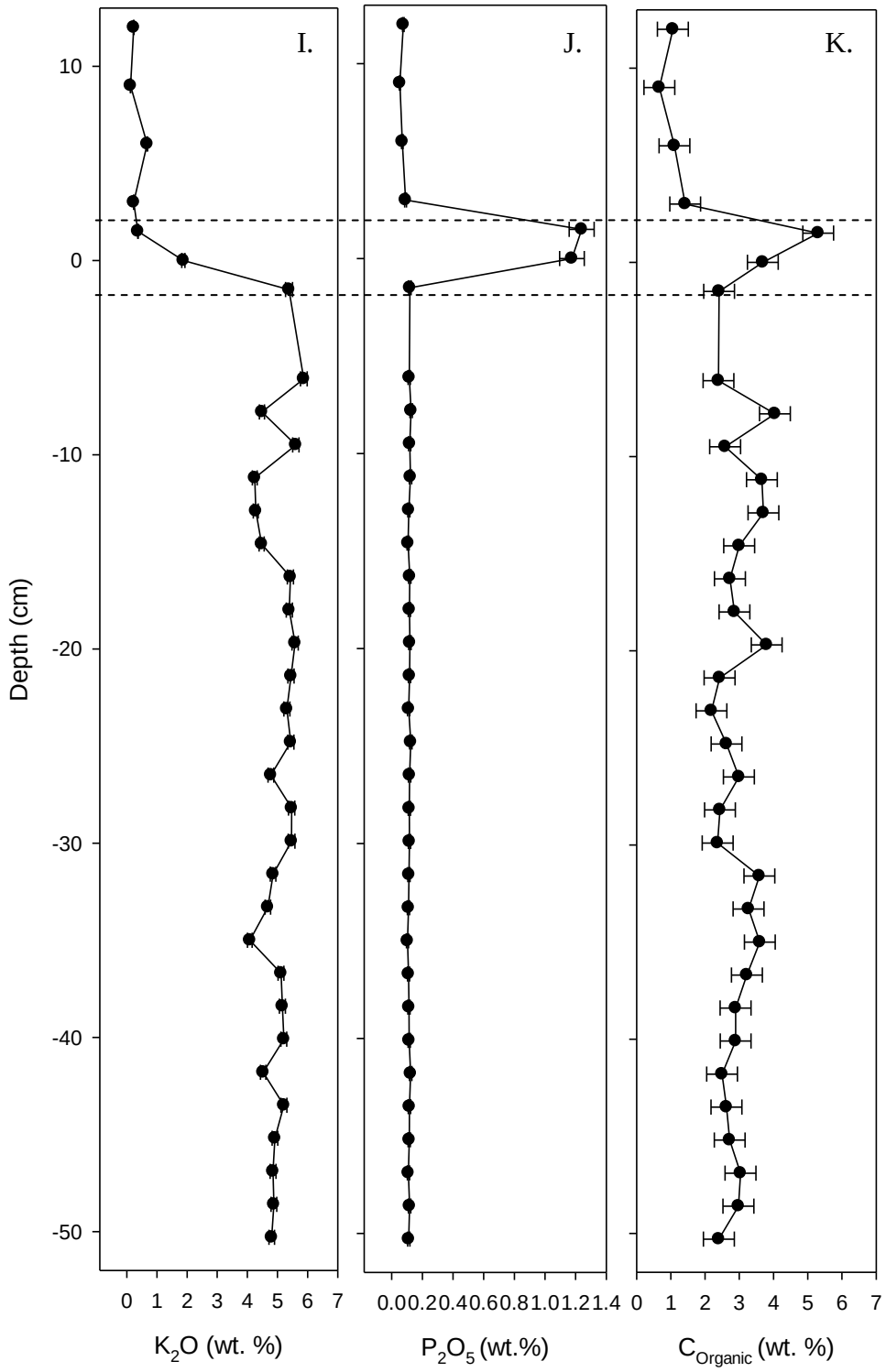
I.
J.
K.
10
0
-10
-20
-30
-40
-50
Depth (cm)
0 1 2 3 4 5 6 7
K2O (wt. %)
0.00.20.40.60.81.01.21.4
P2O5 (wt.%)
0 1 2 3 4 5 6 7
COrganic (wt. %)

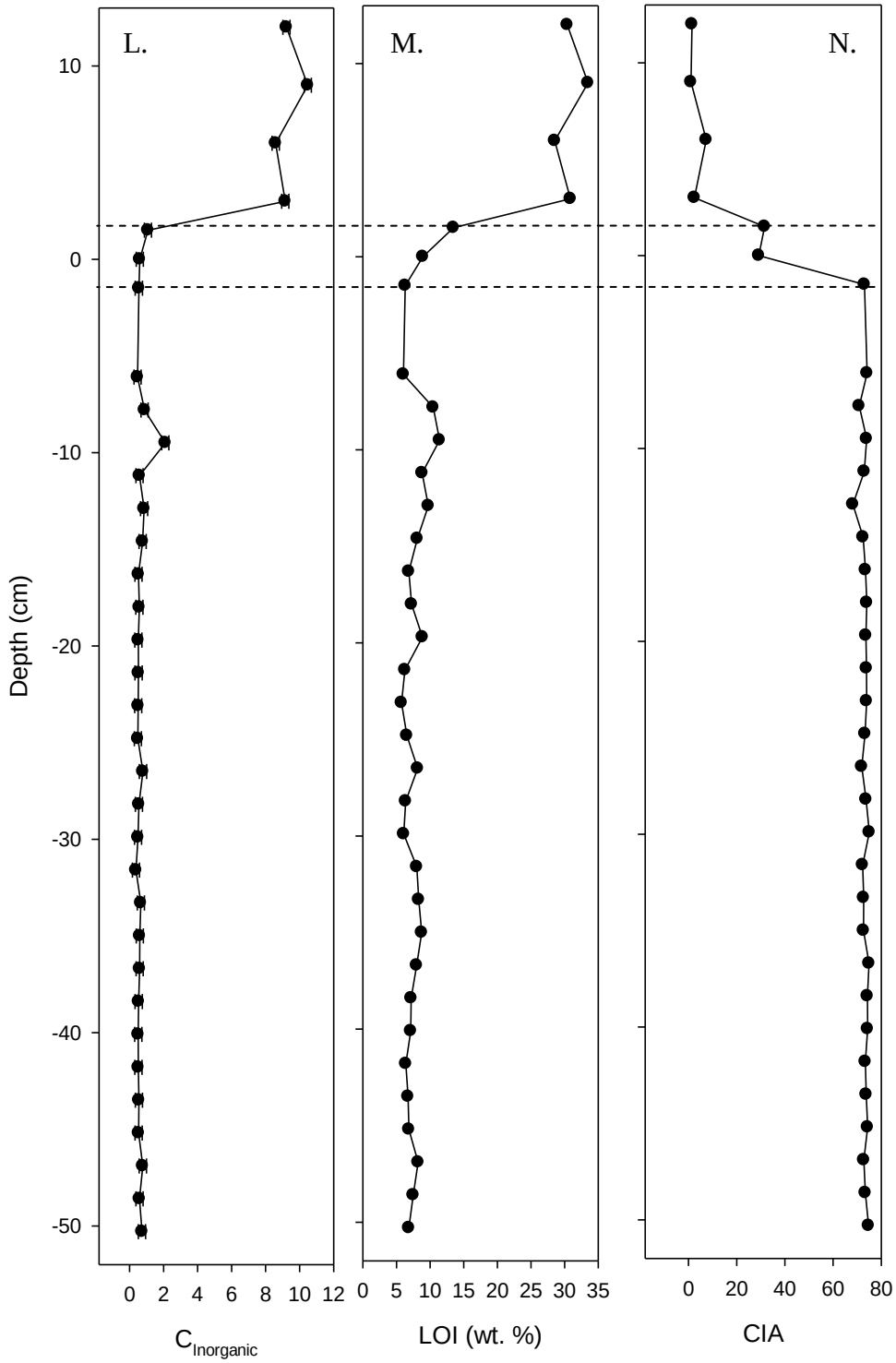
L.
M.
N.
Depth (cm)
10
0
-10
-20
-30
-40
-50
0 2 4 6 8 10 12
0 5 10 15 20 25 30 35
0 20 40 60 80
C Inorganic
LOI (wt. %)
CIA

2.4.1. Ternary Plots

The A-CN-K diagram is useful for evaluating rock compositions and weathering trends because of the dominance of plagioclase and K-feldspar rocks, and clay minerals (Fedo et al., 1995). We used the A-CN-K diagram to evaluate the provenance of the Gungri formation. The relations suggest that Gungri formation and the lower part of the ferruginous layer have lost Na_2O, CaO, and K_2O due to post-depositional alteration (Nesbitt and Young, 1982). The degree of chemical weathering for the Gungri formation and lower part of the ferruginous layer suggest diagenetic transformation from a plagioclase to illite (Figure 2.3). The trend towards the A-K line indicates that Na and Ca have been removed from the Gungri formation most likely caused by a loss of plagioclase (Figure 2.3). Shales loading towards the A-K line suggests that the provenance is possibly K-rich (Figure 2.3); and it appears that the Attargoo PTB has not undergone any K-metasomatism. The geochemistry of the middle and upper ferruginous layer samples (PT-1B and PT-3) suggests a trend from Fe, Ca and Mg enrichment to Al (Figure 2.3).

In order to understand the degree of chemical weathering, and diagenesis, and metamorphism of the Attargoo section we used the the relation between the alkali earths, Mg, and Fe known as the A-CNK-FM diagram or mafic diagram. The A-CNK-FM diagram suggest that shales have an abundace of clay minerals because samples are plotted above the feldspar-orthopryoxene (Nesbitt and Young, 2004). The Gungri samples and the lower ferruginous samples appear to move down the illite-

chlorite line suggesting that the samples have undergone post-depositional weathering due to the presence of illite and diagenesis due to the presence smectite (Hayashi et al., 1997) . The Gungri formation and the lower part of the ferruginous layer appear to have experience some form of low-grade metamorphism as shales trend towards chlorite this is shown on the A-CNK-FM diagram as shales move down the illite-chlorite line (Hayashi et al., 1997) . The relations in Figure 2.4 suggest that the chemical alteration in the Gungri formation may be attirbuted low-grade metamorphism and post depositional processes such as weathering and diagenesis (Figure 2.4). Interestingly, the middle ferruginous layer sample, PT-1B, appears to have a geochemical signature suggestive of goethite (Shukla et al., 2002); PT-3, top of the ferruginous layer, appears to contain aluminous biotite (Figure 2.4). The middle and upper ferruginous layer samples are high in Fe, these samples also fall below the Feldspar-Orthopyroxene line. Falling below the Feldspar-Orthopyroxene line suggests that the samples contain more primary minerals rather than secondary clay minerals, which is indicative of immaturity (Nesbitt and Young, 2004).

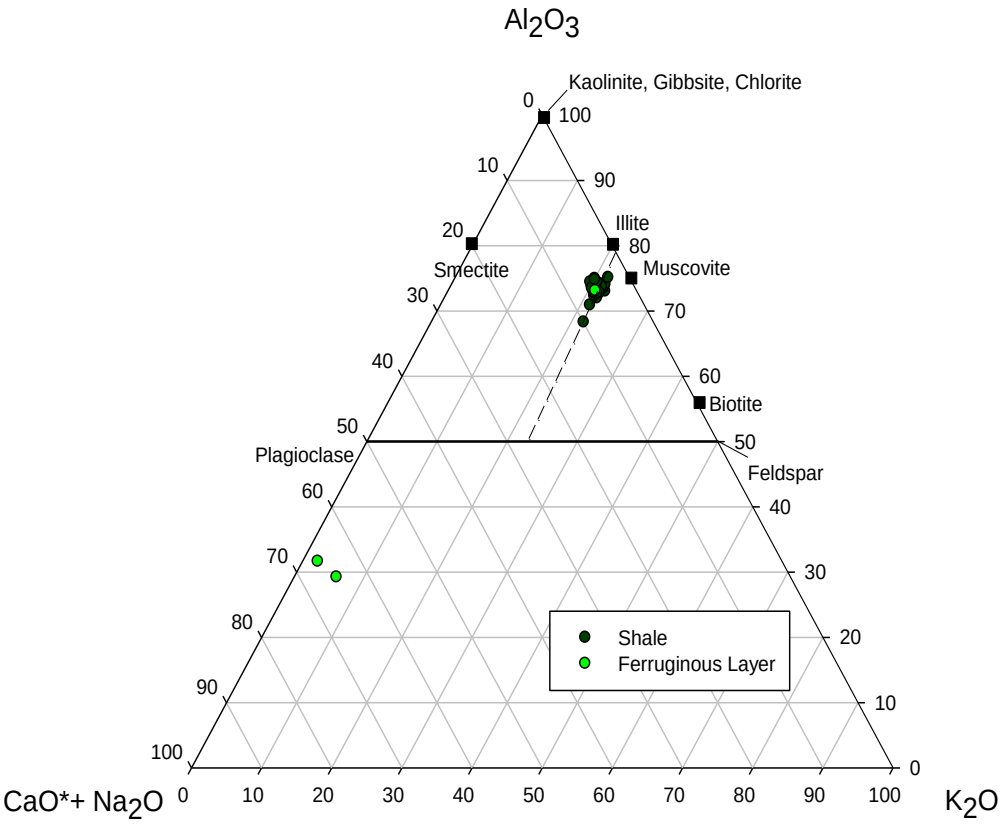

Figure 2.3. Ternary diagram (A-CN-K) for the Gungri Formation and Ferruginous layer. Black line indicates the Plagioclase-Feldspar line.

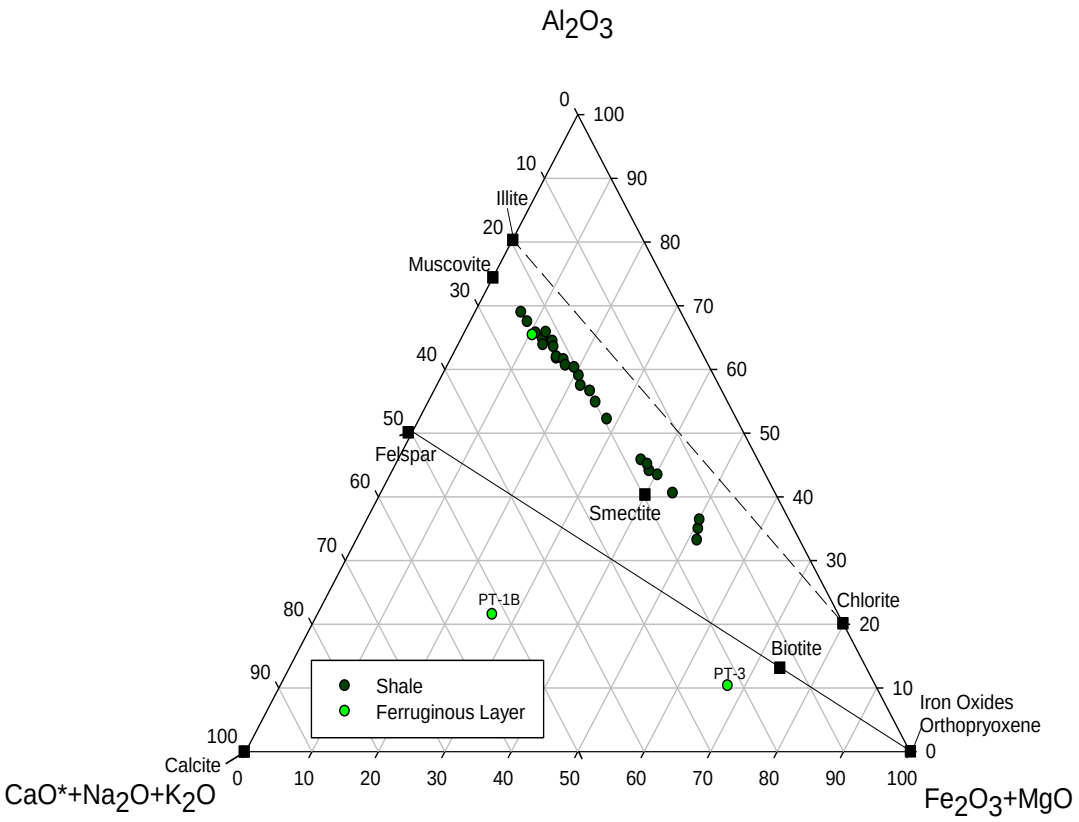

Figure 2.4. Mafic diagram (A-CNK-FM) of the Gungri Formation and Ferruginous layer. The black solid line represents the Feldspar-Orthopryoxene line; the black dotted line represents the Illite-Chlorite line.

2.5. Discussion

2.5.1. Gungri and Mikin Formations

The major element chemistry of the Attagaroo PTB section is significantly different across the three lithologies. The lithological change from the Permian Gungri Shale to the Triassic Mikin Limestone suggests that the Attagaroo PTB section experienced a marine regression (Bhargarva, 1987). The Gungri formation is, geochemically, mature, this maturity can be identified in the major element geochemistry The high content of SiO_2, TiO_2, and Al_2O_3 coupled with low content of alkali metals indicate that the Gungri formation has a substanial amount of clay minerals, which further supports the notion that the Gungri formation is a very mature section(Fedo et al., 1995). The Gungri formation CIA values are within the average range of shales (CIA= 70-75; Nesbitt and Young, 1982; Taylor and McLennan, 1985). The CIA values indicate that the Gungri formation shales have experienced intermediate chemical weathering, 60-80 (Fedo et al., 1995). These results supports our contention that the Gungri formation is suitable for paleo-enivironmental reconstruction.

The major element chemistry and CIA values for the Mikin Limestone (Triassic) are typical of marine limestones. The low CIA value is due to the low content of Al_2O_3 and SiO_2 with higher amounts of CaO and MgO. The low CIA values are probably due to the high content of CaO and MgO, instead of arid or dry conditions stated by Fedo et al. (1995). However, the Mikin formation appears to be weathered signficantly, the color of the Mikin limestone is noted as brown

(Bhargarva et al., 2004). The Mikin formation particularly the lower region appears as a dolomitic limestone (Bhargarva et al., 2004); the MgO and CaO values of the Mikin formation supports the notion that Mikin formation has dolomite characteristics.The geochemistry suggest that the limestone has a low alkali metal content, the alkali metals may have been lost from leaching and chemical weathering of the formation. In all the major element chemistry of the suggest that the Mikin formation at Attargoo can be characterized as a "muddy" or "dirty" limestone, due to the color and major element content.

The major element ternary plots reveal the extent of weathering (Roser and Korsch, 1988) in the Gungri shales. The Gungri shales appear to have lost K_2O and are enriched in Al_2O_3 suggesting re-mineralization. Major element composition of the Gungri suggests the presence of illite; illite is a product of post-depositional weathering. The Gungri shales are low in Na and Ca which may be due to weathering and loss of less stable minerals such as feldspars. It appears that "K-feldspar"-like phase remains and continues to leach (Nesbitt and Young, 2004) in the Gungri formation. Overall the major element relations suggest that the parent material of the Gungri shales is a K-rich granite; it also appears that the Attargoo PTB section did not experience K-metasomatism. This suggestion is supported by Fedo et al. (1995; Figure 3A).

The major element geochemistry of the Gungri is indicative of not only post-depositional alteration, but also low-grade metamorphism. The presence of illite and smectite suggest that secondary minerals occur in the Gungri shales; the relative of

abundace of smectite and illite are directly related to the CIA values of the Gungri formation (Hayashi et al., 1997). This presence of illite and smectite suggest that the Gungri formation has undergone post-depositional weathering (Nesbitt and Young, 2004). Therefore, the presence of smectite illite further supports the contention that the shales have experienced intermediate rather than significant levels of weathering because they are secondary minerals to feldspar (Eggleton, 1986; Meunier and Velde, 1976). In general, the Gungri formation appears to be diagenetically altered and has experienced some chloritization; the evidence of chlorite can be seen on the A-CNK-FM diagram as the shales trend towards chlorite. Eventhough the Gungri formation experienced both weathering and low-grade metamorphism, the sediments in the Gungri formation are not significantly altered to an extent where sediments can not be used for paleo-reconstruction. Therefore, we propose that Attargoo section has been diagenetically altered; this is supported by the presence of smectite. The section has experienced intermediate weathering and chlorization; with no evidence of K-metasomastism. However, the extent of chemical weathering and chlorization do not appear to be significant in which samples are altered from the original chemical composition this is reflective in the shale CIA values and both ternary plots.

2.5.2. Ferruginous Layer

The ferruginous layer is solely found at Permian-Triassic sequences located in the Spiti Valley basin, this layer is different from the Late Permian Event Horizon (LPEH) seen at Guryul Ravine PTB section. The major element chemistry and CIA value of lower ferruginous layer (PT-2) resembles the Gungri formation, while the

middle (PT-1B) and upper (PT-3) ferruginous layer do not resemble either shale or limestone major elemental chemistry. Our analysis of major elements of the middle and upper ferruginous layer contains a substainal amount of Fe, Ca, and P, with a small amount of alkali metals, Si, Ti, and Al. Even though the lower part (PT-2) contains an abundance of clay minerals, the major element chemistry of the middle and upper ferruginous layers does not suggest an abundance of clay mineral due to the low content of SiO_2, TiO_2, and Al_2O_3. Instead it seems that the middle and upper sections of the ferruginous layer is immature. However, the low content of alkali metals except for Ca may suggest that the middle and upper ferruginous layer is post-depositionally altered. The CIA values suggest that the middle and upper ferruginous layer reflects cool and/or arid conditions during deposition (Fedo et al., 1995).

Our findings suggest that the middle and upper parts of the ferruginous layer has a high content of Fe and P . The A-CN-K ternary plots suggest that the lower ferruginous layer has an abundace of illite similiar to the Gungri formation . The middle and upper ferruginous layer fall along the A-CN line close to the CN, indicating that these units contain significant concentrations of Ca in comparison to K and Al, and the loss of K perhaps is due to weathering or environmental conditions during formation.

The middle and upper ferruginous layer appears to be altered and may contain goethite (FeO(OH)) suggesting that this layer has been impacted by weathering (Şengör and Atayman, 2002). The major element data suggest that the upper part of the ferruginous layer (PT-3) contains an abundance of biotite and iron oxide minerals.

The abundance of Fe in the middle and upper ferruginous layers suggests that this layer is post-depositionally altered. Eventhough, the A-CNK-FM diagram suggests that the middle and upper ferruginous layer contains more primary than secondary minerals, the presence of geothite found at the ferruginous layer may be a secondary mineral of hematite commonly seen in shales from weathering (Şengör and Atayman, 2002); whereas the siliciclastic minerals present in ferruginous layer suggest that it is immature (e.g. feldspar and quartz). Red hematite may weather to geothite, therefore it changes the color of a red sedimentary rock a yellowish-brown color (Şengör and Atayman, 2002). A similar yellow-brownish color description has been used to describe the ferruginous layer (Bhatt et al., 1981; Shukla et al., 2002), which may suggest that the middle and upper ferruginous layer has a compisition of an iron-rich shale.

The ferruginous layer is characterize as a pebbly limonitic layer (Bhandari, 1998; Bhargarva, 1987; Bhatt et al., 1981; Ghosh et al., 2002; Shukla et al., 2002), composed of maganese with minor iron indicating a marine component, and consists of goethite, quartz, gypsum and feldspar minerals (Shukla et al., 2002). The presence of geothite suggest that some are implying that the ferruginous layers contains an abundance of hydrated iron oxides. We suggest that lower part of the ferruginous layer displays Gungri shale like characteristics because the major element geochemistry suggest that the bottom ferruginous layer has an abundance of clay minerals and is similar to Gungri shale. The major element chemistry of the middle and upper ferruginous layer suggest is iron-rich, with a high content of P and Ca. The

composition of the iron-rich layers appears to contain geothite (Shukla et al., 2002). The presence of geothite in the middle and upper ferruginous layer may suggest this mineral formed as a product of weathering hematite, this characteristics may imply that the middle and upper ferruginous layer has iron-rich shale characteristics.

The term "limonitic" used to describe the ferruginous layer suggest that the ferruginous layer consist of iron oxides and/or hydrated iron oxides. In all, the term limonitic maybe suggestive that the ferruginous layer formed by subaerial exposure or deposited under anoxic conditons. Sub-aerial exposure is is a theory use to explain the formation of the ferruginous layer. The biostratgraphy of Spiti contains an absent fossil record in the Gungri Formation (Kapoor, 2004). According to Kapoor (2004) the highest *Cyclobus* bed noted in Spiti is 20cm from the top of the Gungri formation. Bhatt et al. (1981) suggest that the ferruginous layer in Spiti marked a subaerial exposure event that followed the deposition of the Kuling formation (Gungri Formation). This subaerial exposure caused the ocean to withdraw during or soon after the deposition of sediments that contain *Cyclobus* creating a void in the fossil record (Bhatt et al., 1981) by volcanism (Kapoor, 2004) or impact (Shukla et al., 2002). Shukla et al. (2002) suggest that the mixed mineral assemblage present at the ferruginous layer, along with the presence of gypsum as an evaporite supports the theory that the ferruginous layer formed under sub-aerial orgin during oxic conditions. The major element chemistry and CIA values of the middle and upper ferruginous layer may suggest that sub-aerial exposure could have caused the formation of the ferruginous layer, evidence for sub-aerial exposure are associated

with high Ca, Fe, and P values (Reolid et al., 2008) and low CIA values that result from arid conditions during formation.

The presence of gypsum (Şengör and Atayman, 2009) and geothite at the ferruginous layer may imply that the ferruginous layer could have been deposited under anoxic conditions instead of being formed during a sub aerial exposure event (Shukla et al., 2002). Under anoxic conditions decomposition of organismal tissue through sulfur-reducing bacteria releases hydrogen sulfide, hydrogen sulfide oxidizes and dissolves calcite in surface waters which gives rise to the mineral gypsum (Şengör and Atayman, 2009). The middle and upper ferruginous layer has a high content of $C_{Organic}$ (PT-1B= 3.69%, PT-3=5.31%, Table 2.1, Figure 2.2), perhaps this $C_{Organic}$ content maybe associated with the production of sulfur needed to produce gypsum. However, we do not have any evidence of gypsum as a primary mineral, sulfide bearing minerals (e.g. frambiodal pyrite) along the ferruginous layer, or sulfur concentrations that suggest anoxic conditions. Other evidence that is suggestive of anoxia is the presence geothite at the ferruginous layers. Limonite mainly composed of geothite, may occur as a secondary mineral to pyrite through chemical weathering (Dennen and Anderson, 1967). In the case of the ferruginous layer, pyrite formed during diagenesis could have been abundant at the formation of the ferruginous layer, but due to chemical weathering pyrite oxidize into limonite, creating the limonitic ferruginous layer. Wignall et al. (2004) found evidence of pyrite at the PTB section Guryul Ravine, which is located in the Neo-Tethyan region simliar to the Attargoo section. Shukla et al. (2002) concluded that the ferruginous layer was deposited

during anoxia, despite the depositional and lithological changes seen in Spiti Valley from Permian Gungri shale to Triassic Mikin Limestone. The U, Th/U, Th, and $(Ce/La)_N$ values supports wide-spread anoxia, as Th/U (~3.8) and $(Ce/La)_N$ values in the lower part of the Permian start decreasing approximately 20-30cm below the ferruginous layer implying that anoxia starts before the deposition of the ferruginous layer (Shukla et al., 2002 see Figure 3 and 4A). Evidence gypsum along with maganese-bearing iron oxide phases suggest evaporitic conditions common during anoxia (Shukla et al. 2002). Shukla et al. (2002) suggest that wide-spread anoxia was short based on the occurrence of both Changxingian and Greisbachian fossils.

From our analysis, the organic carbon content from LOI at the ferruginous layer, specifically the upper part of the layer (PT-3=5.31%) is significantly higher than the rest of the Attargoo section. This value supports the idea that an event occurred during the formation of the ferruginous layer at the Attargoo section, due to the abrupt increase in organic carbon. In addition, we suggest that the ferruginous layer at Attargoo is a iron rich shale created *in situ* during a non-depositional event due to the high content of Fe, Ca, and P and low CIA values. The high content of P may suggest that the ferruginous layer is a representation of a phosphatic lag. The idea of a phosphatic lag may imply that the ferruginous layer is a short hiatus in sedimentation. Our supposition that the ferruginous layer at Attargoo represents the PT boundary and possibly marks a hiatus in sedimentation is aligned along with the sharp contact seen at the Attargoo PTB section with the work of others characterizing the ferruginous layer as a hiatus in sedimentation that was caused by subaerial

exposure (Bhargarva, 1987; Bhargarva and Bassi, 1998; Bhatt et al., 1981). This idea is contrary to the idea Shukla et al. (2002) proposed that the ferruginous layer could be of extraneous origin and was not desopsited *in situ.*

2.6. Conclusion

The Gungri formation contains an abundance of clay minerals, this is reflective in the CIA values, high content of SiO_2, TiO_2, and Al_2O_3, and low content of alkali metals. Based on the CIA values, the Gungri formation has undergone intermediate weathering; these values are also within the average range of shales, making the Gungri formation sediments suitable for paleo-environmental reconstruction. The idea of interemdiate weathering is supported by the presence of secondary minerals illite and smectite suggested by the A-CNK-FM diagram. The Mikin formation consist of a high content of CaO and MgO; and a low content of SiO_2, TiO_2, Al_2O_3, MnO, Na_2O, K_2O, and P_2O_5. The low CIA values are probably due to the high content of CaO and MgO. The Mikin, in terms of major element chemistry, is similiar of a dolomite limestone. This formation can be characterize as a "muddy" or "dirty" limestone due to the color and low content of alkali metals.

The A-CN-K diagram suggest that the provenance for the Attargoo section is a K-rich granite and the section did not undergo K-metasomatism. According to the A-CN-K diagram the Gungri formation has an abundance of clay minerals such as smectite and illite. The A-CNK-FM diagram indicates that the Attargoo section has been altered by post-depositional weathering, diagenesis, and very little low-grade metamorphism. The presence of illite suggests that the Gungri formation is altered

through post-depositional weathering, and diagenetically altered due to the presence of smectite. According to the A-CNK-FM diagram it appears that the Gungri formation has undergone chlorization. Although the major element geochemistry of the shales did reveal some post-depositional alteration the CIA values are in line with a typical black.

The ferruginous layer major element chemistry at Attargoo significantly changes from bottom to top. The lower ferruginous layer (PT-2) major element chemistry is identical to the Gungri formation. The middle and upper ferruginous layer major element chemistry are distinct from both the Gungri and Mikin formations. The lower ferruginous layer, like the Gungri shales below it, shows major element chemistry indicative of clay minerals. However, the middle and upper ferruginous layer show high Ca compared to Al and K. The middle and upper ferruginous layer geochemically, appears to contain goethite with both the middle and upper layers having high concentrations of Fe. The low CIA values of the middle and upper ferruginous layer suggest that arid conditions were present during the formation of the ferruginous layer. The ferruginous layer appears, like the surrounding shales and limestones, to also have been impacted by both weathering, diagenesis, and low-grade metamorphism. The A-CNK-FM diagram suggest that the ferruginous layer does not contain an abundance of secondary silicate minerals which is supported by the finding of quartz and feldspar at the ferruginous layer. The A-CNK-FM diagram also suggest that the middle and upper ferruginous layer is a immature unit in the Attargoo PTB section.

The ferruginous layer has been characterized as a limonitic layer which indicates that the layer consist iron oxides. This description may imply that the layer formed during sub-aerial exposure or anoxia. Previous studies have identified that the minerology of the ferruginous layer consists of geothite, quartz, feldspar, and gypsum. The presence of geothite and gypsum both support the two theories of sub-aerial exposure and anoxia. The high content of $C_{Org.}$ in the middle and upper ferruginous layer supports the idea that the ferruginous layers marks a catastrophic event . We suggest that the ferruginous layer is a iron-rich shale that was created *in situ* during a non-depositional event due to the high content of Fe, Ca, P, C_{Org}, and low CIA values quantified at the ferruginous layer. Sub-aerial exposure can possibly result in the non-depositional event rather than an extraterrestrial event. Moreover, the P_2O_5 content quantified at the middle and upper ferruginous layer suggest a phosphatic lag which is normally associated with a hiatus in sedimentation.

Reference List

Algeo, T.J., Hannigan, R., Rowe, H., Brookfield, M., Baud, A., and Krystyn, L., 2007, Sequencing events across the Permian-Triassic boundary, Guryul Ravine (Kashmir, India): Palaeogeography Palaeoclimatology Palaeoecology, v. 252, p. 328-346.

Bayon, G., German, C.R., Boella, R.M., Milton, J.A., Taylor, R.N., and Nesbitt, R.W., 2002, An improved method for extracting marine sediment fractions and its application to Sr and Nd isotopic analysis: Chemical Geology, v. 187, p. 179-199.

Bhandari, N., 1998, Astronomical and terrestrial causes of physical, chemical, and biological changes at geological boundaries: Proc. India Acad. Sci. (Earth Planet. Sci.), v. 107, p. 251-263.

Bhandari, N., Shukla, P.N., and Azmi, R.J., 1992, POSITIVE EUROPIUM ANOMALY AT THE PERMO-TRIASSIC BOUNDARY, SPITI, INDIA: Geophysical Research Letters, v. 19, p. 1531-1534.

Bhargarva, O.N., 1987, Stratigraphy, microfacies and paleoenvironment of the Lilang group (Scythian-Dogger), Spiti Valley, Himachal Himalaya, India: Journal of Palaeontological Society of India, v. 25, p. 91-107.

Bhargarva, O.N., and Bassi, U.K., 1998, Geology of the Spiti-Kinnaur Himachal Himalaya, Geological Survey of India Memoirs, v124, 1998. In Krystyn, L., Balini, M., and Nicora, A., (eds). 2005. Lower and middle stage and substage boundaries in Spiti, Special publication of Association of Geologist,, v. 1, p. 66-77.

Bhargarva, O.N., Krystyn, L., Balini, R., Lein, R., and Nicora, A., 2004, Revised Litho- and Sequence Stratigraphy of the Spiti Triassic Albertiana, v. 30.

Bhatt, D.K., V.K., J., and Arora, R.K., 1981, Conodonts of Otoceras beds of Spiti: Journal of Palaeontological Society of India, v. 25, p. 91-107.

Brookfield, M.E., Twitchett, R.J., and Goodings, C., 2003, Palaeoenvironments of the Permian-Triassic transition sections in Kashmir, India: Palaeogeography Palaeoclimatology Palaeoecology, v. 198, p. 353-371.

Dennen, W.H., and Anderson, P.J., 1967, Chemical changes in incipient rock weathering: Geological Society of America Bulletin, v. 73, p. 375-384.

Dèzes, P., 1999, Tectonic and metamorphic evolution of the Central Himalayan domian in southeast Zanskar (Kashmir, India). Mem. Geol., v. 32, p. 1-149.

Diener, C., 1897, Cephalopods of the Lower Trias. : Ibid., v. Ser 15., 5(1),, p. 204.

Diener, C., 1908, Landinic, Carnic and Noric fauna of Spiti: Ibid., v. 15, 5(3), p. 157.

Diener, C., 1912, The Trias of the Himalayas: Mem. Geol. Surv. India, v. 36, p. 202-358.

Eggleton, R.A., 1986, The relation between crystal structure and silicate weathering rates in Rates of Chemical Weathering of Rocks and Minerals, S. M. Colman and D, P. Dethier, eds.,: New York.

Erwin, D.H., 1993, The Great Paleozoic Crisis: Life and Death in the Permian: Columbia University Press, New York.

Fedo, C.M., Nesbitt, H.W., and Young, G.M., 1995, UNRAVELING THE EFFECTS OF POTASSIUM METASOMATISM IN SEDIMENTARY-ROCKS AND PALEOSOLS, WITH IMPLICATIONS FOR PALEOWEATHERING CONDITIONS AND PROVENANCE: Geology, v. 23, p. 921-924.

Ghosh, P., Bhattacharya, S.K., Shukla, A.D., Shukla, P.N., Bhandari, N., Parthasarathy, G., and Kunwar, A.C., 2002, Negative delta C-13 excursion and anoxia at the Permo-Triassic boundary in the Tethys Sea: Current Science, v. 83, p. 498-502.

Hayashi, K.-I., Fujisawa, H., Holland, H.D., and Ohmoto, H., 1997, Geochemistry of ~1.9 Ga sedimentary rocks from northeastern Labrador, Canada: Geochimica Et Cosmochimica Acta, v. 61, p. 4115-4137.

Hayden, H.H., 1904, The geology of Spiti with parts of Bashahr Rupshu: Mem. Geol. Surv. India, v. 36(1), p. 121.

Herren, E., 1987, ZANSKAR SHEAR ZONE - NORTHEAST-SOUTHWEST EXTENSION WITHIN THE HIGHER HIMALAYAS (LADAKH, INDIA): Geology, v. 15, p. 409-413.

Hotinski, R.M., Bice, K.L., Kump, L.R., Najjar, R.G., and Arthur, M.A., 2001, Ocean stagnation and end-Permian anoxia: Geology, v. 29, p. 7-10.

Isozaki, Y., 1997a, Permo-triassic boundary superanoxia and stratified superocean: Records from lost deep sea: Science, v. 276, p. 235-238.

Isozaki, Y., 1997b, Timing of Permian-Triassic anoxia: Science, v. 277, p. 1748-1749.

Kakuwa, Y., 2008, Evaluation of palaeo-oxygenation of the ocean bottom across the Permian-Triassic boundary: Global and Planetary Change, v. 63, p. 40-56.

Kapoor, H.M., 2004, Permo-Triassic of the Indian subcontinent and its intercontinental correlation In: Sweet, W.C., Yang, Z., Dickens, J.M., Yin, H. (Eds.), 2004. Permo-Triassic Events in the Eastern Tethys. Stratigraphy, Classification and Relations with the Western Tethys.: Cambridge University Press, Cambridge.

Kato, Y., and Isozaki, Y., 2009, Comment on "Evaluation of palaeo-oxygenation of the ocean bottom cross the Permian-Triassic boundary" by Kakuwa (2008): Was the Late Permian deep-superocean really oxic? Discussion: Global and Planetary Change, v. 69, p. 79-81.

Korte, C., Kozur, H.W., and Partoazar, H., 2004b, Negative carbon istope excursion at the Permian/Triassic boundary section at Zal, NWIran.: Hallesches Jahrbuch fur Geowissenschaften.Reihe B Beiheft, v. 18, p. 69-71.

Kozur, H., 2006, Biostratigraphy and event stratigraphy in Iran around the Permo-Triassic Boundary Implications forthe causes of the PTB biotic crisis In: Yin, H., Feng, Q., Lai, X., Baud, A., Tong, J (Eds). 2007. The protracted Perno-Triassic crisisand multi-episode extinction around the Permian-Triassic boundary. Global and Planetary Change 55, 1-20: Global and Planetary Change, v. 55, p. 155-176.

Kraft von, A., and Diener, C., 1909b, Lower Triassic Cephelapod from Spiti, Malla Johar and Byans: Pal. Indica, v. 15 6(1), p. 186.

Kraus, S.H., Siegert, S., Mette, W., Struck, U., and Korte, C., 2009, Stratigraphic significance of carbon isotope variations in the shallow-marine Seis/Siusi Permian-Triassic boundary section (Southern Alps, Italy): Fossil Record, v. 12, p. 197-205.

Krull, E.S., Retallack, G.J., Campbell, H.J., and Lyons, G.L., 2000, $\delta^{13}C_{org}$ chemostratigraphy of the Permian-Triassic boundary in the Maitai Group, New Zealand: evidence for high-latitudinal methane release: New Zealand Journal of Geology and Geophysics, v. 43, p. 21-32.

Krystyn, L., Richoz, S., Gallet, S., Bouquerel, H., Kürschner, W.M., and Spötl, C., 2007, Updated bio- and magnetostratigraphy from Steinbergkogel (Austria),

candidate GSSP for the base of the Rhaetian Stage. : Albertiana, v. 36, p. 164-174.

Matsuda, T., 1985, Late Permian to Early Triassic conodant paleobiogeography in the Tethys Realm. In: Nakazawa, K., Dickins, J.M. (Eds.), The Tethys, her Paleogeography and Paleobiogeography from Paleozoic to Mesozoic.: Tokai University Press, p. 57 – 1–70.

Meunier, A., and Velde, B., 1976, Mineral Reactions At Grain Contacts In Early Stages Of Granite Weathering: Clay Miner., v. 11(3), p. 235-240.

Murray, R.W., and Leinen, I., 1993, Chemical transport to the seafloor of the equatorial Pacific across a latitudinal transect at 135°W: tracking sedimentary major, trace, and rare earth element fluxes at the Equator and the ITCZ.: Geochim. Cosmochim. Acta v. 57, p. 414-4163.

Musashi, M., Isozaki, Y., Koike, T., and Kreulen, R., 2001, Stable carbon isotope signature in mid-Panthalassa shallow-water carbonates across the Permo-Triassic boundary: evidence for C-13-depleted superocean: Earth and Planetary Science Letters, v. 191, p. 9-20.

Nesbitt, H.W., and Young, G.M., 1982, EARLY PROTEROZOIC CLIMATES AND PLATE MOTIONS INFERRED FROM MAJOR ELEMENT CHEMISTRY OF LUTITES: Nature, v. 299, p. 715-717.

Nesbitt, H.W., and Young, G.M., 2004, Ancient Climatic and Tectonic Settings Inferred from Paleosols Developed on Igneous Rocks. In Eriksson, P., Altermann, W., Nelson, D.R., Mueller, W.U. and Catuneanu, O., (eds.) 2004.The Precambrian Earth: Tempos and Events: Developments in Pre-Cambrian

Renne, P.R., and Basu, A.R., 1991, RAPID ERUPTION OF THE SIBERIAN TRAPS FLOOD BASALTS AT THE PERMO-TRIASSIC BOUNDARY: Science, v. 253, p. 176-179.

Renne, P.R., Zhang, Z.C., Richards, M.A., Black, M.T., and Basu, A.R., 1995, SYNCHRONY AND CAUSAL RELATIONS BETWEEN PERMIAN-TRIASSIC BOUNDARY CRISES AND SIBERIAN FLOOD VOLCANISM: Science, v. 269, p. 1413-1416.

Reolid, M., Abad, I., and Martín-García, J.M., 2008, Palaeoenvironmental implications of ferruginous deposits related to a Middle-Upper Jurassic

discontinuity (Prebetic Zone, Betic Cordillera, Southern Spain): Sedimentary Geology, v. 203, p. 1-16.

Retallack, G.J., Greaver, T., and Jahren, A.H., 2007, Return to Coalsack Bluff and the Permian-Triassic boundary in Antarctica: Global and Planetary Change, v. 55, p. 90-108.

Richoz, S., Krystyn, L., Horacek, C., and Spötl, C., 2007, Carbon isotope record of the Induan-Olenekian candidate GSSP Mud and comparison with other sections.: Albertiana, v. 35, p. 35-45.

Roser, B.P., and Korsch, R.T., 1988, Determination of tectonic setting of sandstone-mudstone suites using SiO_2 content and K_2O/Na_2O ratio: Journal of Geology, v. 94, p. 635-650.

Şengör, A.M.C., and Atayman, S., 2002, The Permian Extinction and the Tethys:An Exercise in Global Geology: geological Society of America Special Papers, v. 448.

Sheldon, N.D., and Tabor, N.J., 2009, Quantitative paleoenvironmental and paleoclimatic reconstruction using paleosols: Earth-Science Reviews, v. 95, p. 1-52.

Shukla, A.D., Bhandari, N., and Shukla, P.N., 2002, Chemical signatures of the Permian-Triassic transitional environment in Spiti Valley, India: Geological Society of America Special Papers, v. 356, p. 445-453.

Singh, J., Mahanti, S., and Singh, K., 2004, Geology and evaluation of hydrocarbon prospects of Tethyan sediments in Spiti Valley, Spiti, and Zanskar, Himanchal Pradesh: Himalayan Journal of Sciences, v. 2.

Smith, J.P., 2007, Short-to-medium term sediment accumulation in low-energy subtidal areas of the lower Hudson River estuary: geochemical tracers and applications. : Boston, University of Massachusetts Boston.

Stoliczka, F., 1865, Geological section across the Himalayan Mountain range from Wangtu Bridge on the river Sutlej to Sungdeo with an account of the formations in Spiti accompanied by a revision of all known fossils from district.: Mem. Geol. Surv. India, v. 5.

Taylor, S.R., and McLennan, S., 1985, The Continental Crust: its Composition and Evolution. : Blackwell, Oxford, Blackwell Scientific Publications.

Wignall, P.B., and Hallam, A., 1992, ANOXIA AS A CAUSE OF THE PERMIAN TRIASSIC MASS EXTINCTION - FACIES EVIDENCE FROM NORTHERN ITALY AND THE WESTERN UNITED-STATES: Palaeogeography Palaeoclimatology Palaeoecology, v. 93, p. 21-46.

Wignall, P.B., Newton, R., and Brookfield, M.E., 2004, Pyrite framboid for oxygen-poor deposition during the Permian-Triassic crisis in Kashmir: Palaeogeography Palaeoclimatology Palaeoecology, v. 216, p. 183-188.

Wignall, P.B., and Twitchett, R.J., 1996, Oceanic anoxia and the end Permian mass extinction: Science, v. 272, p. 1155-1158.

Yin, H.F., Feng, Q.L., Lai, X.L., Baud, A., and Tong, J.N., 2007, The protracted Permo-Triassic crisis and multi-episode extinction around the Permian-Triassic boundary: Global and Planetary Change, v. 55, p. 1-20.

Zhang, R., Follows, M.J., Grotzinger, J.P., and Marshall, J., 2001, Could the Late Permian deep ocean have been anoxic?: Paleoceanography, v. 16, p. 317-329.

APPENDIX I

SPECTRO XEPOS BENCHTOP ENERGY DISPERSIVE X-RAY

FLUORESCENCE (ED-XRF)

STANDARD MODE OPERATION PROCEDURE

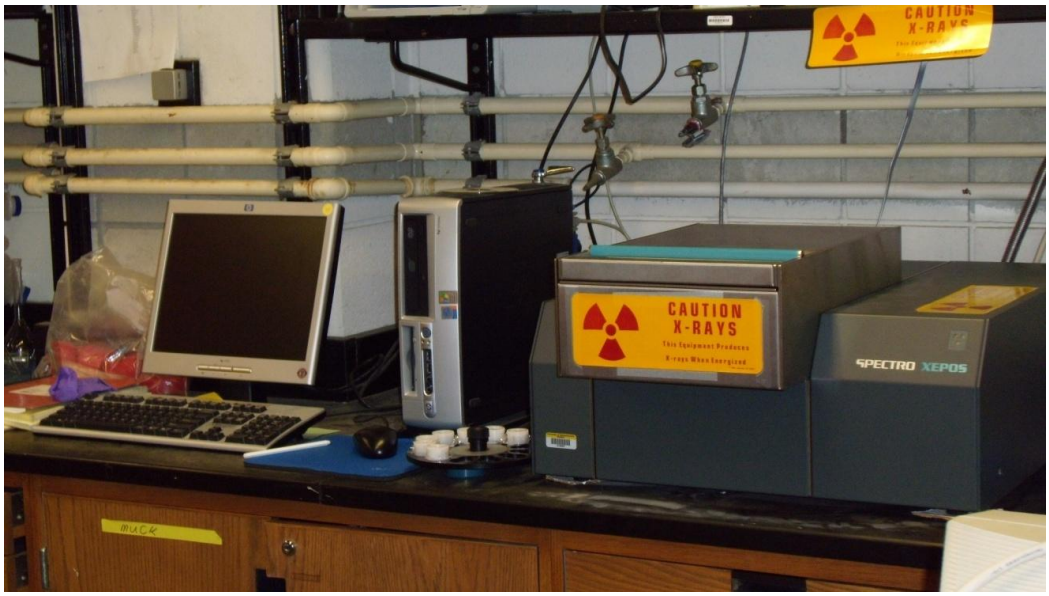

1. Turn on the ED-XRF; the power switch is on the back of the instrument.
2. Click on X-Lab Pro Routine Dialog.

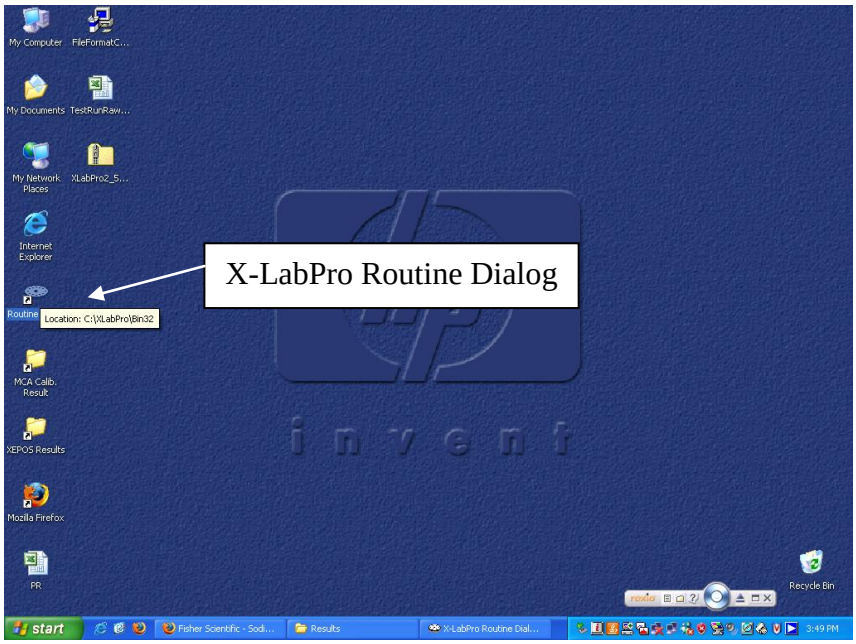

3. Click standby and allow the instrument to warm up for at least 8 hours.

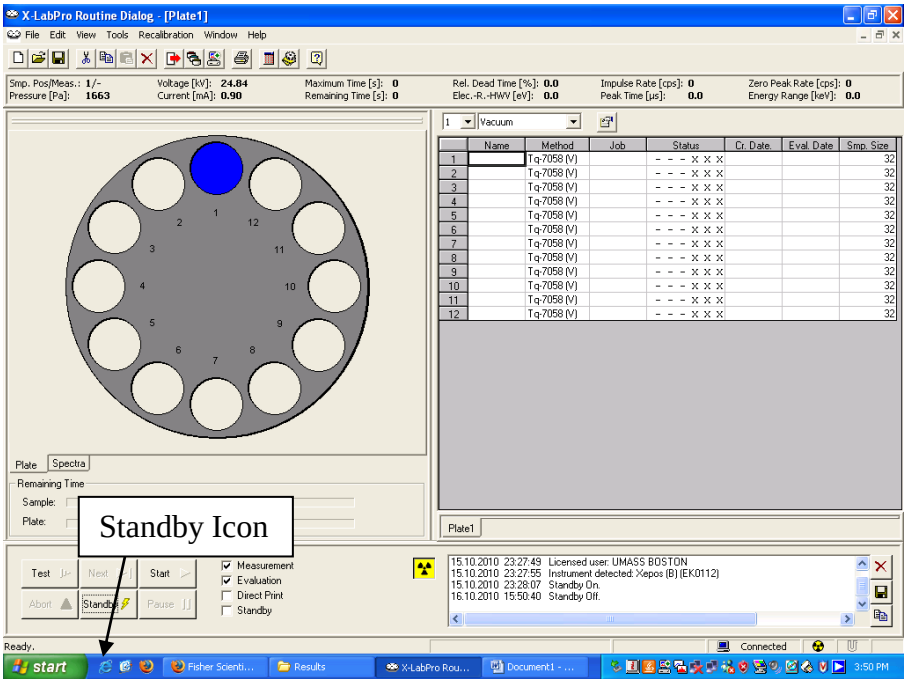

4. Once the instrument has stayed on standby for 9 hours. Select the total number of runs for each sample.

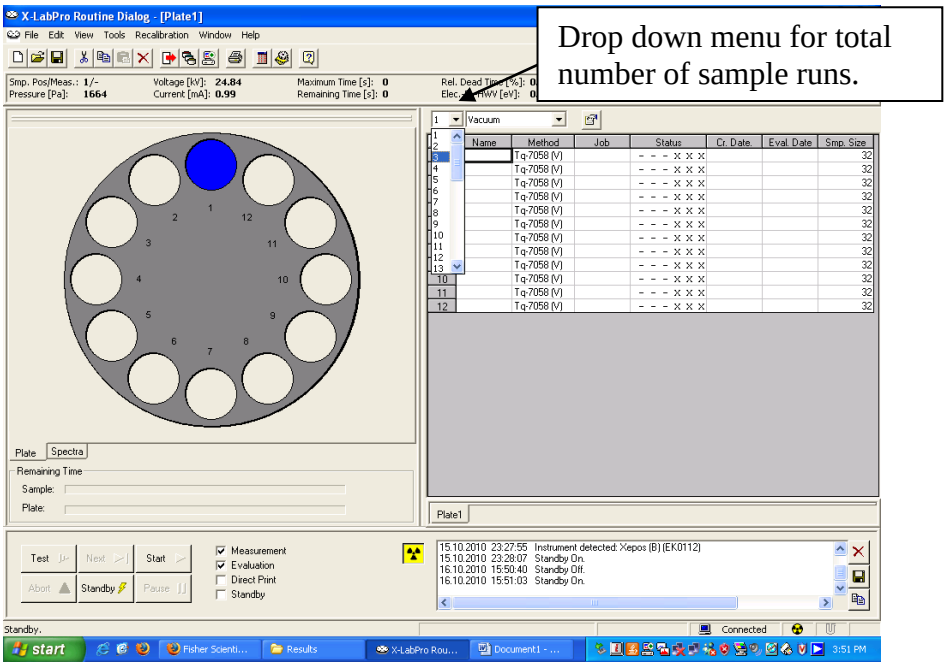

5. Select gas flush in which the samples will be analyzed under.

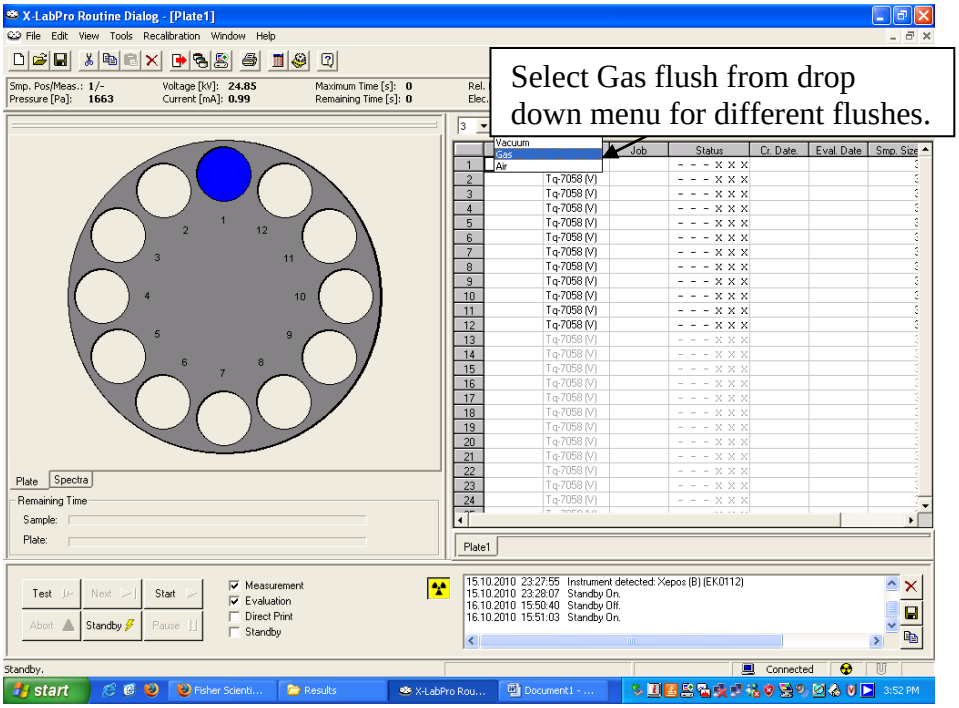

6. Select the Tqk-7058 (G) method from spreadsheet for each sample that is being analyzed under the column titled Method.

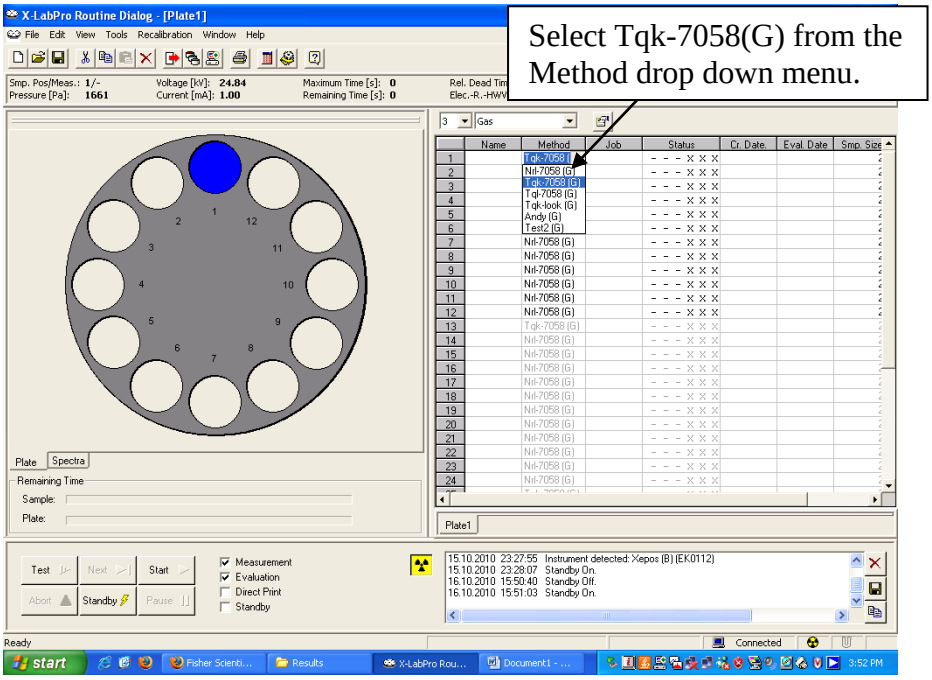

7. Type in Sample ID under the column titled Name.

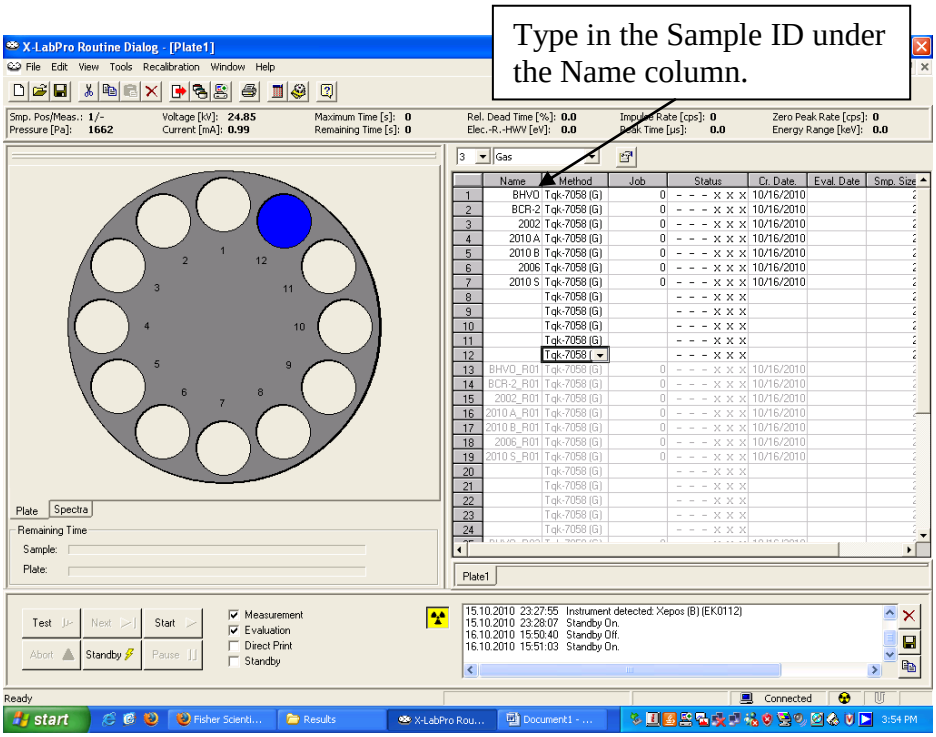

8. Type in the Job name for each sample under the column titled Job.

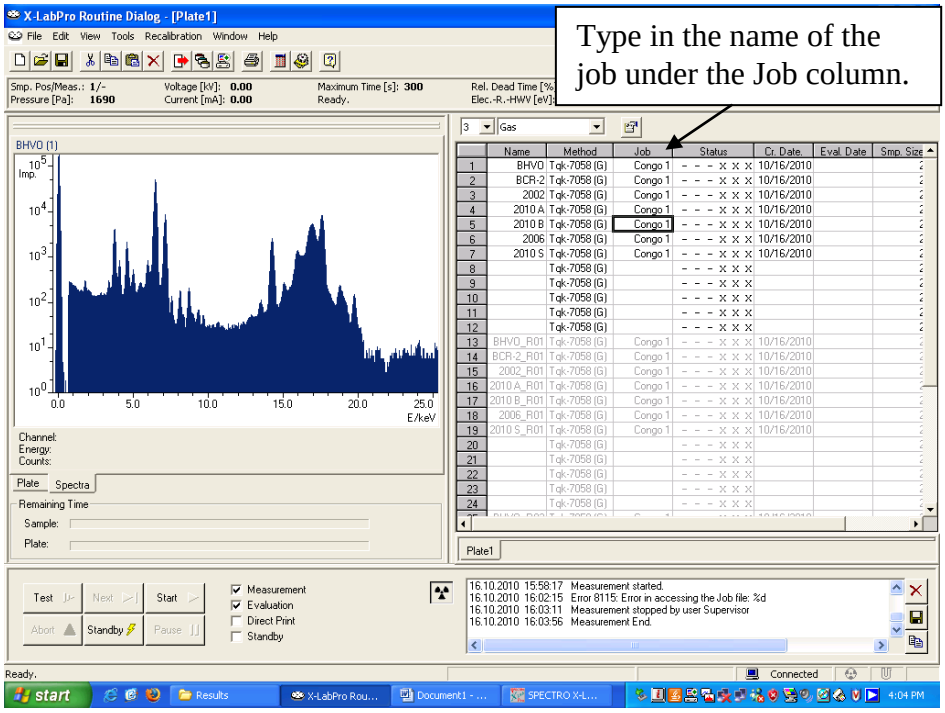

9. Turn the Instrument off of Standby and uncheck the vacuum valve open in order to stop the vacuum valve during the standby mode.

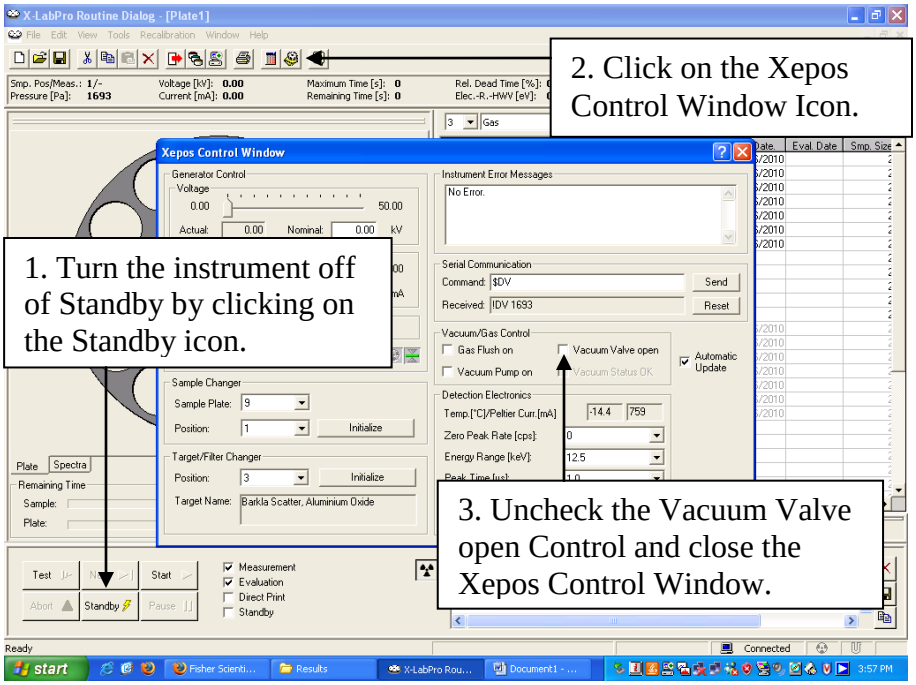

10. Load the samples inside of the instrument and turn on the gas, the gas pressure should be set to 70kPa.

11. Click on the Start Icon to begin instrument analysis. The computer will inform the user that the samples will be measured under gas flush, click Yes. If the computer warns the user that the samples will be measured under another flush besides gas, click No and change the flush to Gas.

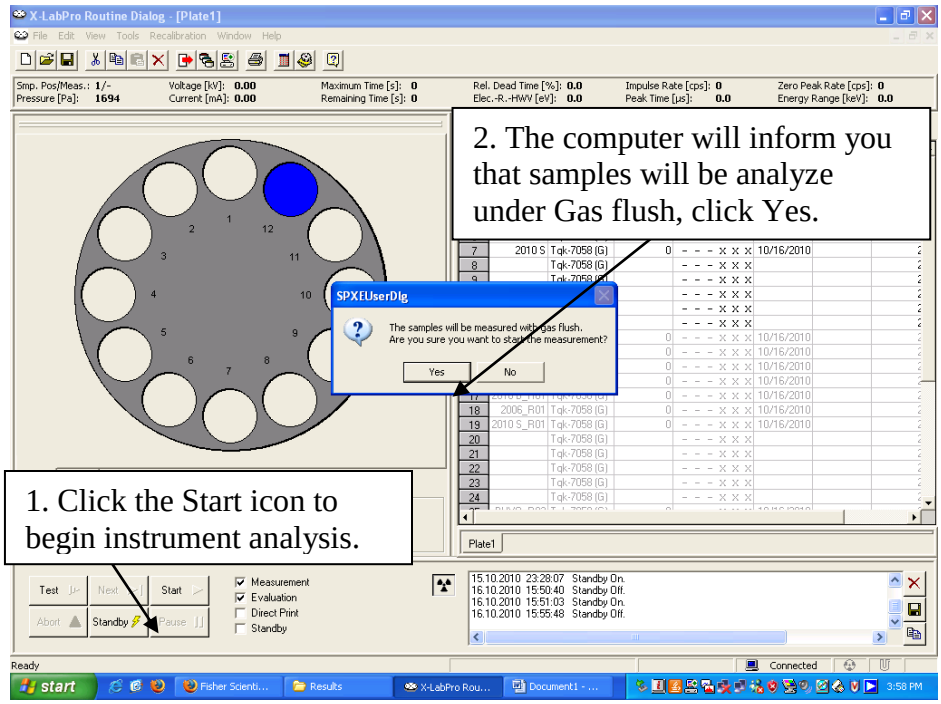

12. Once the instrument analysis is completed, remove the samples from the instrument and close the remove samples pop up box.

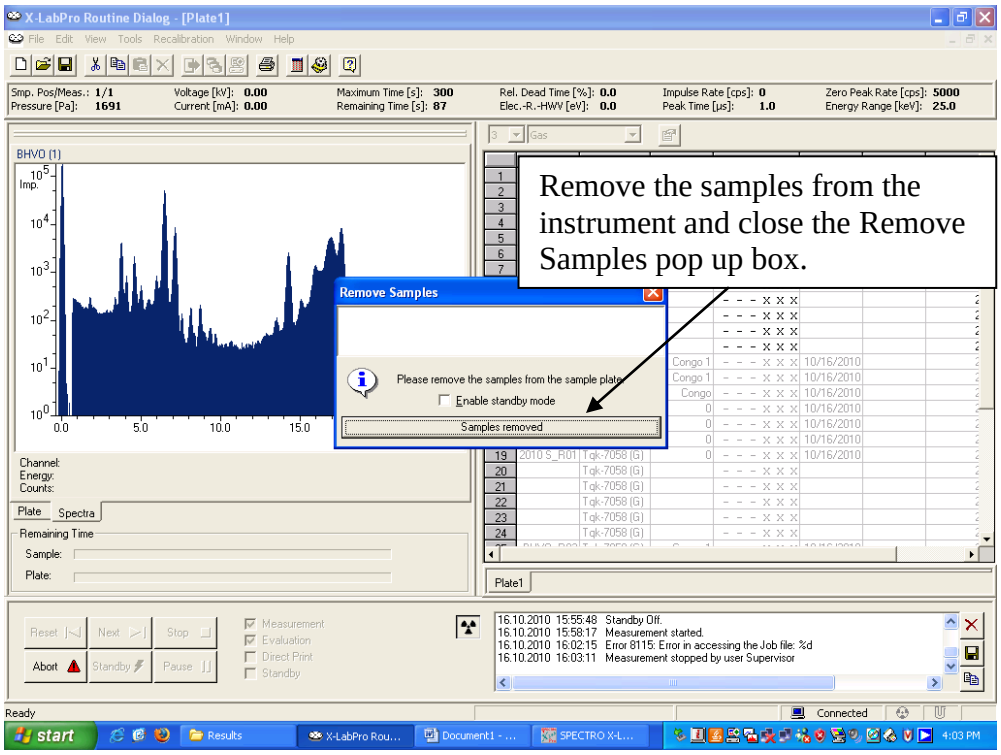

13. Once the samples are removed from the instrument:
    a. Turn off the He gas.
    b. Place the instrument on Standby for next analysis or leave it on standby for at least 9 hours before turning off the instrument.

APPENDIX II

LOSS ON IGNITION (LOI): MUFFLE FURNACE

STANDARD MODE OPERATION PROCEDURE

Loss on Ignition – Organic Carbon

1. Record the mass of the crucible(s).
2. Place approximately 0.5-2g of sample in the crucible, and record the mass of the crucible.
3. Heat the crucible(s) for 1 hour at 550ºC.
4. Let the crucible(s) cool down to room temperature and stir.
5. Heat the crucible(s) for 1 hour at 550°C.
6. Let the crucible(s) cool down to room temperature and weigh.

Loss on Ignition- Carbonate Carbon

1. Heat the crucible(s) for 2 hours at 850°C.
2. Stir the sample(s) at least once during the 850°C.
3. Let the crucible(s) cool down to room temperature and weigh.

APPENDIX III

PERKINELMER OPTIMA 3000XL INDUCTIVELY COUPLED PLASMA OPTICAL EMISSION SPECTROMETER (ICP-OES)

STANDARD MODE OPERATION PROCEDURE

1. Turn on the instrument in the following sequences:
    a. Computer
    b. Liquid Nitrogen Gas and Argon Gas (Ultra Pure).
    c. Water chiller, located alone on the left side against the wall.
    d. Main power, located on the right of the ICP-OES.
    e. RF Power, located on the right of the ICP-OES.
    f. Computer software WinLab 32

2. Check the gas pressure, water pressure on the chiller, and the temperature on the chiller. The parameters are pre-set, make sure that the readings are correct.
   - Gas pressure
     - N_2: 62 psi
     - Ar: 80psi
   - Chiller
     - Water Pressure-50
     - Temperature- 18°C

3. Let the instrument warm-up for 1.5hrs, the remain time is displayed on the computer screen.

4. Clamp the tubing on the roller of the peristaltic pump. The Green taped line is the autosampler line, the autosampler should be placed on the top row. The red taped line is the waste line, the waste line should be place on the second row below the autosampler line.
   Note: Make sure the flow directions are right. If not it will damage the instrument.

5. Turn on the perstaltic pump.

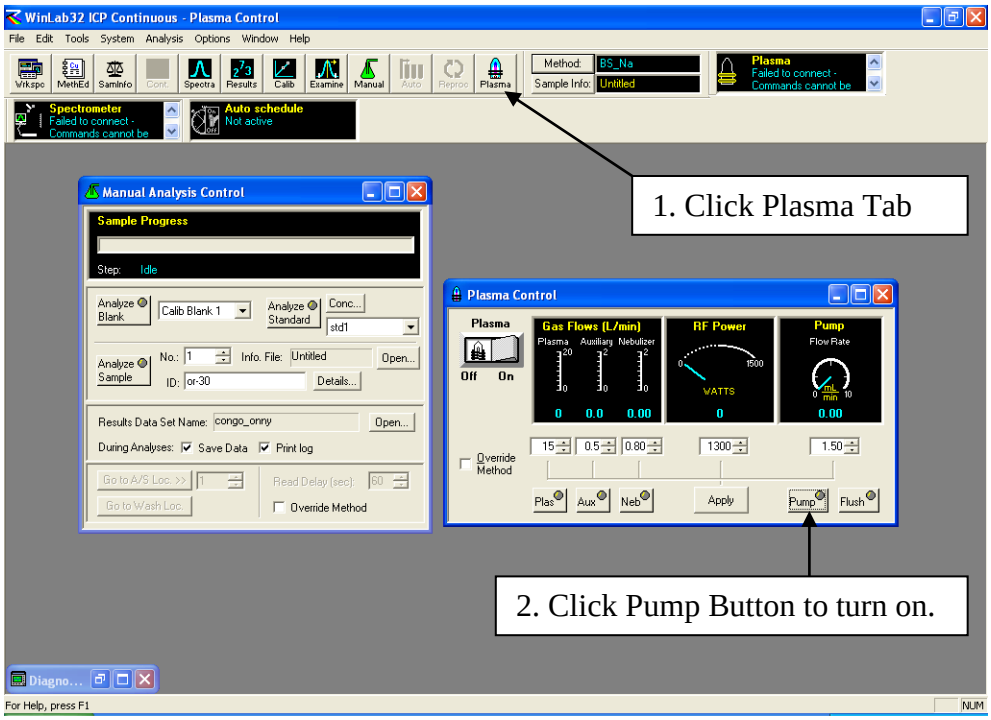

6. Make sure the flow is smooth by introducing a few air bubbles.

7. Turn off the perstaltic pump

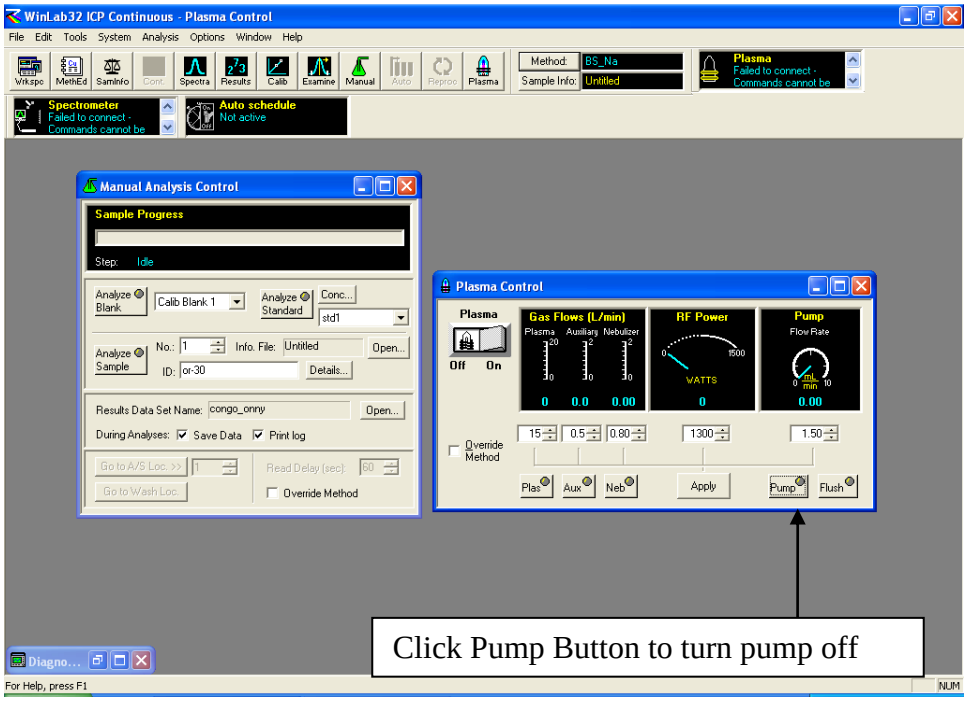

8. The ICP-OES is ready for sample analysis., but in order to guarantee reproducilibilty, the instrument should be idle at least 15 minutes.

9. Set up the measurement procedures by choosing elements, wavelength and entering standard solution concentration.

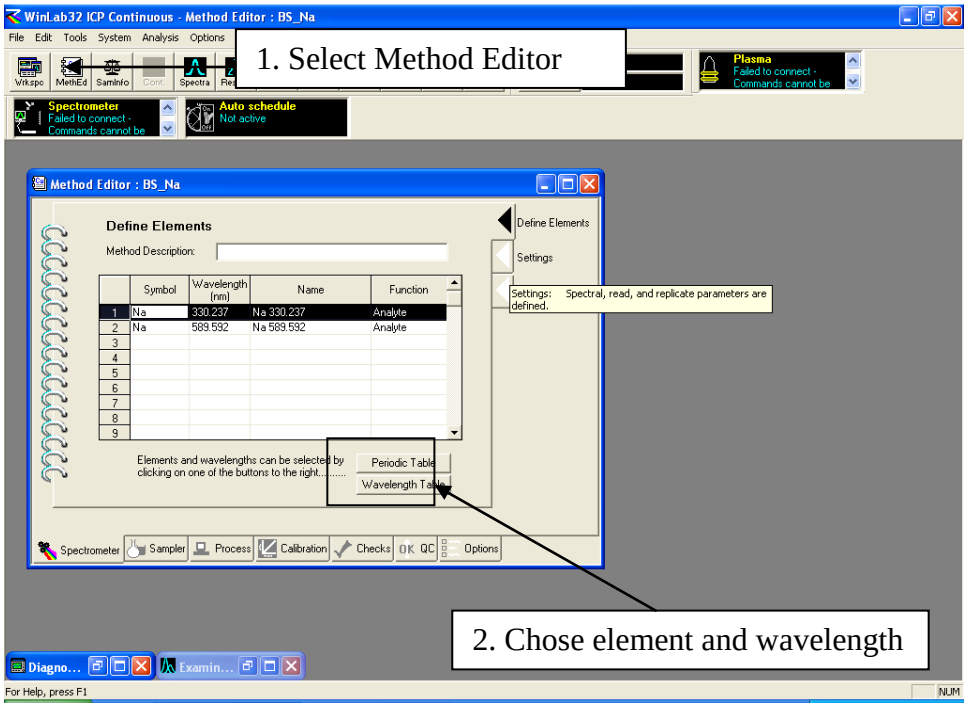

10. Analyze the Blank, once the blank is analyze turn off the perstaltic pump.

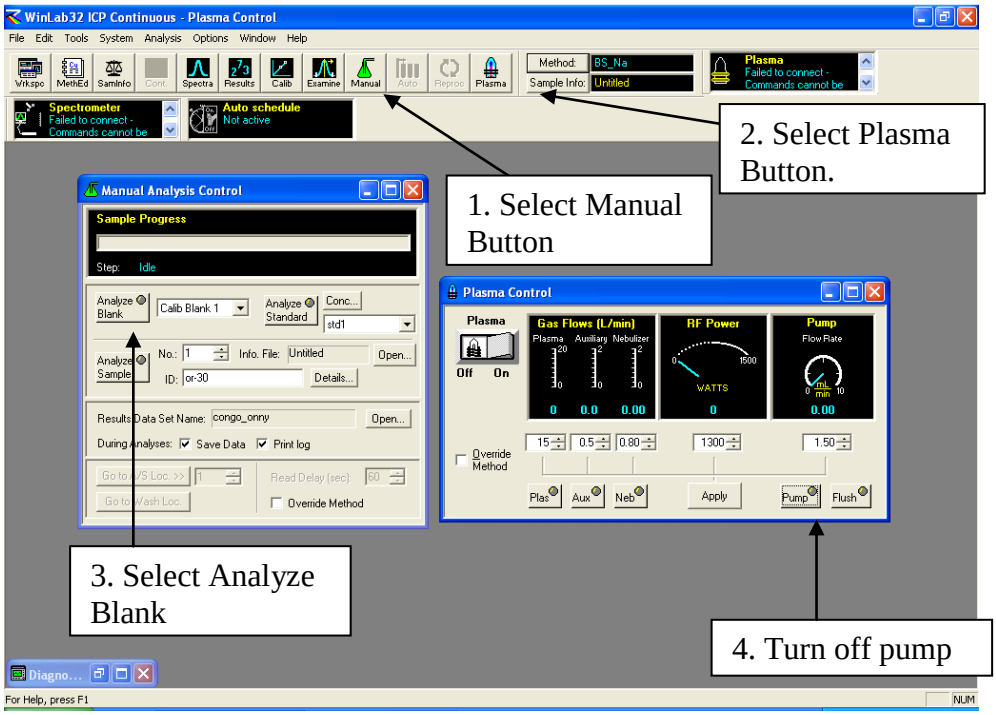

11. Analyze Standard(s), once the standard(s) is/are analyzed turn off the perstaltic pump.

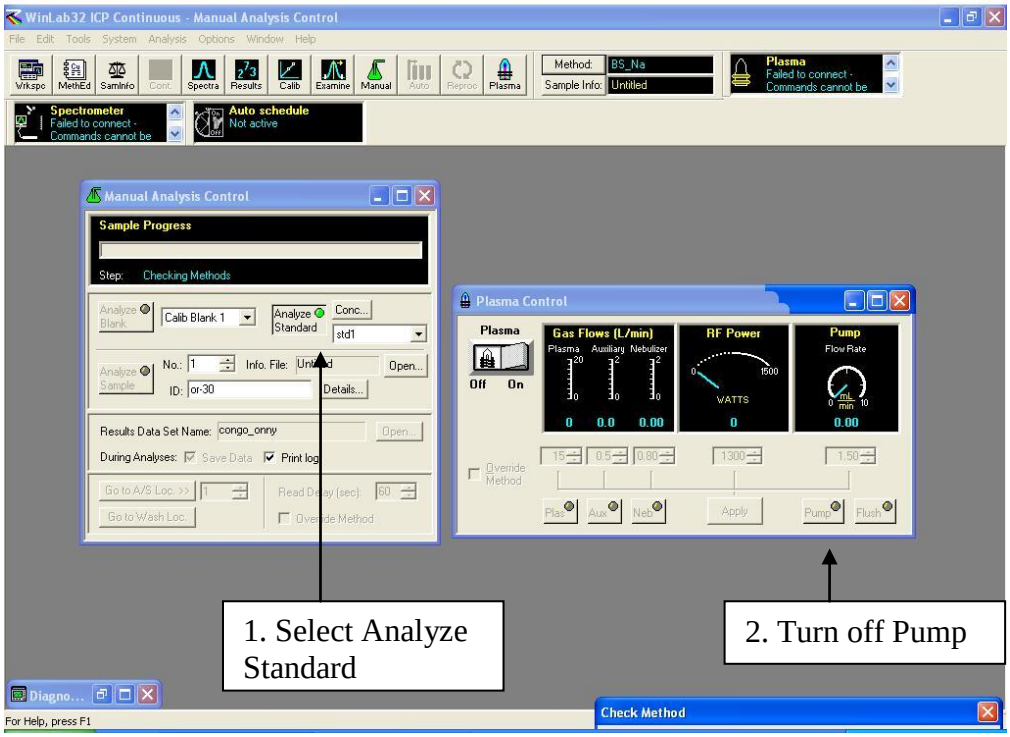

12. Analyze the sample(s):
    a. Type in the sample name in the ID space.
    b. Select analyze sample
    c. Once the sample is analyzed, turn off pump

Note: This procedure must be done for each sample.

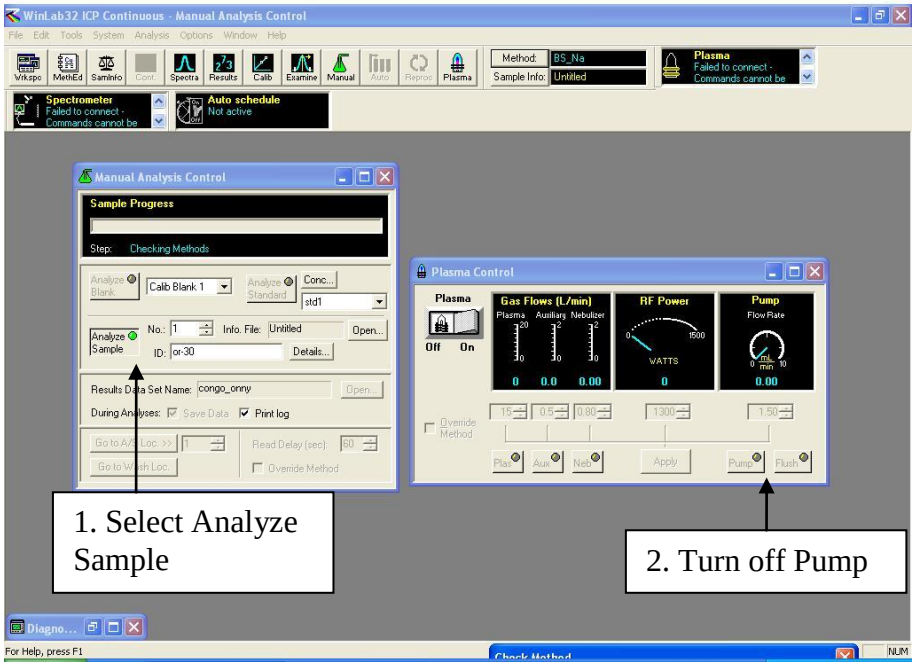

13. Between the individual sample run and after the entire sample run, 2% HNO_3 solution should be used to rinse the system for 20 seconds.

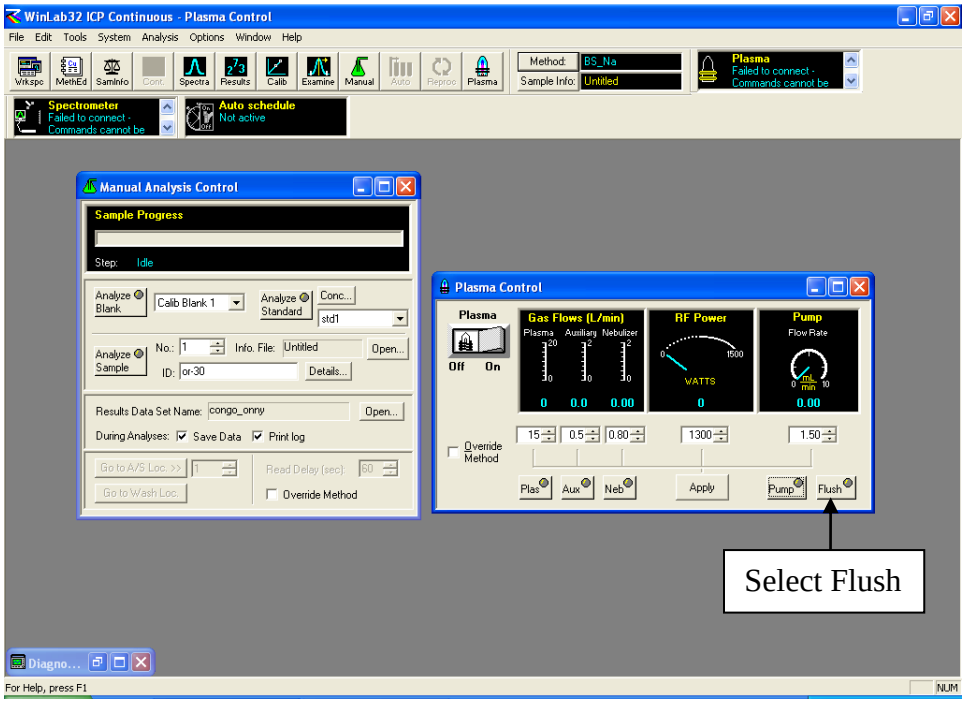

14. Rinse the instument with 2% HNO_3 and DI water, by immersing the sample probe tip in DI water before shutting down.

15. Shut down procedure:
    a. Shut down Plasma
    b. Turn off RT power
    c. Turn off Main Power
    d. Turn off chiller
    e. Turn off Liguid Nitrogen and Argon Gas (Ultrapure).
    f. Close out WinLab 32

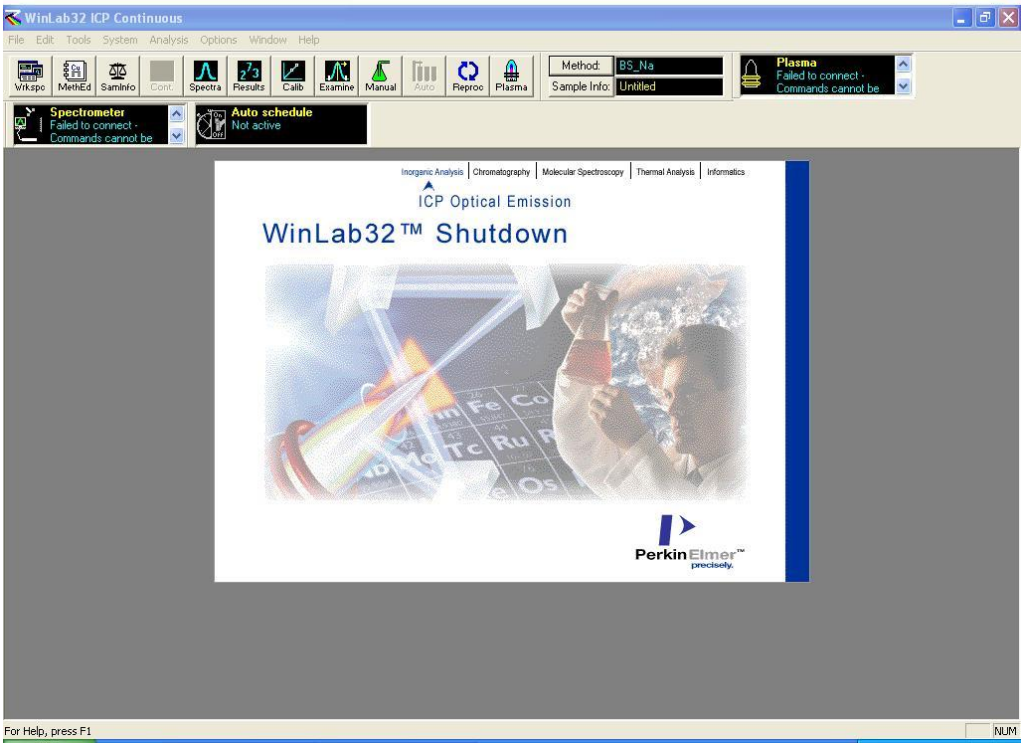

REFERENCE LIST

Abanda, P.A., and Hannigan, R., 2006, Diagenetic controls of trace element partitioning in shales: Chemical Geology, v. 230, p. 42-59.

Algeo, T.J., Ellwood, B., Nguyen, T.K.T., Rowe, H., and Maynard, J.B., 2007a, The Permian-Triassic boundary at Nhi Tao, Vietnam: Evidence for recurrent influx of sulfidic water masses to a shallow-marine carbonate platform: Palaeogeography, Palaeoclimatology, Palaeoecology, v. 252, p. 304-327.

Algeo, T.J., Hannigan, R., Rowe, H., Brookfield, M., Baud, A., and Krystyn, L., 2007b, Sequencing events across the Permian-Triassic boundary, Guryul Ravine (Kashmir, India): Palaeogeography Palaeoclimatology Palaeoecology, v. 252, p. 328-346.

Algeo, T.J., Hannigan, R., Rowe, H., Brookfield, M., Baud, A., Krystyn, L., and Ellwood, B.B., 2007c, Sequencing events across the Permian-Triassic boundary, Guryul Ravine (Kashmir, India): Palaeogeography, Palaeoclimatology, Palaeoecology, v. 252, p. 328-346.

Bassoullet, J.P., Colchen, M., Juteau, T., Marcoux, J., Mascle, G., and Reibel, F., 1983, Geological studies in the Indus suture zone of Ladakh (Himalayas), *in* Gupta, V.J., ed., Stratigraphy and structure of Kashmir and Ladakh Himalaya: Contributions to Himalayan Geology, Volume 2: India, HPC Publishers, p. 96-124.

Basu, A.R., Petaev, M.I., Poreda, R.J., Jacobsen, S.B., and Becker, L., 2003, Chondritic meteorite fragments associated with the Permian-Triassic boundary in Antarctica: Science, v. 302, p. 1388-1392.

Baud, A., Atudorei, V., and Sharp, Z., 1996, Late Permian and early Triassic evolution of the Northern Indian margin: Carbon isotope and sequence stratigraphy: Geodinamica Acta, v. 9, p. 57-77.

Baud, A., Magaritz, M., and Holser, W.T., 1989, Permian-Triassic of the Tethys: Carbon isotope studies: International Journal of Earth Sciences, v. 78, p. 649-677.

Bayon, G., German, C.R., Boella, R.M., Milton, J.A., Taylor, R.N., and Nesbitt, R.W., 2002, An improved method for extracting marine sediment fractions and its application to Sr and Nd isotopic analysis: Chemical Geology, v. 187, p. 179-199.

Becker, L., Poreda, R.J., Basu, A.R., Pope, K.O., Harrison, T.M., Nicholson, C., and Iasky, R., 2004, Bedout: A possible end-Permian impact crater offshore of Northwestern Australia: Science, v. 304, p. 1469-1476.

Beerling, D.J., and Berner, R.A., 2005, Feedbacks and the coevolution of plants and atmospheric CO2: Proceedings of the National Academy of Sciences of the United States of America, v. 102, p. 1302-1305.

Berner, R.A., 2005, The carbon and sulfur cycles and atmospheric oxygen from middle Permian to middle Triassic: Geochimica Et Cosmochimica Acta, v. 69, p. 3211-3217.

Berner, R.A., VandenBrooks, J.M., and Ward, P.D., 2007, Evolution - Oxygen and evolution: Science, v. 316, p. 557-558.

Bhandari, N., 1998, Astronomical and terrestrial causes of physical, chemical, and biological changes at geological boundaries: Proc. India Acad. Sci. (Earth Planet. Sci.), v. 107, p. 251-263.

Bhandari, N., Shukla, P.N., and Azmi, R.J., 1992, POSITIVE EUROPIUM ANOMALY AT THE PERMO-TRIASSIC BOUNDARY, SPITI, INDIA: Geophysical Research Letters, v. 19, p. 1531-1534.

Bhargava, O.N., 1987, Stratigraphy, microfacies and paleoenvironment of the Lilang group (Scythian-Dogger), Spiti Valley, Himachal Himalaya, India: Journal of the Palaeontological Society of India, v. 25, p. 91-107.

Bhargarva, O.N., and Bassi, U.K., 1998, Geology of the Spiti-Kinnaur Himachal Himalaya, Geological Survey of India Memoirs, v124, 1998. In Krystyn, L., Balini, M., and Nicora, A., (eds). 2005. Lower and middle stage and substage boundaries in Spiti, Special publication of Association of Geologist,, v. 1, p. 66-77.

Bhargava, O.N., Krystyn, L., Balini, M., Lein, R., and Nicora, A., 2004, Revised litho- and sequence stratigraphy of the Spiti Triassic: Albertiana, v. 30, p. 21-39.

Bhargava, O.N., Srivastava, R.N., and Gadhoke, S.K., 1985, *Zoophycos* from the Permian Gungri Member (Kuling Formation), Spiti Valley, Himachal Himalaya: Journal of the Geological Society of India, v. 26, p. 137-140.

Bhatt, D.K., Fuchs, G., Prashara, K.C., Krysten, L., Arora, R.K., and Golebiowski, R., 1981, Conodonts of Otoceras beds of Spiti: Journal of the Palaeontological Society of India, v. 25, p. 130-134.

Bice, D.M., Newton, C.R., McCauley, S., Reiners, P.W., and McRoberts, C.A., 1992, SHOCKED QUARTZ AT THE TRIASSIC-JURASSIC BOUNDARY IN ITALY: Science, v. 255, p. 443-446.

Brookfield, M.E., 1993, THE HIMALAYAN PASSIVE MARGIN FROM PRECAMBRIAN TO CRETACEOUS TIMES: Sedimentary Geology, v. 84, p. 1-35.

Brookfield, M.E., Twitchett, R.J., and Goodings, C., 2003, Palaeoenvironments of the Permian-Triassic transition sections in Kashmir, India: Palaeogeography Palaeoclimatology Palaeoecology, v. 198, p. 353-371.

Canfield, D.E., and Thamdrup, B., 1994, THE PRODUCTION OF S-34-DEPLETED SULFIDE DURING BACTERIAL DISPROPORTIONATION OF ELEMENTAL SULFUR: Science, v. 266, p. 1973-1975.

Catalano, R., Distefano, P., and Kozur, H., 1991, PERMIAN CIRCUMPACIFIC DEEP-WATER FAUNAS FROM THE WESTERN TETHYS (SICILY, ITALY) - NEW EVIDENCES FOR THE POSITION OF THE PERMIAN TETHYS: Palaeogeography Palaeoclimatology Palaeoecology, v. 87, p. 75-108.

Condie, K.C., 1993, Chemical-composition and evolution of the upper continental crust - contrasting results from surface samples and shales: Chemical Geology, v. 104, p. 1-37.

Corsetti, F.A., Baud, A., Marenco, P.J., and Richoz, S., 2005, Summary of Early Triassic carbon isotope records: Comptes Rendus Palevol, v. 4, p. 473-486.

Dennen, W.H., and Anderson, P.J., 1967, Chemical changes in incipient rock weathering: Geological Society of America Bulletin, v. 73, p. 375-384.

Dèzes, P., 1999, Tectonic and metamorphic evolution of the Central Himalayan domian in southeast Zanskar (Kashmir, India). Mem. Geol., v. 32, p. 1-149.

Diener, C., 1897, Himalayan fossils. The Cephalopoda of the Lower Trias: Palaeontologia Indica, (ser.15), v. 2, p. 1-191.

Diener, C., 1908, Ladinic, Carnic and Noric faunae of Spiti: Palaeontologia Indica, (ser.15), v. 5, p. 1-157.

Diener, C., 1912, The Trias of the Himalayas: Memoirs of the Geological Survey of India, v. 36, p. 202-367.

Dyer, B.D., Lyalikova, N.N., Murray, D., Doyle, M., Kolesov, G.M., and Krumbein, W.E., 1989, ROLE FOR MICROORGANISMS IN THE FORMATION OF IRIDIUM ANOMALIES: Geology, v. 17, p. 1036-1039.

Eggleton, R.A., 1986, The relation between crystal structure and silicate weathering rates in Rates of Chemical Weathering of Rocks and Minerals, S. M. Colman and D, P. Dethier, eds.,: New York.

Erwin, D.H., 1993, The Great Paleozoic Crisis: Life and Death in the Permian: Columbia University Press, New York.

Erwin, D.H., 1994, THE PERMO-TRIASSIC EXTINCTION: Nature, v. 367, p. 231-236.

Farley, K.A., and Mukhopadhyay, S., 2001, An extraterrestrial impact at the Permian-Triassic boundary?: Science, v. 293, p. 2343-+.

Fedo, C.M., Wayne Nesbitt, H., and Young, G.M., 1995, Unraveling the effects of potassium metasomatism in sedimentary rocks and paleosols, with implications for paleoweathering conditions and provenance: Geology, v. 23, p. 921-924.

Gaetani, M., and Garzanti, E., 1991a, MULTICYCLIC HISTORY OF THE NORTHERN INDIA CONTINENTAL-MARGIN (NORTHWESTERN HIMALAYA): Aapg Bulletin-American Association of Petroleum Geologists, v. 75, p. 1427-1446.

Gaetani, M., and Garzanti, E., 1991b, Multicyclic history of the northern India continental margin (Northwestern Himalaya): American Association of Petroleum Geologists Bulletin, v. 75, p. 1427-1446.

Gardner, L.R., 1992, Long-term isovolumetric leaching of aluminum from rocks during weathering: Implications for the genesis of saprolite: CATENA, v. 19, p. 521-537.

Garzanti, E., 1993a, Himalayan ironstones, "superplumes," and the breakup of Gondwana: Geology, v. 21, p. 105-108.

Garzanti, E., 1993b, Sedimentary evolution and drowning of a passive margin shelf (Giumal Group; Zanskar Tethys Himalaya, India): palaeoenvironmental changes during final break-up of Gondwanaland: Geological Society, London, Special Publications, v. 74, p. 277-298.

Garzanti, E., Angiolini, L., and Sciunnach, D., 1996, The Permian Kuling Group (Spiti, Lahaul and Zanskar; NW Himalaya): sedimentary evolution during rift/drift transition and initial opening of Neo-Tethys: Rivista Italiana di Paleontologia e Stratigrafia, v. 102, p. 175-200.

Garzanti, E., Jadoul, F., Nicora, A., and Berra, F., 1995, Triassic of Spiti (Tethys Himalaya; N. India): Rivista Italiana di Paleontologia e Stratigrafia, v. 101, p. 267-300.

Garzanti, E., Nicora, A., and Rettori, R., 1998, Permo-Triassic boundary and lower to middle Triassic in South Tibet: Journal of Asian Earth Sciences, v. 16, p. 143-157.

Ghosh, P., Bhattacharya, S.K., Shukla, A.D., Shukla, P.N., Bhandari, N., Parthasarathy, G., and Kunwar, A.C., 2002, Negative delta C-13 excursion and anoxia at the Permo-Triassic boundary in the Tethys Sea: Current Science, v. 83, p. 498-502.

Grice, K., Cao, C.Q., Love, G.D., Bottcher, M.E., Twitchett, R.J., Grosjean, E., Summons, R.E., Turgeon, S.C., Dunning, W., and Jin, Y.G., 2005, Photic zone euxinia during the Permian-Triassic superanoxic event: Science, v. 307, p. 706-709.

Haas, J., Demeny, A., Hips, K., Zajzon, N., Weiszbury, T.G., and Sundar, M., 2007 Biotic and environmental changes in the Permian-Triassic boundaryinterval recorded on a western Tethyan ramp in the Bukk Mountains, Hungary: Global and Planetary Change, v. 55, p. 136-154

Hallam, A., and Wignall, P.B., 1997, Mass Extinction and their aftermath: Oxford University Press, New York.

Hayashi, K.-I., Fujisawa, H., Holland, H.D., and Ohmoto, H., 1997, Geochemistry of ~1.9 Ga sedimentary rocks from northeastern Labrador, Canada: Geochimica Et Cosmochimica Acta, v. 61, p. 4115-4137.

Hayden, H.H., 1904, The geology of Spiti with parts of Bashahr and Rupshu: Memoirs of the Geological Survey of India, v. 36, p. 1-129.

Herren, E., 1987, ZANSKAR SHEAR ZONE - NORTHEAST-SOUTHWEST EXTENSION WITHIN THE HIGHER HIMALAYAS (LADAKH, INDIA): Geology, v. 15, p. 409-413.

Hongfu, Y., Dickins, J.M., Shi, G.R., and T.Jinnan, 2000, Permian-Triassic Evolution of Tethys and Western Circum-Pacific, Developments in Palaeontology and Stratigraphy: Amsterdam, Elsevier, p. 412.

Hotinski, R.M., Bice, K.L., Kump, L.R., Najjar, R.G., and Arthur, M.A., 2001, Ocean stagnation and end-Permian anoxia: Geology, v. 29, p. 7-10.

Isozaki, Y., 1997a, Permo-triassic boundary superanoxia and stratified superocean: Records from lost deep sea: Science, v. 276, p. 235-238.

Isozaki, Y., 1997b, Timing of Permian-Triassic anoxia: Science, v. 277, p. 1748-1749.

Isozaki, Y., Kawahata, H., and Ota, A., 2007, A unique carbon isotope recordacross the Guadalupian-Lopingian (Middle-Upper Permian) boundary in the mid-oceanic paleo-atoll carbonates: The high productivity "Kamura event: and its collapse in Panthalassa.: Global and Planetary Change, v. 55, p. 21-38.

Izett, G.A., 1990, The Cretaceous-Tertiary (KT) boundary interval, Raton Basin Colorado and New Mexico, and its content of minerals: Evidence relevant to the Crateceous-Tertiary impact extinction hypothesis: Geological Society of America Special Papers, v. 249, p. 100.

Jin, Y.G., Wang, Y., Wang, W., Shang, Q.H., Cao, C.Q., and Erwin, D.H., 2000, Pattern of marine mass extinction near the Permian-Triassic boundary in South China: Science, v. 289, p. 432-436.

Kakuwa, Y., 2008, Evaluation of palaeo-oxygenation of the ocean bottom across the Permian-Triassic boundary: Global and Planetary Change, v. 63, p. 40-56.

Kakuwa, Y., and Matsumoto, R., 2006, Cerium negative anomaly just before the Permian and Triassic boundary event - The upward expansion of anoxia in the water column: Palaeogeography Palaeoclimatology Palaeoecology, v. 229, p. 335-344.

Kapoor, H.M., 2004, Permo-Triassic of the Indian subcontinent and its intercontinental correlation In: Sweet, W.C., Yang, Z., Dickens, J.M., Yin, H. (Eds.), 2004. Permo-Triassic Events in the Eastern Tethys. Stratigraphy, Classification and Relations with the Western Tethys.: Cambridge University Press, Cambridge.

Kato, Y., and Isozaki, Y., 2009, Comment on "Evaluation of palaeo-oxygenation of the ocean bottom cross the Permian-Triassic boundary" by Kakuwa (2008): Was the Late Permian deep-superocean really oxic? Discussion: Global and Planetary Change, v. 69, p. 79-81.

Kato, Y., Nakao, K., and Isozaki, Y., 2002, Geochemistry of Late Permian to Early Triassic pelagic cherts from southwest Japan: implications for an oceanic redox change: Chemical Geology, v. 182, p. 15-34.

Korte, C., Kozur, H., and Mohtat-Aghai, P., 2004a, Dzhulfian tolowermost Triassic d13C record at the Permian/Triassic section at Shahreza, Central, Iran In: Yin, H., Feng, Q., Lai, X., Baud, A., Tong, J (Eds). 2007. The protracted Perno-Triassic crisisand multi-episode extinction around the Permian-Triassic boundary. Global and Planetary Change 55, 1-20: Hallesches Jahrbuch der Geowissenchaften, B, v. 18, p. 73-78.

Korte, C., Kozur, H.W., and Partoazar, H., 2004b, Negative carbon istope excursion at the Permian/Triassic boundary section at Zal, NWIran.: Hallesches Jahrbuch fur Geowissenschaften.Reihe B Beiheft, v. 18, p. 69-71.

Korte, C., and Kozur, H.W., 2010, Carbon-isotope stratigraphy across the Permian-Triassic boundary: A review: Journal of Asian Earth Sciences, v. 39, p. 215-235.

Korte, C., Kozur, H.W., Joachimski, M.M., Strauss, H., Veizer, J., and Schwark, L., 2004b, Carbon, sulfur, oxygen,and strontium isotope records, organic geochemistry and biostratigraphy across the Permian /Triassic boundary in Abadeh, Iran In: Yin, H., Feng, Q., Lai, X., Baud, A., Tong, J (Eds). 2007. The protracted Perno-Triassic crisisand multi-episode extinction around the Permian-Triassic boundary. Global and Planetary Change 55, 1-20: Geological Rundschau, v. 93, p. 565-581.

Kozur, H., 2006, Biostratigraphy and event stratigraphy in Iran around the Permo-Triassic Boundary Implications forthe causes of the PTB biotic crisis In: Yin, H., Feng, Q., Lai, X., Baud, A., Tong, J (Eds). 2007. The protracted Perno-Triassic crisisand multi-episode extinction around the Permian-Triassic boundary. Global and Planetary Change 55, 1-20: Global and Planetary Change, v. 55, p. 155-176.

Krafft, A., and Diener, C., 1909, Himalayan fossils. Lower Triassic Cephalopoda from Spiti, Malla Johar, and Byans: Palaeont. Indica, (ser. 15), v. 6, p. 1-186.

Kraft von, A., and Diener, C., 1909, Lower Triassic Cephelapod from Spiti, Malla Johar and Byans: Pal. Indica, v. 15 6(1), p. 186.

Kraus, S.H., Siegert, S., Mette, W., Struck, U., and Korte, C., 2009, Stratigraphic significance of carbon isotope variations in the shallow-marine Seis/Siusi Permian-Triassic boundary section (Southern Alps, Italy): Fossil Record, v. 12, p. 197-205.

Krull, E.S., Retallack, G.J., Campbell, H.J., and Lyons, G.L., 2000, $\delta^{13}C_{org}$ chemostratigraphy of the Permian-Triassic boundary in the Maitai Group, New Zealand: evidence for high-latitudinal methane release: New Zealand Journal of Geology and Geophysics, v. 43, p. 21-32.

Krystyn, L., Richoz, S., Gallet, S., Bouquerel, H., Kürschner, W.M., and Spötl, C., 2007, Updated bio- and magnetostratigraphy from Steinbergkogel (Austria), candidate GSSP for the base of the Rhaetian Stage. : Albertiana, v. 36, p. 164-174.

Matsuda, T., 1985, Late Permian to early Triassic conodont paleobiogeography in the "Tethys Realm", *in* Nakazawa, K., and Dickens, J.M., eds., The Tethys–Her Paleogeography and Paleobiogeography from Paleozoic to Mesozoic: Tokyo, Tokai University Press, p. 157–170.

McBride, E.F., 1974, Significance of color in red, green, olive, brown, and grey beds of Difunta Group, northeastern Mexico.: Journal of Sedimentary Petrology, v. 44, p. 760-773.

Meunier, A., and Velde, B., 1976, Mineral Reactions At Grain Contacts In Early Stages Of Granite Weathering: Clay Miner., v. 11(3), p. 235-240.

Murray, R.W., and Leinen, I., 1993, Chemical transport to the seafloor of the equatorial Pacific across a latitudinal transect at 135°W: tracking sedimentary major, trace, and rare earth element fluxes at the Equator and the ITCZ.: Geochim. Cosmochim. Acta v. 57, p. 414-4163.

Musashi, M., Isozaki, Y., Koike, T., and Kreulen, R., 2001, Stable carbon isotope signature in mid-Panthalassa shallow-water carbonates across the Permo-Triassic boundary: evidence for C-13-depleted superocean: Earth and Planetary Science Letters, v. 191, p. 9-20.

Nesbitt, H.W., and Young, G.M., 1982, Early Proterozoic climates and plate motions inferred from major element chemistry of lutites: Nature, v. 299, p. 715-717.

Nesbitt, H.W., and Young, G.M., 2004, Ancient Climatic and Tectonic Settings Inferred from Paleosols Developed on Igneous Rocks. In Eriksson, P., Altermann, W., Nelson, D.R., Mueller, W.U. and Catuneanu, O., (eds.) 2004.The Precambrian Earth: Tempos and Events: Developments in Pre-Cambrian

Payne, J.L., Lehrmann, D.J., Follett, D., Seibel, M., Kump, L.R., Riccardi, A., Altiner, D., Sano, H., and Wei, J., 2007, Erosional truncation of uppermost Permian shallow-marine carbonates and implications for Permian-Triassic boundary events: Geological Society of America Bulletin, v. 119, p. 771-784.

Payne, J.L., Lehrmann, D.J., Wei, J.Y., Orchard, M.J., Schrag, D.P., and Knoll, A.H., 2004, Large perturbations of the carbon cycle during recovery from the end-Permian extinction: Science, v. 305, p. 506-509.

Payne, J.L., Turchyn, A.V., Paytan, A., DePaolo, D.J., Lehrmann, D.J., Yu, M.Y., and Wei, J.Y., 2010, Calcium isotope constraints on the end-Permian mass extinction: Proceedings of the National Academy of Sciences of the United States of America, v. 107, p. 8543-8548.

Raiswell, R., and Berner, R.A., 1985, PYRITE FORMATION IN EUXINIC AND SEMI-EUXINIC SEDIMENTS: American Journal of Science, v. 285, p. 710-724.

Raymond, A., Parker, W.C., and Parrish, J.T., 1985, Phtyogeography and paleoclimate of the early Carboniferous in Tiffney B.H. (eds). Geological Factors and the Evolution of Plants.: New Haven, Yale University Press, p. 166-222.

Reeburgh, W.S., Ward, B.B., Whalen, S.C., Sandbeck, K.A., Kilpatrick, K.A., and Kerkhof, L.J., 1991, Black Sea methane geochemistry: Deep-Sea Res., v. 38, p. 1189–1210.

Renne, P.R., and Basu, A.R., 1991, RAPID ERUPTION OF THE SIBERIAN TRAPS FLOOD BASALTS AT THE PERMO-TRIASSIC BOUNDARY: Science, v. 253, p. 176-179.

Renne, P.R., Zhang, Z.C., Richards, M.A., Black, M.T., and Basu, A.R., 1995, SYNCHRONY AND CAUSAL RELATIONS BETWEEN PERMIAN-TRIASSIC BOUNDARY CRISES AND SIBERIAN FLOOD VOLCANISM: Science, v. 269, p. 1413-1416.

Reolid, M., Abad, I., and Martín-García, J.M., 2008, Palaeoenvironmental implications of ferruginous deposits related to a Middle-Upper Jurassic discontinuity (Prebetic Zone, Betic Cordillera, Southern Spain): Sedimentary Geology, v. 203, p. 1-16.

Retallack, G.J., Greaver, T., and Jahren, A.H., 2007, Return to Coalsack Bluff and the Permian-Triassic boundary in Antarctica: Global and Planetary Change, v. 55, p. 90-108.

Retallack, G.J., Seyedolali, A., Krull, E.S., Holser, W.T., Ambers, C.P., and Kyte, F.T., 1998, Search for evidence of impact at the Permian-Triassic boundary in Antarctica and Australia: Geology, v. 26, p. 979-982.

Retallack, G.J., Veevers, J.J., and Morante, R., 1996, Global coal gap between Permian-Triassic extinction and Middle Triassic recovery of peat-forming plants: Geological Society of America Bulletin, v. 108, p. 195-207.

Richoz, S., Krystyn, L., Horacek, C., and Spötl, C., 2007, Carbon isotope record of the Induan-Olenekian candidate GSSP Mud and comparison with other sections.: Albertiana, v. 35, p. 35-45.

Roser, B.P., and Korsch, R.T., 1988, Determination of tectonic setting of sandstone-mudstone suites using SiO_2 content and K_2O/Na_2O ratio: Journal of Geology, v. 94, p. 635-650.

Rowley, D.B., Raymond, A., Parrish, J.T., Lottes, A.L., Scotese, C.R., and Ziegler, A.M., 1985, CARBONIFEROUS PALEOGEOGRAPHIC, PHYTOGEOGRAPHIC, AND PALEOCLIMATIC RECONSTRUCTIONS: International Journal of Coal Geology, v. 5, p. 7-42.

Schubert, C.J., Durisch-Kaiser, E., Klauser, L., Vazquez, F., Wehrli, B., and Holzner, C.P., 2006, Recent studies in sources and sinks of methane in Black Sea, in Neretin, L.N., (eds). Past Present Water Column Anoxia: Dordrecht Springer, p. 419-441.

Şengör, A.M.C., Altmer, D., Cin, A., Utsaomer, T., and Hsu, K.J., 1988, Origin and assembly of the Tethyside orogenic collage at the expense of Gondawana Land, *in* Audley-Charles, M.G., and Hallam, A., eds., Gondawa and Tethys, Volume 37: Special Publication: Boulder, Geological Society of America, p. 119-181.

Şengör, A.M.C., and Atayman, S., 2009, The Permian Extinction and the Tethys:An Exercise in Global Geology: geological Society of America Special Papers, v. 448.

Shao, L.Y., Zhang, P.F., Duo, J.W., and Shen, S.Z., 2000, Carbon isotope compositions of the late Permian carbonate rocks in southern China: their variations between Wujiaping and Changxing formations.: Palaeogeography Palaeoclimatology Palaeoecology, v. 161, p. 179-192.

Shoemaker, E.M., 1959, Impact mechanics at Meteor crater, Arizona, U.S.: Atomic Energy Commission Open File Report.

Sholkovitz, E.R., Landing, W.M., and Lewis, B.L., 1994, OCEAN PARTICLE CHEMISTRY - THE FRACTIONATION OF RARE-EARTH ELEMENTS BETWEEN SUSPENDED PARTICLES AND SEAWATER: Geochimica Et Cosmochimica Acta, v. 58, p. 1567-1579.

Shukla, A.D., Bhandari, N., and Shukla, P.N., 2002a, Chemical signatures of the Permian-Triassic transitional environment in Spiti Valley, India, *in* Koeberl, C., and MacLeod, K.G., eds., Catastrophic Events and Mass Extinctions: Impacts and Beyond, Volume Special Paper 356: Boulder, Geological Society of America, p. 445-453.

Shukla, A.D., Bhandari, N., and Shukla, P.N., 2002b, Chemical signatures of the Permian-Triassic transitional environment in Spiti Valley, India: Geological Society of America Special Papers, v. 356, p. 445-453.

Singh, T., Tiwari, R., Vijaya, S., and Avtar, R., 1995, Stratigraphy and palynology of Carboniferous-Permian-Triassic succession in Spiti Valley, Tethys Himalaya, India: Journal of the Palaeontological Society of India, v. 40, p. 55-76.

Singh, J., Mahanti, S., and Singh, K., 2004, Geology and evaluation of hydrocarbon prospects of Tethyan sediments in Spiti Valley, Spiti, and Zanskar, Himanchal Pradesh: Himalayan Journal of Sciences, v. 2.

Smith, J.P., 2007, Short-to-medium term sediment accumulation in low-energy subtidal areas of the lower Hudson River estuary: geochemical tracers and applications. Boston, University of Massachusetts Boston.

Srikantia, S.V., and Bhargava, O.N., 1998, Geology of Himachal Pradesh: Bangalore, Geological Society of India.

Stoliczka, F., 1866, Geological section across the Himalayan Mountains, from Wangtu bridge on the River Sutlej to Sungdo on the Indus: with an account of the formations of Spiti, accompanied by a revision of all known fossils from that district: Memoirs of the Geological Survey of India, v. 5, p. 1-173.

Stutz, E., 1988, Geologie de la chaine de Mylmaling aux confins du Ladakh et du Rupshu (NW Himalaya, Inde): Evolution, paleogeographique et tectonique d' un segment de la marge nord-indienne, 149 p.

Sweet, W.C., Zunyi, Y., Dickins, J.M., and Yin, H., 1992, Permo-Triassic Events in the Eastern Tethys: Cambridge, Cambridge University Press.

Taylor, S.R., and McLennan, S., 1985, The Continental Crust: its Composition and Evolution. : Blackwell, Oxford, Blackwell Scientific Publications.

Tong, J.N., Erwin, D.H., Zuo, J.X., and Zhao, L.S., 2005, Lower Triassic carbon isotope stratigraphy in Chaohu, Anhui: implaction to biotic and ecological recovery.: Albertiana, v. 33, p. 75-76.

Veevers, J.J., and Powell, C.M., 1987, Late Paleozoic glacial episodes in Gondwanaland reflected in trasngressive-regressive depositional sequences in Euramerica: Geological Society of America Bulletin, v. 98, p. 475-487.

Warmer, J.G., and Sandberg, C.A., 1996, Alamo megabreccia: Record of late Devonian impact in southern Nevada, U.S.A.: GSA Today, v. 104, p. 171-176.

Waterhouse, J.B., 2010, Lopingian (Late Permian) stratigraphy of the Salt Range, Pakistan and Himalayan region: Geological Journal, v. 45, p. 264-284.

Wignall, P.B., 1994, Black Shales: Oxford, Oxford University Press, , v. 30.

Wignall, P.B., and Hallam, A., 1992, ANOXIA AS A CAUSE OF THE PERMIAN TRIASSIC MASS EXTINCTION - FACIES EVIDENCE FROM NORTHERN ITALY AND THE WESTERN UNITED-STATES: Palaeogeography Palaeoclimatology Palaeoecology, v. 93, p. 21-46.

Wignall, P.B., and Hallam, A., 1996, Facies change and the end-Permian mass extinction in SE Sichuan, China: Palaios, v. 11, p. 587-596.

Wignall, P.B., Newton, R., and Brookfield, M.E., 2004, Pyrite framboid for oxygen-poor deposition during the Permian-Triassic crisis in Kashmir: Palaeogeography Palaeoclimatology Palaeoecology, v. 216, p. 183-188.

Wignall, P.B., and Twitchett, R.J., 1996, Oceanic anoxia and the end Permian mass extinction: Science, v. 272, p. 1155-1158.

Wilkin, R.T., and Barnes, H.L., 1997, Pyrite formation in an anoxic estuarine basin: American Journal of Science, v. 297, p. 620-650.

Willis, K., and McElwain, J.C., 2002, The Evolution of Plants: Oxford University Press, v. 378.

Xie, S.C., Pancost, R.P., Yin, E.F., Wang, H., and Evershed, R.P., 2006, Two episodes of microbial changes associated with Permo-Triassic faunal mass extinction.: Nature, v. 434, p. 494-497.

Yin, H.F., Feng, Q.L., Lai, X.L., Baud, A., and Tong, J.N., 2007, The protracted Permo-Triassic crisis and multi-episode extinction around the Permian-Triassic boundary: Global and Planetary Change, v. 55, p. 1-20.

Zakharov, Y.D., Biakov, A.S., Baud, A., and Kozur, H., 2005, Carbon isotope standard for the Upper Permian and Lower Triassic in Caucasus and its correlation with the Permian of northeastern Russia: Albertiana, v. 33, p. 102-103.

Zhang, R., Follows, M.J., Grotzinger, J.P., and Marshall, J., 2001, Could the Late Permian deep ocean have been anoxic?: Paleoceanography, v. 16, p. 317-329.

Zhang, H.J., Tong, J.N., and Zuo, J.X., 2005, Lower Triassic and carbon isotope excursion in West Guangxi, southwest China: Albertiana, v. 33, p. 103-104.

Zhao, G., Sun, M., Wilde, S.A., and Li, S.Z., 2004, A Paleo-Mesoproterozoic supercontinent: assembly, growth and breakup: Earth-Science Reviews, v. 67, p. 91-123.